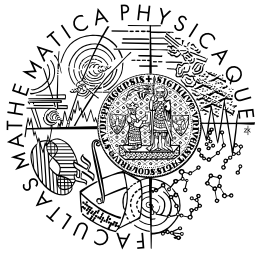

FACULTY
OF MATHEMATICS
AND PHYSICS
Charles University

MASTER THESIS

Kristián Farkaš

Two-loop chiral corrections to the neutral pion decay to electron-positron pair

Faculty of Mathematics and Physics

Supervisor of the master thesis: RNDr. Jiří Novotný, CSc.

Study programme: Physics

Study branch: Nuclear and Subnuclear Physics

Prague 2019

I declare that I carried out this master thesis independently, and only with the cited sources, literature and other professional sources.

I understand that my work relates to the rights and obligations under the Act No. 121/2000 Sb., the Copyright Act, as amended, in particular the fact that the Charles University has the right to conclude a license agreement on the use of this work as a school work pursuant to Section 60 subsection 1 of the Copyright Act.

In ..... date ..... signature of the author

At this place I would like to thank to my supervisor RNDr. Jiří Novotný, CSc. who explained me all knowledge necessary for the elaboration of this diploma thesis in detail and patiently discussed all the problems which I encountered during this process. I would also like to thank to prof. RNDr. Jiří Hořejší, DrSc. whose lectures on quantum field theory helped me to understand the problem discussed in this work.

Title: Two-loop chiral corrections to the neutral pion decay to electron-positron pair

Author: Kristián Farkaš

Institute of Particle and Nuclear Physics: Faculty of Mathematics and Physics

Supervisor: RNDr. Jiří Novotný, CSc., Institute of Particle and Nuclear Physics

Abstract: This thesis is devoted to the rare decay $\pi^0 \to e^+e^-$. We firstly introduce all theoretical knowledge necessary for the description of the vertices used in this work. Subsequently, we introduce three two-loop chiral Feynman diagrams, which are of order $O(\alpha^2 p^4)$. These diagrams are firstly decomposed to master integrals by Laporta algorithm. After that, we calculate each master integral individually by the differential equation technique. We also focus on the renormalization of the process. Since we are working with the effective field theory, finite corrections χ from counterterm diagrams naturally appear. With use of the calculations listed in this thesis, the determination of the parameter χ_R could be further improved taking into account the whole two-loop correction.

Keywords: rare decay $\pi^0 \to e^+e^-$, effective field theory, chiral perturbation theory, two-loop corrections, next leading order calculations, master integrals, pion transition form factor, modern methods of amplitude calculation

Contents

Introduction

Decay $\pi^0 \to e^+e^-$ is thoroughly studied over the years. The major reasons are following. Firstly, the direct confrontation of the experimental data with theoretical predictions gives us a good tool for testing a low-energy dynamics of the Standard Model (SM) and possible physics beyond the SM. Secondly, the process is even in the lowest order described by the exchange of two virtual photons and therefore is connected directly with a pion transition form factor $\mathrm{F}_{\pi^0\to\gamma\gamma}$ which cannot be calculated from the first principles. Better understanding of this form factor is for example important in the muon anomalous magnetic moment g - 2 [1].

The very first theoretical prediction of the decay rate was performed by Drell [2]. This calculation initiated various attempts to calculate amplitude within the leading order based on various approaches by which was pion transition form factor $\mathrm{F}_{\pi^0\to\gamma\gamma}$ determined [3, 4, 5, 6, 7, 8]. Renowned theoretical interest appeared after the publication of the branching ratio $\pi^0 \to e^+e^-$ from the KTeV-E799-II experiment at Fermilab [9] with the result

$$B(\pi^0 \to e^+e^-(\gamma), x_D > 0.95) = (6.44 \pm 0.25 \pm 0.22) \times 10^{-8}, \tag{1}$$

where the first uncertainty corresponds to statistical and second to systematical error. In the above expression, x_D is a Dalitz variable defined as

$$x_D = \frac{m^2_{e^+e^-}}{M^2_{\pi^0}} = 1 - 2\frac{E_\gamma}{M_{\pi^0}}, \tag{2}$$

where M_{π^0} is mass of neutral pion, $m^2_{e^+e^-}$ corresponds to the mass of the electron-positron pair $(q_{e^+} + q_{e^-})^2$ and E_γ is the photon energy. Constraint to the variable x_D of the type (1) is imposed to get rid of the Dalitz decay $\pi^0 \to e^+e^-\gamma$ which is dominant at low x_D. In order to subtract the radiative corrections the collaborants of KTeV-E799-II experiment used the theoretical work of Bergström [10] with the result

$$B^{no-rad}_{KTeV}(\pi^0 \to e^+e^-) = (7.48 \pm 0.29 \pm 0.25) \times 10^{-8}. \tag{3}$$

This result was confronted with the SM prediction in [11] where the calculation was done for the various form factor $\mathrm{F}_{\pi^0\to\gamma\gamma}$ models. They shown that the result was almost insensitive on the chosen model. Within the model using the data of CLEO combined with the operator product expansion (CLEO + OPE model) [12] they came to the result

$$B^{no-rad}_{SM}(\pi^0 \to e^+e^-) = (6.23 \pm 0.09) \times 10^{-8}. \tag{4}$$

which can be interpreted as a discrepancy of 3.3 σ in comparison with (3). After this result a big amount of the theoretical work (e.g. [13]) including NLO corrections was performed. However, only the work [14] calculated two-loop QED radiative corrections of the order $O(\alpha^3 p^2)$ without any approximation (except of the estimate of the ξ parameter [1]). Adding of this contribution reduced the discrepancy between prediction of the SM and experiment to 2 σ.

Another important ingredient naturally appearing in the loop correction calculations using effective theory are the finite contributions of the counterterm diagrams which are described by a parameter χ. This parameter describes high-energy loop contribution since the effective theory is not usable in this energy region and can be obtained by comparison with the model dependent calculation. In our particular case this comparison was done in the lowest order by [7] within a model using the large N_C limit and Lowest Meson Dominance (LMD) approximation with the result

$$\chi^R_{LMD}(770MeV) = 2.2 \pm 0.9. \tag{5}$$

Different approach was chosen in [15]. The parameter χ^R was obtained by the fit of the experimental data with the result

$$\chi^R_{fit}(770MeV) = 4.5 \pm 1.0. \tag{6}$$

In this paper also the NLO chiral contributions in the leading log (LL) approximation were considered. However, as was shown, this contribution at least in this approximation, can be neglected.

In this thesis we want to pick up on the work [14] and calculate part of the NLO contribution of the order $O(\alpha^2 p^4)$ stemming from the chiral perturbation theory (χPT) [16, 17, 18] enriched by photons and leptons [19, 20]. The contribution of this order consists of three Feynman diagrams, namely one tadpole diagram and two diagrams with the bubble insertion. Last, but not least it is possible use also this chiral NLO contributions to improve the estimate of the theoretical uncertainty of the parameter χ_R.

Thesis is organized as follows. The first chapter is devoted to the short review of the chiral perturbation theory. In the second chapter we set the notation and discuss general dynamical and kinematical properties of the process $\pi \to e^+e^-$. All relevant Feynman diagrams are introduced here, too. The third chapter consist of subchapters in which the whole technique of the calculation of two-loop diagrams is described. The general structure of a renormalization is discussed in the fourth chapter. This concept is then applied on our particular case in the fifth chapter. In the sixth chapter all the analytical results associated with the calculated two-loop graphs are presented. The appendix A is dedicated to the Feynman rules used in this thesis. IBP identities are listed in the appendix B. In the appendix C, (generalized) harmonic polylogarithms are introduced. The last two appendices are devoted to master integrals. In the appendix D, the decomposition of all B functions used in this thesis to master integrals is listed. The results for the individual master integrals are listed in appendix E.

[1] This parameter correspond to the finite contribution of QED NLO counterterms

Chapter 1

Chiral effective theory

In the first part of this chapter we briefly introduce the idea of an effective field theory (EFT). After that we discuss the symmetries of QCD in the chiral limit and we will show why the existence of light particles (in comparison with other particles in the spectrum) with dynamical properties of Goldstone bosons (pseudo Goldstone bosons) should be expected even in the real case, where the masses of three lightest quarks are non-zero, but much lower than the QCD scale parameter Λ_{QCD}. The biggest part of the chapter will be devoted to the transformation properties of Goldstone bosons and to the chiral perturbation theory (χPT).

1.1 Effective field theory

Effective field theory (EFT) approximately describes low-energy dynamics of the underlying fundamental theory. This approximation is valid in regions of the energy which are (much) lower than some energy scale Λ. In EFT we work only with degrees of freedom suitable for the particular energy domain. Perhaps the most famous effective theory is the Fermi theory where the baryons and leptons were used as degrees of freedom instead of quarks, leptons and gauge bosons. This theory is valid in regions of the momentum transfer $q^2 << M_W^2$, where M_W is the mass of the W boson. In general, these theories are non-renormalizable as we need to use the most general Lagrangian to assure that observables calculated in EFT are related to those in the underlying theory. This means if we want to achieve the same accuracy as in the underlying theory we need to include infinite number of terms (increasing in the parameter $\frac{p}{\Lambda}$) of the EFT Lagrangian and the theory becomes non-renormalizable. Any term of the Lagrangian is described by its own coefficient so-called low-energy constant (LEC). However, if we are satisfied with the calculation to particular order of the $\frac{p}{\Lambda}$ we can perform a renormalization by redefining fields and LEC occurring only in the part of the EFT Lagrangian describing dynamics to the desired order $\frac{p}{\Lambda}$.

1.2 Goldstone theorem

Let us consider a Lagrangian which is invariant under some Lie group G. Then between the generators of this group Q_i and the Hamiltonian $\mathcal{H}$ corresponding to this theory exists a relation

$$[\mathcal{H}, Q_i] = 0. \tag{1.1}$$

Assume now existence of the generators Q_a which do not belong to the subgroup of G which annihilate ground state of the system, i.e. the ground state is not invariant under these generators

$$Q_a \left|0\right\rangle \neq 0. \tag{1.2}$$

This conditions immediately imply a degeneracy of a vacuum state. This phenomenon is called spontaneous symmetry breaking. In the manner of the relativistic quantum field theory this means that in this theory there have to exist as many spinless massless bosons (Goldstone bosons) [21] as is the number of the generators Q_a.

1.3 Quantum Chromodynamics

The Lagrangian of QCD is of the form

$$\mathcal{L}_{QCD} = -\frac{1}{4} G^A_{\mu\nu} G^{\mu\nu}_A - \mathcal{M}_{ij} \overline{q}^i_a q^j_a + \mathrm{i} \overline{q}^i_k \not{D}_{kl} q^i_l, \tag{1.3}$$

where $-\frac{1}{4} G^A_{\mu\nu} G^{\mu\nu}_A$ includes the kinetic term of gluons and the pure interaction between gluons, $\mathcal{M}_{ij} \overline{q}^i_a q^i_a$ is the mass term for quarks and $\mathrm{i} \overline{q}^i_k \not{D}_{kl} q^i_l$ contains the kinetic term for quarks as well as the interaction term between quarks and gluons. D_{kl} denote covariant derivative defined as

$$D^\mu_{kl} = \delta_{kl} \partial^\mu + \mathrm{i} g_s (\lambda_A G^\mu_A)_{kl}, \tag{1.4}$$

where g_s is the strong coupling constant, λ_A are Gell-Mann matrices ($A = 1, ..., 8$) and G^μ_A is the gluon field. The big latin index in (1.3) is related to the colour group $SU(3)_C$ in the adjoint representation ($A = 1$, ..., 8) and greek index to the Lorentz group. Small upper latin indices represent flavour indices and lower latin indices correspond to the colour group $SU(3)_C$ in the fundamental representation ($a = 1, 2, 3$). Quark field is in general six dimensional vector in the flavour space. However, in the low energy limit we are working only with three lightest quarks, since the other three can be integrated out from the theory. Schematically

$$q^i = \begin{pmatrix} u \\ d \\ s \end{pmatrix}, \tag{1.5}$$

$$\mathcal{M}_{ij} = \begin{pmatrix} m_u & 0 & 0 \\ 0 & m_d & 0 \\ 0 & 0 & m_s \end{pmatrix}. \tag{1.6}$$

As we can see, the Lagrangian (1.3) is invariant just under the local non-abelian group $SU(3)_C$. Focus now on dynamical aspects of this theory. The basic parameters of bare QCD are the bare coupling constants $g_{s,0}$ and quark masses $m_{q,0}$. However, on the loop level these quantities must be renormalized since we want to get rid of infinities appearing in loop calculations. At the one loop level in the dimensional regularization scheme we get for the renormalized coupling constant

$$g_s = g_{s,0} + \frac{g_{s,0}^3}{16\pi^2}\Big(\frac{11}{2} - \frac{1}{3}N_f\Big)\frac{1}{\epsilon} + O(g_{s,0}^5), \tag{1.7}$$

where N_f is the number of quark flavours. Change ratio of the g_s with respect to renormalization scale μ_{REN} is given by the β function

$$\beta(g_s) = \mu_{REN}\frac{\partial g_s}{\partial \mu_{REN}} = \frac{g_s}{2}\frac{\partial}{\partial \epsilon^{-1}}\Big(Z_G^{-1/2} Z_\psi^{-1} Z_g\Big), \tag{1.8}$$

where Z_G, Z_ψ and Z_g are the normalization functions of the gluon field, the quark field and the vertex respectively . In the lowest order we get for the β function

$$\beta(g_s) = -\Big(11 - \frac{2}{3}N_f\Big)\frac{g_s^3}{16\pi^2} + O(g_s^5). \tag{1.9}$$

As we can see, the β function is negative in the case of $N_f = 6$. We can interpret this as the decrease of the coupling constant g_s with increasing of the renormalization scale μ_{REN}. Let us now derive the expression which relate the coupling constant g_s and the renormalization scale μ_{REN} to one equation. For this purpose we put the solution in the lowest order for the β function (1.9) to (1.8) and we get

$$\frac{g_s(\mu_{REN})}{(4\pi)^2} = \frac{1}{\Big(11 - \frac{2}{3}N_f\Big)\ln(\mu_{REN}^2/\Lambda_{QCD}^2)}, \tag{1.10}$$

where Λ_{QCD} is the integration constant of the (1.8). This quantity is independent of the renormalization scheme μ_{REN} and thus represent a significant parameter of QCD. In fact, the theory is characterized by mass scale Λ_{QCD} instead of the coupling constant g_s (so-called dimensional transmutation). This parameter can be experimentally measured. It recent value is

$$\Lambda_{QCD} = 218 \pm 24\text{MeV}. \tag{1.11}$$

The interpretation of (1.10) is following. When the energies are much higher than Λ_{QCD} ($E >> \Lambda_{QCD}$) the theory is weakly coupled (asymptotic freedom) and the dynamics can be described by the perturbative QCD. In case of $E \sim \Lambda_{QCD}$ the theory is strongly coupled and cannot be described by the perturbative QCD. This is the reason why we are forced to use the chiral perturbation theory in our calculations.

1.3.1 Massless quarks

In the case of massless quarks the QCD Lagrangian is richer in terms of the symmetries. Let us firstly focus on the chirality of quark fields. Left- and right-

handed quark fields are defined as

$$q_R = P_R q = \frac{1}{2}(1+\gamma_5)q, \tag{1.12a}$$

$$q_L = P_L q = \frac{1}{2}(1-\gamma_5)q. \tag{1.12b}$$

Then with the use of $P_R + P_L = 1$ and $P_R P_L = P_L P_R = 0$ we can divide the part of the QCD Lagrangian with quark fields to two independent parts (the colour and flavour indices are suppressed)

$$\mathcal{L}^{chir}_{QCD,q} = \overline{q}\not{D}q = \overline{q_R}\not{D}q_R + \overline{q_L}\not{D}q_L. \tag{1.13}$$

In this case the Lagrangian remains invariant under the chiral rotation $U(N_f)_R \times U(N_f)_L$, where the N_f is the number of quark flavours. Vector and axial Noether currents corresponding to this symmetry are given by

$$V^\mu_a = \frac{1}{2}\overline{q}\gamma_\mu\Sigma_a q, \tag{1.14a}$$

$$V^\mu_0 = \frac{1}{2}\overline{q}\gamma_\mu q, \tag{1.14b}$$

$$A^\mu_a = \frac{1}{2}\overline{q}\gamma_\mu\gamma_5\Sigma_a q, \tag{1.14c}$$

$$A^\mu_0 = \frac{1}{2}\overline{q}\gamma_\mu\gamma_5 q, \tag{1.14d}$$

$$\tag{1.14e}$$

where Σ_a are in the case of $N_f = 2$ Pauli matrices and in the case of $N_f = 3$ Gell-Mann matrices in the flavour space. However, the axial current A^μ_0 is not conserved due to the anomaly. So, the symmetry group of QCD in the chiral limit can be written in the form

$$G = SU(N_f)_R \times SU(N_f)_L \times U(1)_V. \tag{1.15}$$

Focus now on the ground state of the theory. From an experimental fact that there does not exist a baryon octet with negative parity we can deduce that a charge operator Q^A_a related to A^μ_a does not annihilate QCD vacuum. Schematically

$$Q^A_a \left|0\right\rangle \neq 0. \tag{1.16}$$

The ground state is then invariant under H $\subset$ G, where

$$H = SU(N_f)_V \times U(1)_V. \tag{1.17}$$

This spontaneously broken symmetry gives rise in the chiral limit to $N_f^2 - 1$ Goldstone bosons. In the next subchapter we illustrate why we should expect the spectrum of pseudo Goldstone bosons (particles with dynamical properties as Goldstone bosons which have finite masses but are much lighter than other particles of the spectrum) even in the real case of massive quarks.

1.3.2 Massive quarks

The mass pattern of the quarks is of the following form [22]

Type of quark	Mass of quark
u	$2.2^{+0.5}_{-0.4}$ MeV
d	$4.7^{+0.5}_{-0.3}$ MeV
s	95^{+9}_{-3} MeV
c	$1.275^{+0.025}_{-0.035}$ GeV
b	$4.18^{+0.04}_{-0.03}$ GeV
t	$173^{+0.4}_{-0.4}$ GeV

Table 1.1: Table of the mass pattern of quarks.

In the table 1.1 u, d, and s masses are estimates of so-called "current-quark masses" in a mass-independent subtraction scheme such as $\overline{MS}$ at a scale $\mu \approx 2$ GeV. The c and b quark masses are the "running" masses in the $\overline{MS}$ scheme at $\mu = m_q$. The mass of t is estimated from direct measurements.

The divergence of currents is now determined by the mass quark matrix $\mathcal{M}$

$$\partial_\mu V_a^\mu = \frac{1}{2}\mathrm{i}\overline{q}(\mathcal{M}\Sigma_a - \Sigma_a\mathcal{M})q, \tag{1.18a}$$

$$\partial_\mu V_0^\mu = 0, \tag{1.18b}$$

$$\partial_\mu A_a^\mu = \frac{1}{2}\mathrm{i}\overline{q}(\mathcal{M}\Sigma_a + \Sigma_a\mathcal{M})\gamma_5 q, \tag{1.18c}$$

$$\partial_\mu A_0^\mu = 2\mathrm{i}\overline{q}\mathcal{M}\gamma_5 q + \frac{N_f}{8\pi^2}\mathrm{Tr}_C G_{\mu\nu}\tilde{G}^{\mu\nu}. \tag{1.18d}$$

In the case of the most general mass matrix $\mathcal{M}$, the only exactly conserved current is the diagonal vector current. That means only one charge per quark flavour is conserved. However, in special cases of the mass matrix $\mathcal{M}$ also the other currents can be conserved. Baryon number, strangeness, electric charge, etc. are linear combinations of the charge corresponding to conserved currents.

Let us now illustrate, why we should expect existence of pseudo Goldstone bosons in the real case. In general, pseudo Goldstone bosons exists in the theory where the symmetry is spontaneously broken and in addition also explicit broken. This means that the current corresponding to the generators which break the symmetry spontaneously is no more conserved. However, if the parameter which cause the non-conservation of the current mentioned above is small in comparison with other parameters (e. g. the mass of u, d and s quarks in comparison with Λ_{QCD}) we should expect the existence of pseudo Goldstone bosons in the spectrum. Assume that the u and d quarks have same masses $m_u = m_d$. Then the QCD Lagrangian has the exact $SU(2)$ isospin symmetry. In the case that masses of the u and d quarks are much lower than masses of the other quarks (as they really are, see table 1.1) and Λ_{QCD} we should expect three lightest particles composite from the u and d quarks in the spectrum. These correspond to pseudo Goldstone bosons which should have the same masses in the limit $m_u = m_d$. Now, if we assume that the masses m_u and m_d are almost equal, then we can

assume approximative isospin $SU(2)$ symmetry. If we rewrite the mass term to the form

$$m_u\overline{u}u + m_d\overline{d}d = \frac{1}{2}(m_u + m_d)(\overline{u}u + \overline{d}d) + \frac{1}{2}(m_u - m_d)(\overline{u}u - \overline{d}d), \tag{1.19}$$

it can be seen that the QCD Hamiltonian for 2 quarks consist of the isospin symmetry part and the isospin breaking part

$$\mathcal{H} = \mathcal{H}_{sym} + \mathcal{H}_{break}, \tag{1.20a}$$

$$\mathcal{H}_{break} = \int \mathrm{d}^3x \frac{1}{2}(m_u - m_d)(\overline{u}u - \overline{d}d). \tag{1.20b}$$

If the term $\mathcal{H}_{break}$ is small in the comparison with $\mathcal{H}_{sym}$ then we can assume the isospin symmetry $SU(2)$ as approximative. This approximative symmetry leads to the existence of three pseudo Goldstone bosons with very similar but non-identical masses (isotriplet of Goldstone bosons). In fact, we can really observe the isotriplet of spinless bosonic particles, which are much lighter than other particles (triplet of pions π^+, π^- and π^0) with very similar masses. This idea can be extended to the case of three quarks (u, d and s) which are much lighter than the other three quarks (c, b and t). In this case the approximative symmetry is $SU(3)$ symmetry known as eightfold way, which leads to the octet of pseudo Goldstone bosons. These pseudo Goldstone bosons really appear in a nature (note that the pion triplet is much lighter than the other five pseudo Goldstone bosons containing much heavier s quarks). The meson octet mentioned above is depicted in the figure 1.1.

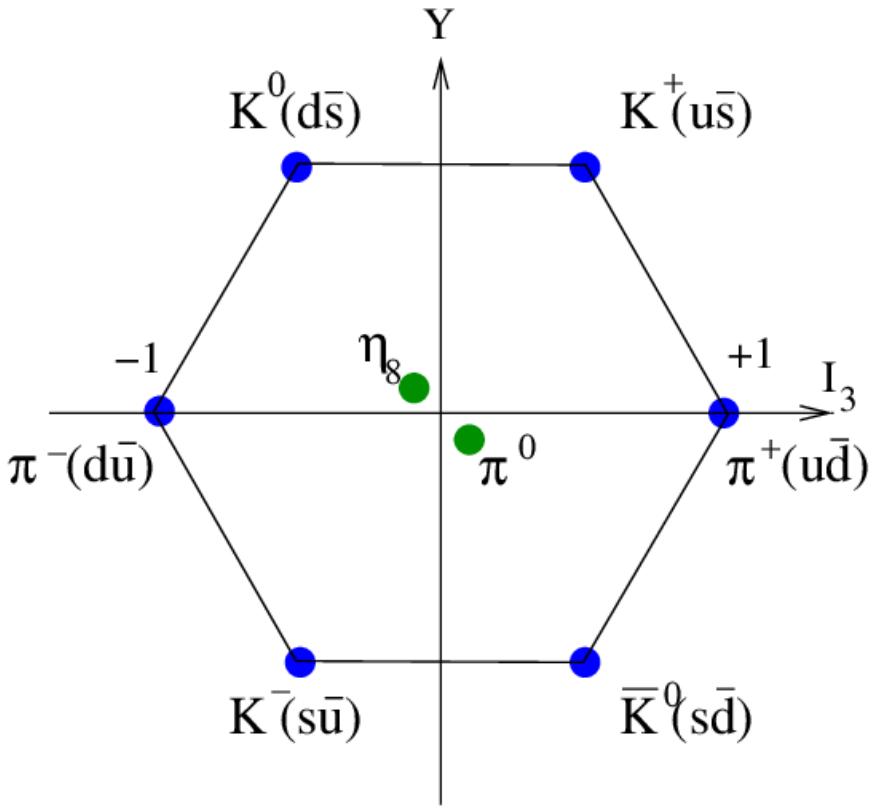

Figure 1.1: Meson octet of pseudo Goldstone bosons.

1.4 Chiral perturbation theory

In this chapter we firstly define Goldstone boson fields as the low-energy degrees of freedom and set their transformation properties. Then we show how to create the effective Lagrangian consisting of these bosons. In the end, we introduce the effective Lagrangians used in calculations of this thesis.

1.4.1 Transformation properties of Goldstone bosons in QCD

Let us consider an underlying theory the Lagrangian of which is invariant under Lie group G and the ground state is invariant under subgroup H $\subset$ G. The effective Lagrangian describing the underlying theory on some scale Λ should have the following properties:

1. Degrees of freedom of the underlying theory should be replaced by degrees of freedom relevant to the energy region $E << \Lambda$
2. The effective Lagrangian should be invariant under the same symmetry group as the fundamental theory
3. The ground state of the system (Goldstone bosons) should stay invariant under the subgroup H

Illustration of this process will be shown on the example of QCD with two and three massless quarks. In the former (latter) case we expect three (eight) degrees of freedom describing the triplet of pions (octet of lightest mesons). In general, Goldstone boson fields are functions on Minkowski space M^4 collected to n component vector $\Phi = (\phi_1, ..., \phi_n)$, defining the real vector space

$$M \equiv \{\Phi : M^4 \to \mathrm{R}^n \,|\, \phi_i : M^4 \to \mathrm{R}\}. \tag{1.21}$$

Our aim is to find a mapping φ which maps $(g,\Phi) \in \mathrm{G} \times M$ to $\varphi(g,\Phi) \in M$. For this mapping we require following properties

$$\varphi(e, \Phi) = \Phi, \tag{1.22a}$$
$$\varphi(g_1, \varphi(g_2, \Phi)) = \varphi(g_1 g_2, \Phi)), \tag{1.22b}$$
$$\varphi(h, \Phi_{\mathrm{vac}}) = \Phi_{\mathrm{vac}}, \tag{1.22c}$$

where $g_1, g_2 \in G$, $h \in H$ and Φ_{vac} corresponds to the classical ground state $\Phi_{\mathrm{vac}} = 0$. To fulfill the desired condition on the theory we choose Goldstone bosons as left cosets $\{gH \,|\, g \in G\}$

$$\Phi = \varphi(gH, 0). \tag{1.23}$$

Let us now show that the origin is mapped onto the same vector in R^n under all elements of a given coset gH

$$\varphi(gh, 0) = \varphi(g, \varphi(h, 0)) = \varphi(g, 0). \tag{1.24}$$

Another important property is that the mapping is injective with respect to all the left cosets $\{gH \,|\, g \in G\}$. Let us consider two elements $g, \overline{g} \in G$ so that $\overline{g} \notin gH$. Let us assume $\varphi(g,0) = \varphi(\overline{g},0)$

$$0 = \varphi(e,0) = \varphi(g^{-1}g,0) = \varphi(g^{-1},\varphi(g,0)) = \varphi(g^{-1},\varphi(\overline{g},0)) = \varphi(g^{-1}\overline{g},0), \tag{1.25}$$

but this implies $\overline{g} \in gH$ in contradiction with the assumption and therefore $\varphi(g,0) \neq \varphi(\overline{g},0)$. It means there exists an isomorphic mapping between the left cosets $\{gH \,|\, g \in G\}$ and Goldstone boson fields.

In QCD ($G = SU(N_f)_L \times SU(N_f)_R$ and $H = SU(N_f)_V$) let $g = (L,R) \in G$. Left cosets can be characterized through $SU(N)$ matrices $U = RL^\dagger$ such that $gH = (1, RL^\dagger)H$. With this parametrization it can be shown that U transforms under $\overline{g} = (\overline{L}, \overline{R})$ as

$$U = RL^\dagger \mapsto U' = \overline{R}U\overline{L}^\dagger. \tag{1.26}$$

In the special case of QCD with massless quarks we can define $U = \exp\left(\frac{\mathrm{i}\phi}{F_0}\right)$ where

$$\phi = \sum_{i=1}^{N_f^2-1} \phi_i \Sigma_i, \tag{1.27}$$

here $N_f^2 - 1$ is the number of corresponding generators Σ_i of the $SU(N_f)$ group. F_0 is the constant with the dimension of the energy. This constant correspond to the decay constant of Goldstone bosons in the chiral limit. In a special case of two and three massless quarks we get for the ϕ

$$\phi_{(2)} = \sum_{i=1}^{3} \phi_i \tau_i = \begin{pmatrix} \pi^0 & \sqrt{2}\pi^+ \\ \sqrt{2}\pi^- & -\pi^0 \end{pmatrix}, \tag{1.28}$$

$$\phi_{(3)} = \sum_{i=1}^{8} \phi_i \lambda_i = \begin{pmatrix} \pi^0 + \frac{1}{\sqrt{3}}\eta & \sqrt{2}\pi^+ & \sqrt{2}K^+ \\ \sqrt{2}\pi^- & -\pi^0 + \frac{1}{\sqrt{3}}\eta & \sqrt{2}K^0 \\ \sqrt{2}K^- & \sqrt{2}\overline{K}^0 & -\frac{\sqrt{2}}{3}\eta \end{pmatrix}. \tag{1.29}$$

where τ_i and λ_i are Pauli matrices and Gell-Mann matrices respectively. The ground state of the system now corresponds to $U = 1$ ($\phi = 0$). Let us check, if this state is really invariant under the subgroup $H = \{(V,V) | V \in SU(2)\}$

$$\varphi\left(g = (V,V), 1\right) = V1V^\dagger = 1. \tag{1.30}$$

Much more information about transformation properties of Goldstone bosons can be found in [23].

1.4.2 Lagrangian of the chiral perturbation theory

The Lagrangian with the minimal number of derivatives constructed using $U = \exp\left(\frac{\mathrm{i}\phi}{F_0}\right)$ and its derivatives as the building blocks has the form

$$\mathcal{L}_{\text{eff}}^{(2)} = \frac{F_0^2}{4}\mathrm{Tr}(\partial_\mu U \partial^\mu U^\dagger), \tag{1.31}$$

where the superscript (2) denote the second order in the power counting scheme. Let us now show, that the Lagrangian has desired properties of the effective Lagrangian. Firstly, if we expand both U it can be rewritten as

$$\mathcal{L}_{\text{eff}}^{(2)} = \frac{F_0^2}{4}[... + \frac{1}{F_0^2}\partial_\mu\phi_a\partial^\mu\phi_b\text{Tr}(\tau_a\tau_b) + ...] = \frac{1}{2}\partial_\mu\phi_a\partial^\mu\phi_a + \mathcal{L}_{\text{eff}}^{int,(2)}, \tag{1.32}$$

where two parts correspond to the kinetic term of the Lagrangian and to the interaction part containing infinite number of terms. Another property of the Lagrangian which should be fulfilled is the invariance under $SU(N)_R \times SU(N)_L \times U(1)$. The invariance under $U(1)$ is trivially satisfied since the baryon number of Goldstone bosons is zero, thus $\phi \mapsto \phi$ and $U \mapsto U$. The invariance under $SU(N)_R \times SU(N)_L$ can be proved if we realize $\partial_\mu L = \partial_\mu R = 0$. Then, because $U \mapsto RUL^\dagger$ [1]

$$\mathcal{L}_{\text{eff}}^{(2)} \mapsto \frac{F_0^2}{4}\text{Tr}(R\partial_\mu UL^\dagger L\partial^\mu U^\dagger R^\dagger) = \frac{F_0^2}{4}\text{Tr}(\partial_\mu U\partial^\mu U^\dagger) = \mathcal{L}_{eff}^{(2)}. \tag{1.33}$$

1.4.3 Mass term in the Lagrangian of the chiral perturbation theory

In the previous section we saw how the breaking of exact symmetry $SU(N)_L \times SU(N)_R \mapsto SU(N)$ leads to the appearance of pseudo Goldstone bosons with finite masses. Additionally, masses of pseudo Goldstone bosons are different if masses of compositing quarks are different. The general form of the mass term in QCD for three lightest quarks can be written as

$$\mathcal{L}_{\mathcal{M}} = -\overline{q}_R\mathcal{M}q_L - \overline{q}_L\mathcal{M}^\dagger q_R, \tag{1.34}$$

$$\mathcal{M} = \begin{pmatrix} m_u & 0 & 0 \\ 0 & m_d & 0 \\ 0 & 0 & m_s \end{pmatrix}. \tag{1.35}$$

If we want to achieve an invariance of $\mathcal{L}_{\mathcal{M}}$, we need to demand from $\mathcal{M}$ to transform as $\mathcal{M} \mapsto R\mathcal{M}L^\dagger$, although $\mathcal{M}$ is a constant matrix. With this transformation property, we can construct the invariant effective Lagrangian in the lowest order which has the form

$$\mathcal{L}_{\text{eff},\mathcal{M}}^{(2)} = \frac{F_0^2B_0}{2}\text{Tr}(\mathcal{M}U^\dagger + U\mathcal{M}^\dagger), \tag{1.36}$$

where B_0 is constant with the dimension of energy. For better interpretation let us determine a mass term from Lagrangian (1.36) which obviously originate from term

$$-\frac{B_0}{2}\text{Tr}(\phi^2\mathcal{M}), \tag{1.37}$$

which explicit form is

$$\begin{aligned}\text{Tr}(\phi^2\mathcal{M}) =& 2(m_u + m_d)\pi^+\pi^- + 2(m_u + m_s)K^+K^- + 2(m_d + m_s)K^0K^0 \\ &+ (m_u + m_d)\pi^0\pi^0 + \frac{m_u + m_d + 4m_s}{3}\eta^2 + \frac{2}{\sqrt{3}}(m_u - m_d)\pi^0\eta.\end{aligned} \tag{1.38}$$

[1] Please note, in all cases U represent the function on the Minkowski space, e.g. $U(x)$.

For simplicity of solution, let us get rid of mixing term of $\pi^0\eta$ with assumptions $m_u = m_d = \overline{m}$. Then we get for masses of pseudo Goldstone bosons

$$M_\pi^2 = 2B_0\overline{m}, \tag{1.39a}$$
$$M_K^2 = B_0(\overline{m} + m_s), \tag{1.39b}$$
$$M_\eta^2 = \frac{2}{3}B_0(\overline{m} + 2m_s). \tag{1.39c}$$

As we can see, constant B_0 serve as "dimension regularizator" in the relation of mass terms [2]. In power counting scheme (see the following subchapter) quark masses should be taken as $O(p^2)$ because of $m_q \sim M_{PGB}^2$. Let us also remark that from the linear combination of the (1.39), we can derive famous Gell-Mann-Okubo relation

$$4M_K^2 = 3M_\eta^2 + M_\pi^2. \tag{1.40}$$

For completeness, let us add that in this thesis we work in the approximation $m_u = m_d$, what leads to $M_{\pi^\pm}^2 = M_{\pi^0}^2$.

1.4.4 Power counting scheme

A main purpose to define EFT is to calculate Feynman amplitudes of the process for some particular energy domain. As was mentioned, the most general EFT Lagrangian has infinite number of terms. However, this Lagrangian can be organized in terms of the increasing number of derivatives and quark masses. Schematically

$$\mathcal{L}_{\text{eff}} = \mathcal{L}_{\text{eff}}^{(2)} + \mathcal{L}_{\text{eff}}^{(4)} + \mathcal{L}_{\text{eff}}^{(6)} + \dots . \tag{1.41}$$

This power counting scheme is essential in determination of the accuracy in our calculation. The biggest contribution to some particular process will be from Feynman diagrams using lowest possible orders. In the chiral perturbation theory the lowest possible Lagrangian is of the order two, since the derivatives which count as $O(p)$ must be always coupled with Lorentz indices and the quark mass is counted as $O(p)^2$ (see 1.39). In addition, if we want to make the chiral perturbation theory locally invariant, we need to introduce external fields with the coupling constant. The one of our interest is the electric charge, since in our Feynman diagrams the interaction between pions and photons is included. The electric charge is counted in the power counting scheme as $O(p)$.

Let us now show how can we perform the power counting analysis on the arbitrary amplitude. For this purpose let us rescale all external momenta $q_i \mapsto tq_i$ and quark masses $m_q \mapsto t^2 m_q$. The calculated amplitude is then rescaled as

$$\mathfrak{M} \mapsto t^D \mathfrak{M}, \tag{1.42}$$

[2] in general constant B_0 is related to the quark condensate $\langle 0|\overline{q}q|0\rangle$ as $3F_0^2B_0 = -\langle 0|\overline{q}q|0\rangle$

where D is so-called chiral dimension which is given by (see [23])

$$\begin{aligned} D &= nN_L - 2N_I + \sum_{k=1}^{\infty} 2kN_{2k}, \\ &= 2 + (n-2)N_L + \sum_{k=1}^{\infty}(2k-2)N_{2k}, \end{aligned} \tag{1.43}$$

where n is the number of space-time dimensions, N_L is the number of loops, N_I is the number of internal Goldstone boson lines and N_{2k} is the number of vertices from $\mathcal{L}_{2k}$. Let us now interpret, why should we expect lowering of the contribution (1.42) with increasing of the chiral dimension D. From the definition of $U = \exp\left(\frac{\mathrm{i}\phi}{F_0}\right)$ we see that every momentum (stemmed from derivative) which appear in the arbitrary vertex is divided by the factor $\sim F_0$ of some particular order. Since the constant F_0 is connected with chiral symmetry breaking scale as $\Lambda_\chi = 4\pi F_0 = O(1\mathrm{GeV})$, and the energy with which we are working in the chiral perturbation theory is $E < 1\,\mathrm{GeV}$. Therefore the implication of the constrain $0 < t < 1$ is reasonably.

As an example we calculate the chiral dimension D of diagrams, with which we are working in this thesis. For the leading order diagram depicted in the figure 2.2 is the corresponding $D_{LO} = 4$ and for NLO contributions depicted in the figure 2.3 we get $D_{tadpole} = D_{bubble} = 6$.

1.5 Wess-Zumino-Witten Lagrangian

In this section we only outline principles by which the Wess-Zumino-Witten Lagrangian can be derived. More details about enriching the χPT by photons and leptons can be found in [23, 19, 20]. The principle of the addition of the external field to the effective field theory is same as in underlying theories. Firstly, we need to show how external fields can be added to QCD, in order to satisfy the $SU(3)_L \times SU(3)_R \times U(1)_V$ (in case of three quarks) symmetry. We will follow procedure of Gasser and Leutwyler [24, 25]. In this procedure we add to the Lagrangian in the chiral limit terms corresponding to couplings of nine vector, eight axial currents, scalar and pseudoscalar quark densities with external fields. Schematically

$$\mathcal{L} = \mathcal{L}_{QCD}^{chir} + \mathcal{L}_{ext}, \tag{1.44}$$

$$\begin{aligned} \mathcal{L}_{ext} = &\sum_{i=1}^{N_f^2-1} v_i^\mu \overline{q}\gamma_\mu \frac{\Sigma_i}{2} q + \frac{1}{3} v_{(s)}^\mu \overline{q}\gamma_\mu q + \sum_{i=1}^{N_f^2-1} a_i^\mu \overline{q}\gamma_\mu\gamma_5 \frac{\Sigma_i}{2} q \\ &- \sum_{i=1}^{N_f^2-1} s_i^\mu \overline{q}\Sigma_i q + \mathrm{i} \sum_{i=1}^{N_f^2-1} p_i^\mu \overline{q}\gamma_5 \Sigma_i q \\ =&\overline{q}\gamma_\mu(v^\mu + \frac{1}{3}v_{(s)}^\mu + \gamma_5 a^\mu)q + \overline{q}(\mathrm{i}\gamma_5 p - s)q, \end{aligned} \tag{1.45}$$

where in the last line we introduced denotation where we omit the group index and the corresponding generator. For recovering the Lagrangian in the limit of three

lightest quarks, we need to set $v^\mu = v^\mu_{(s)} = a^\mu = p = 0$ and $s = \mathrm{diag}(m_u, m_d, m_s)$. For further convenience, we introduce external fields r^μ and l^μ defined as

$$r^\mu = v^\mu + a^\mu, \tag{1.46a}$$
$$l^\mu = v^\mu - a^\mu. \tag{1.46b}$$

Let us now go through to the local invariance of the Lagrangian (1.45). If we denote the quark field transformation as

$$\begin{aligned} q_R &\mapsto \exp(-\mathrm{i}\frac{\theta(x)}{3})V_R(x)q_R, \\ q_L &\mapsto \exp(-\mathrm{i}\frac{\theta(x)}{3})V_L(x)q_L, \end{aligned} \tag{1.47}$$

then the demand of the local invariance is fulfilled, if external fields transform as (in what follows the space-time dependence of functions is omitted)

$$\begin{aligned} r^\mu &\mapsto V_R r^\mu V_R^\dagger + \mathrm{i}V_R\partial_\mu V_R^\dagger, \\ l^\mu &\mapsto V_L l^\mu V_L^\dagger + \mathrm{i}V_L\partial^\mu V_L^\dagger, \\ v^\mu_{(s)} &\mapsto v^\mu_{(s)} - \partial^\mu\theta, \\ s + \mathrm{i}p &\mapsto V_R(s + \mathrm{i}p)V_L^\dagger, \\ s - \mathrm{i}p &\mapsto V_L(s + \mathrm{i}p)V_R^\dagger, \end{aligned} \tag{1.48}$$

where V_R, V_L and $\exp(-\mathrm{i}\frac{\theta(x)}{3})$ in the (1.47, 1.48) are members of $SU(3)_R, SU(3)_L$ and $U(1)$ group respectively. Let us now turn our attention to the particular case, in which we want to add the photon field to our Lagrangian. In the case of three quarks, the photon field A_μ is given by

$$r^\mu = l^\mu = -eA^\mu Q, \tag{1.49}$$

where e is absolute value of the elementary charge and $Q = \mathrm{diag}(2/3, -1/3, -1/3)$ is the quark charge matrix. The external Lagrangian $\mathcal{L}_{ext}$ is given by

$$\begin{aligned} \mathcal{L}_{ext} =& - eA^\mu(\overline{q_L}Q\gamma_\mu q_L + \overline{q_R}Q\gamma_\mu q_R = -eA^\mu\overline{q}Q\gamma_\mu q \\ =& - eA^\mu(\frac{2}{3}\overline{u}Q\gamma_\mu u - \frac{1}{3}\overline{d}Q\gamma_\mu d - \frac{1}{3}\overline{s}Q\gamma_\mu s = -eA^\mu J_\mu. \end{aligned} \tag{1.50}$$

In order to achieve the form of $\mathcal{L}_{ext}$ as (1.50) in case of two quarks, we need to define the photon field A^μ through

$$\begin{aligned} r^\mu =& l^\mu = -eA^\mu\frac{\tau_3}{2}, \\ v^\mu_{(s)} =& -\frac{e}{2}A^\mu. \end{aligned} \tag{1.51}$$

Let us now concentrate on the demand of the locally invariant χPT Lagrangian. The matrix U then transform as

$$U(x) \mapsto V_R(x)U(x)V_L(x)^\dagger. \tag{1.52}$$

Due to this requirement in theories invariant under $SU(N)_R \times SU(N)_L \times U(1)$, the classical derivative changes to the covariant derivative in the following form

$$\partial_\mu U \mapsto D_\mu U \equiv \partial_\mu U - \mathrm{i} r_\mu U + \mathrm{i} U l_\mu, \tag{1.53}$$

where r_μ and l_μ correspond to external fields which transform under $SU(N)_R \times SU(N)_L \times U(1)$ as (1.48). With this transformation a covariant derivative transforms in the desired way

$$D_\mu U \mapsto V_R (D_\mu U) V_L^\dagger. \tag{1.54}$$

In order to describe two-loop diagrams of our interest, we need the part of the interaction χPT Lagrangian describing the interaction of the $2\pi\gamma$, $3\pi\gamma$ and $3\pi 2\gamma$. The vertex $2\pi\gamma$ is obtained after the requirement of the local invariance of the Lagrangian (1.31). Schematically

$$\mathcal{L}^{(2)}_{\pi\pi\gamma} = \frac{F_0^2}{4} \mathrm{Tr}(D_\mu U D^\mu U^\dagger). \tag{1.55}$$

The Lagrangian describing the dynamics of other two vertices has to be minimally of order $O(p^4)$. Corresponding Lagrangian was introduced by Wess-Zumino-Witten [26, 27]. The relevant part of this Lagrangian can be written as

$$\begin{aligned} \mathcal{L}^{(4)}_{WZW} = &- \frac{N_c}{48\pi^2} \epsilon^{\mu\nu\alpha\beta} \mathrm{Tr}\Big[A_u \{ eQ(\partial_\nu U \partial_\alpha U^\dagger \partial_\beta U U^\dagger - \partial_\nu U^\dagger \partial_\alpha U \partial_\beta U^\dagger U) \} \\ &+ 4\mathrm{i} \partial_\mu A_\nu A_\alpha \{ e^2 Q^2 \partial_\beta U U^\dagger + e^2 Q^2 U^\dagger \partial_\beta U - \frac{1}{2} e^2 Q U Q \partial_\beta U^\dagger \\ &+ \frac{1}{2} e^2 Q U^\dagger Q \partial_\beta U \} \Big]. \end{aligned} \tag{1.56}$$

The relevant parts of the Lagrangian (1.56) which describe vertices $3\pi\gamma$ and $3\pi 2\gamma$ can be schematically written as

$$\mathcal{L}_{\pi^0\pi^+\pi^-\gamma} = -\mathrm{i} \frac{e N_c}{12\pi^2 F_0^3} \epsilon^{\mu\nu\alpha\beta} \partial_\nu \pi^+ \partial_\alpha \pi^0 \partial_\beta \pi^-, \tag{1.57}$$

$$\mathcal{L}_{\pi^0\pi^+\pi^-\gamma\gamma} = -\frac{e^2 N_c}{18\pi^2 F_0^3} \epsilon^{\mu\nu\alpha\beta} \partial_\mu A_\nu A_\alpha \Big[\pi^-\pi^0 \partial_\beta \pi^+ - 2\pi^- \partial_\beta \pi^0 \pi^+ + \partial_\beta \pi^- \pi^0 \pi^+ \Big], \tag{1.58}$$

where $\epsilon^{\mu\nu\alpha\beta}$ is fully antisymmetric epsilon tensor and Q is a charge matrix of u and d quarks

$$Q = \frac{1}{3} \begin{pmatrix} 2 & 0 \\ 0 & -1 \end{pmatrix}. \tag{1.59}$$

The introduction of counterterm diagrams is basic technique to get rid of infinities, emerging from multi-loop calculations. For renormalization of two-loop diagrams of our interest, the introduction of one-loop counterterm diagrams and tree counterterm diagram is necessary. For this purpose, the Lagrangian describing $\pi 2\gamma$, $\pi e^+ e^-$ and $3\pi e^+ e^-$ has to be introduced. The very first vertex is described by Wess-Zumino-Witten Lagrangian, the relevant part of which was

introduced in (1.56). Element from this Lagrangian describing process $\pi 2\gamma$ can be written in the compact form as

$$\mathcal{L}^{(4)}_{CT,\pi\gamma\gamma} = \frac{\pi^0}{8} K_{\pi\gamma\gamma}\Big(\frac{\alpha}{\pi}\Big)\epsilon_{\mu\nu\alpha\beta}F^{\mu\nu}F^{\alpha\beta}, \tag{1.60}$$

where in the constants $K_{\pi\gamma\gamma}$ we put all the terms corresponding to differing counterterm vertices and α is the fine structure constant. The part of the χPT Lagrangian describing interactions of the pion fields and the fermionic fields [5] has the form

$$\begin{aligned}\mathcal{L}^{(6)}_{Pe^+e^-} =& \frac{3\mathrm{i}}{32}\Big(\frac{\alpha}{\pi}\Big)^2\overline{\psi}\gamma^\mu\gamma_5\psi\Big[\chi_1\mathrm{Tr}(Q^2D_\mu UU^\dagger - Q^2D_\mu U^\dagger U)\\ &+ \chi_2\mathrm{Tr}(U^\dagger QD_\mu UQ - UQD_\mu U^\dagger Q)\Big].\end{aligned} \tag{1.61}$$

Let us discuss the constants χ_1 and χ_2 in more detail. As was mentioned in the introduction, counterterms in the effective theory has the finite contribution to the amplitude. In our particular case this contribution in LO was calculated in [7] with result $\chi^R_{LMD}(770MeV) = 2.2 \pm 0.9$. This parameter correspond to the linear combination of constants χ_1 and χ_2 as we can write the Lagrangian describing process $\pi^0 \to e^+e^-$ in the form

$$\begin{aligned}\mathcal{L}^{(6),fin}_{\pi^0e^+e^-} &= -\Big(\frac{\alpha}{\pi}\Big)^2\frac{\chi_1(\mu)+\chi_2(\mu)}{16F_0}\overline{\psi}\gamma_\mu\gamma_5\psi\partial^\mu\pi^0\\ &= \frac{\chi(\mu)}{4F_0}\Big(\frac{\alpha}{\pi}\Big)^2\overline{\psi}\gamma_\mu\gamma_5\psi\partial^\mu\pi^0,\end{aligned} \tag{1.62}$$

where we denoted $\chi(\mu) = -\frac{\chi_1(\mu)+\chi_2(\mu)}{4}$. Since in our particular case the function of counterterm graph $\pi^0 \to e^+e^-$ is also to subtract superficial divergences, we write the Lagrangian describing vertex $\pi^0e^+e^-$ as

$$\mathcal{L}^{(6)}_{CT,\pi^0e^+e^-} = \Big(\frac{\alpha}{\pi}\Big)^2\frac{K_{\pi e^+e^-}}{4F_0}\overline{\psi}\gamma_\mu\gamma_5\psi\partial^\mu\pi^0, \tag{1.63}$$

where the constant $K_{\pi e^+e^-}$ contain the finite contribution from the counterterm as well as the part subtracting superficial divergences. The last remaining vertex $3\pi e^+e^-$ is obviously also described by the Lagrangian (1.61). Schematically

$$\begin{aligned}\mathcal{L}^{(6)}_{CT,\pi^0\pi^-\pi^+e^+e^-} =& \frac{K_{\pi^0\pi^-\pi^+e^+e^-}}{24F_0^3}\Big(\frac{\alpha}{\pi}\Big)^2\overline{\psi}\gamma^\mu\gamma_5\psi(\pi^-\pi^0\partial_\mu\pi^+\\ &- 2\pi^-\partial_\mu\pi^0\pi^+ + \partial_\mu\pi^-\pi^0\pi^+).\end{aligned} \tag{1.64}$$

The whole χPT Lagrangian used in this thesis can be then schematically written as

$$\begin{aligned}\mathcal{L}_{\chi PT} =& \frac{F_0^2}{4}\mathrm{Tr}(D_\mu UD^\mu U^\dagger) + \frac{F_0^2B_0}{2}\mathrm{Tr}(\mathcal{M}U^\dagger + U\mathcal{M}^\dagger) + \mathcal{L}^{(4)}_{WZW}\\ &+ \mathcal{L}^{(4)}_{CT,\pi\gamma\gamma} + \mathcal{L}^{(6)}_{CT,\pi e^+e^-} + \mathcal{L}^{(6)}_{CT,\pi\pi\pi e^+e^-}\ .\end{aligned} \tag{1.65}$$

Chapter 2

General structure of the amplitude

In this section we discuss general properties of the amplitude. Firstly, we set the notation and kinematics. As a next step we summarize all the Lagrangians necessary for the description of our particular process. Then we introduce pion transition form factor $\mathrm{F}_{\pi^0\to\gamma\gamma}$ and amplitude $\mathrm{P}_{\pi^0\to e^+e^-}$ which are necessary for the description of the process $\pi^0 \to e^+e^-$. After that, we calculate them in the LO of χPT. Last, but not least we introduce a two-loop diagrams which are calculated in this thesis.

2.1 Notation and kinematics

The matrix element describing process $\pi^0 \to e^+e^-$ is defined as

$$\langle e^+(q_+,s_+)e^-(q_-,s_-);\mathrm{out}|\pi^0(Q);\mathrm{in}\rangle = \mathrm{i}(2\pi)^4\delta^{(4)}(Q-q_+-q_-)\mathcal{M}_{\pi^0\to e^+e^-}\ , \quad (2.1)$$

where the amplitude $\mathcal{M}_{\pi^0\to e^+e^-}$ has the general form

$$\mathcal{M}_{\pi^0\to e^+e^-} = \overline{u}(q_-,s_-)\mathcal{V}(q_+,q_-)v(q_+,s_+), \quad (2.2)$$

where $\mathcal{V}$ is effectively one particle irreducible $\pi^0 \to e^+e^-$ vertex. Because pion is a pseudoscalar particle the form of $\mathcal{V}(q_+,q_-)$ can be only composed as

$$\begin{aligned}\mathrm{i}\mathcal{V}(q_+,q_-) =& P(q_+^2,q_-^2,Q^2)\gamma_5 + A_+(q_+^2,q_-^2,Q^2)\gamma_5(\not{q}_+ + m)\\ &+ (\not{q}_- - m)A_-(q_+^2,q_-^2,Q^2)\gamma_5\\ &+ (\not{q}_- - m)\gamma_5(\not{q}_+ + m)B(q_+^2,q_-^2,Q^2),\end{aligned} \quad (2.3)$$

and after the inclusion of the on-shell condition we are left only with one form factor $P(q_+^2,q_-^2,Q^2)$ and we get

$$\mathrm{i}\overline{u}\mathcal{V}(q_+,q_-)v = P(q_+^2,q_-^2,Q^2)\overline{u}\gamma_5 v. \quad (2.4)$$

The decay rate is then given by

$$\Gamma_{\pi^0\to e^+e^-} = \frac{M_\pi}{8\pi}\beta(M_\pi^2)|P(q_+^2, q_-^2, Q^2)|^2, \tag{2.5}$$

$$\beta(M_\pi^2) = \sqrt{1-\frac{4m^2}{M_\pi^2}}. \tag{2.6}$$

Note that, the form factor $P(q_+^2, q_-^2, Q^2)$ can be expressed by $\mathcal{V}(q_+, q_-)$ as

$$P(m^2, m^2, Q^2) = -\lim_{q_\pm^2\to m^2}\frac{1}{2Q^2}\mathrm{Tr}\Big[(\not{q}_- + m)\mathcal{V}(q_+, q_-)(\not{q}_+ - m)\gamma_5\Big]. \tag{2.7}$$

For further calculations let us also introduce the dimensionless kinematic variable which will be necessary for the further calculation

$$y = \frac{M_\pi^2}{4m^2}. \tag{2.8}$$

2.2 Dynamical aspects of the process $\pi^0 \to e^+e^-$

The $e^+e^-\gamma$ interaction is described by the Lagrangian of the spinor QED

$$\mathcal{L}_{QED} = -\frac{1}{4}F_{\mu\nu}F^{\mu\nu} - m\overline{\psi}\psi + \mathrm{i}\overline{\psi}\not{D}\psi - \frac{1}{2}(\partial_\mu A^\mu)^2, \tag{2.9}$$

where $\frac{1}{4}F_{\mu\nu}F^{\mu\nu}$ and $m\overline{\psi}\psi$ are kinetic terms of photon field and mass term of the fermionic field respectively, $\frac{1}{2}(\partial_\mu A^\mu)^2$ is gauge fixing term, $\mathrm{i}\overline{\psi}\not{D}\psi$ include an interaction term and the kinetic term of the fermionic field and $\not{D}$ denote covariant derivative defined as

$$D_\mu = \partial_\mu + \mathrm{i}eA_\mu. \tag{2.10}$$

The low energy dynamics of the strong interaction cannot be described by the perturbative QCD (quantum chromodynamics). That is the reason why we are forced to use effective theories, where degrees of freedom correspond to composite objects. The effective theory which is used in this diploma thesis is the chiral perturbation theory (χPT) with dynamical leptons and photons [20]. One of the relevant part describing dynamics of pseudo Goldstone bosons (massive bosons with dynamical properties of Goldstone bosons) and photons was introduced by Wess-Zumino-Witten [26, 27] . The whole part of the χPT Lagrangian used in this thesis was discussed in the chapter 1 and is schematically summarized in (1.65).

Whole corresponding Lagrangian describing process $\pi^0 \to e^+e^-$ is then in the form

$$\mathcal{L} = \mathcal{L}_{QED} + \mathcal{L}_{\chi PT}. \tag{2.11}$$

2.3 Pion transition form factor $\mathrm{F}_{\pi^0\to\gamma\gamma}$ and amplitude $\mathrm{P}_{\pi^0\to e^+e^-}$

In this section we introduce the pion transition form factors $\mathrm{F}_{\pi^0\to\gamma\gamma}$ and amplitude $\mathrm{P}_{\pi^0\to e^+e^-}$ with their properties. After that, they will be calculated in the LO of the chiral expansion, thanks to what, we will be able to calculate decay rate of the process $\pi^0 \to e^+e^-$ in the LO.

2.3.1 General structure and properties of the $\mathrm{P}_{\pi^0\to\gamma\gamma}$

Let us introduce the pion transition form factor $\mathrm{F}_{\pi^0\to\gamma\gamma}$ through the strong matrix element as

$$-\mathrm{e}^2\int d^4x e^{\mathrm{i}k\cdot x}\left\langle 0\right|T(j^\mu(x)j^\nu(0))\left|\pi^0(Q)\right\rangle = \mathrm{i}\mathrm{e}^2\epsilon^{\mu\nu\alpha\beta}k_\alpha Q_\beta \mathrm{F}_{\pi^0\to\gamma\gamma}(k^2,(Q-k)^2), \tag{2.12}$$

where $j^\mu(x)$ is the hadronic part of electromagnetic current

$$j^\mu(x) = \frac{2}{3}\overline{u}\gamma^\mu u - \frac{1}{3}\overline{d}\gamma^\mu d. \tag{2.13}$$

At the leading order in e, the one particle irreducible vertex of the amplitude for the decay $\pi^0 \to e^+e^-$ has the form (see figure 2.1)

$$\begin{aligned}\mathrm{i}\mathcal{V}^{LO,QED}_{\pi^0e^+e^-}(q_+,q_-) =& e^4\epsilon^{\mu\nu\alpha\beta}\int\frac{\mathrm{d}^4l}{(2\pi)^4}F_{\pi^0\gamma\gamma}((l+q_+)^2,(l-q_-)^2)\\ &\times\frac{(l+q_+)_\alpha(l-q_-)_\beta}{[(l+q_+)^2+\mathrm{i}0][(l-q_-)^2+\mathrm{i}0]}\gamma_\mu\frac{1}{[\not{l}-m+\mathrm{i}0]}\gamma_\nu.\end{aligned} \tag{2.14}$$

In the figure 2.1 the shaded blob correspond to the strong matrix element (2.12). If we put (2.14) to the formula (2.7) we can obtain a relation at the leading order in e for P of the relevant amplitude in the form [28]

$$P^{LO}_{\pi^0e^+e^-}(m^2,Q^2) = -\mathrm{i}\frac{e^4m}{Q^2}\int\frac{\mathrm{d}^4t}{(2\pi)^4}\frac{F_{\pi^0\gamma\gamma}(D^{(-)},D^{(+)})}{D^{(-)}D^{(+)}D^{(0)}}\lambda(Q^2,D^{(-)},D^{(+)}), \tag{2.15}$$

where

$$D^{(\pm)} = (t\pm q_\pm)^2 + \mathrm{i}0, \tag{2.16}$$

$$D^{(0)} = t^2 - m^2 + \mathrm{i}0, \tag{2.17}$$

and

$$\lambda(a,b,c) = a^2+b^2+c^2-2ab-2ac-2bc \tag{2.18}$$

is the triangle function.

In what follows, we calculate the pion transition form factor $\mathrm{F}_{\pi^0\to\gamma\gamma}$ in the chiral limit to the NLO. It means that the pion transition form factor $\mathrm{F}_{\pi^0\to\gamma\gamma}$ can be written as

$$\mathrm{F}_{\pi^0\to\gamma\gamma} = \mathrm{F}^{LO}_{\pi^0\to\gamma\gamma} + \mathrm{F}^{NLO}_{\pi^0\to\gamma\gamma} + ..., \tag{2.19}$$

where in the $\mathrm{F}^{NLO}_{\pi^0\to\gamma\gamma}$ are included all two-loop terms, each corresponding to the different Feynman diagram.

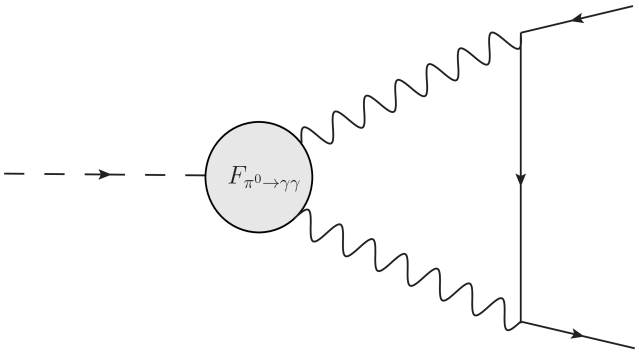

Figure 2.1: Feynman diagram of the process $\pi^0 \to e^- e^+$ with highlighted strong matrix element.

2.3.2 LO amplitude in the chiral expansion

The Feynman diagram at the LO in the chiral expansion is depicted in the figure 2.2. For description of this diagram we need Lagrangian of the spinor QED (2.9) and vertices (1.60, 1.63) introduced in the chapter 1. Schematically

$$\mathcal{L}^{(4)}_{\pi\gamma\gamma} = \frac{\pi^0}{8}\left(\frac{\alpha}{\pi}\right)\epsilon_{\mu\nu\alpha\beta}F^{\mu\nu}F^{\alpha\beta}, \tag{2.20}$$

$$\mathcal{L}^{(4)}_{CT,\pi^0 e^+e^-} = -\frac{\alpha^2}{4\pi^2}\frac{\chi}{F_0^2}\partial_\mu\pi^0\overline{\psi}\gamma^\mu\gamma_5\psi, \tag{2.21}$$

where constants defined in the chapter 1 now correspond to $K_{\pi\gamma\gamma} = 1$ (because now this vertex describes the bare interaction) and $K_{\pi e^+e^-} = -\chi$. If we define χ in $\overline{MS}$

$$\chi = \chi^R(\mu) + \frac{3}{2}\left[\frac{1}{\epsilon} + \ln(4\pi) - \gamma_E\right], \tag{2.22}$$

than the $\chi^R(\mu)$ is the finite contribution of the counterterm diagram at a scale μ. We take its numerical value from [7] where it was calculated in the limit of the large N_C with result

$$\chi^R(770\text{MeV}) = 2.2 \pm 0.9. \tag{2.23}$$

Let us derive $\mathrm{F}^{LO}_{\pi^0\to\gamma\gamma}$. For this purpose we will use the formula (2.12) and vertex $\pi^0 \to \gamma\gamma$ listed in the appendix A and we get

$$\mathrm{F}^{LO}_{\pi^0\to\gamma\gamma} = \frac{1}{4\pi^2}\frac{1}{F_0}, \tag{2.24}$$

Calculation will rapidly simplify with the use of (2.15). We get

$$P^{LO}_{\pi^0\to e^+e^-} = -\mathrm{i}\frac{e^4 m}{Q^2}\frac{1}{4\pi^2}\frac{1}{F_0}\int\frac{\mathrm{d}^4 l}{(2\pi)^4}\frac{1}{D^{(-)}D^{(+)}D^{(0)}}\lambda(Q^2, D^{(-)}, D^{(+)}). \tag{2.25}$$

Computation was done e.g. in [14] . Result reads

$$|P^{LO}_{\pi^0\to e^+e^-}|^2 = (8,90 \pm 0,39)\cdot 10^{-14}, \tag{2.26}$$

where the whole uncertainty is caused by the uncertainty of the χ^R. With the use of (2.5) we get for the decay rate

$$\Gamma^{LO}_{\pi^0\to e^+e^-} = (7,73 \pm 0.34)\cdot 10^{-6}\text{MeV}. \tag{2.27}$$

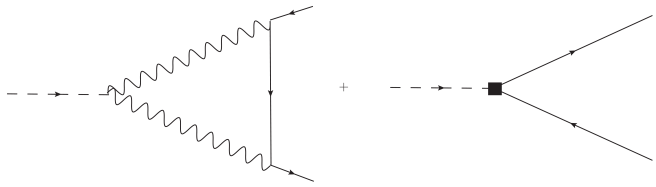

Figure 2.2: LO χPT diagram and corresponding counterterm diagram describing process $\pi^0 \to e^+e^-$.

2.4 Structure of the two-loop diagrams

One of the main aim of this thesis is to calculate two-loop chiral corrections to $P(q_+^2, q_-^2, Q^2)$ of the order $O(\alpha^2 p^4)$ and pick up on the QED two-loop corrections calculated in [14]. Corresponding Feynman diagrams with their counterterm diagrams we are dealing with are shown in the figure 2.3. Whole following chapter is devoted to the calculations of these diagrams.

Feynman rules for vertices describing diagrams in the figure 2.3 are listed in the appendix A.

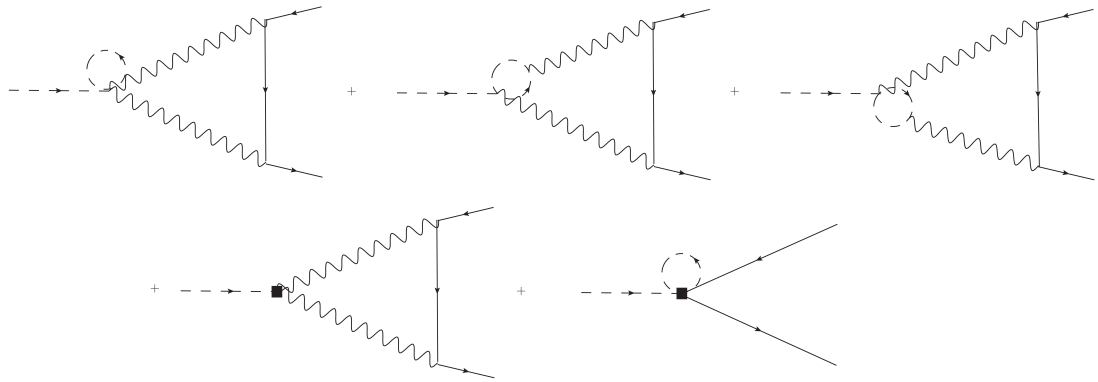

Figure 2.3: List of two-loop chiral Feynman diagrams and their counterterms diagrams of the order $O(\alpha^2 p^4)$.

Remark that to the family of the chiral two-loop corrections of the order $O(\alpha^2 p^4)$ belongs also the diagram which renormalize the on-shell pion. However, this diagram differs from one-loop diagram depicted in the figure 2.2 just by the constant factor (usually denoted as Z factor) and was calculated e. g. in [15].

Chapter 3

Calculation of two-loop graphs

3.1 Generalization of two-loop graphs to auxiliary graph

The goal of this chapter is to express all of the calculated two-loop Feynman diagrams in a compact form. This is done by rewriting all of the Feynman amplitudes as linear combinations of loop integrals containing just scalar propagators. All the scalar propagators necessary for this process are depicted in the so-called Auxiliary graph.

If we consider a general scalar Feynman graph with k loops, E external legs and I internal lines then the amplitude of this graph can be decomposed as a linear combination of the following terms

$$\int \mathrm{d}^n l_1 .... \mathrm{d}^n l_k \frac{\prod_{i=1}^{N_{sp}} F_i^{a_i}}{\prod_{j=1}^{I} P_j}, \tag{3.1}$$

where F_i are independent scalar products of both external and internal momenta, N_{sp} is the number of these scalar products, a_i is the non-negative integer number and P_j is the propagator of the given Feynman graph. Quantity N_{sp} can be expressed in terms E and k as follows

$$N_{sp} = k(E-1) + \frac{k(k+1)}{2}. \tag{3.2}$$

As a next step we would like to write all independent scalar products in terms of denominators of propagators. This decomposition of scalar products allow us to rewrite linear combinations of the terms (3.1) in terms of the linear combination of the integrals

$$B(n_1, ..., n_I) = \int \mathrm{d}^n l_1 .... \mathrm{d}^d l_k \frac{1}{\prod_{j=1}^{I} (P_j)^{n_j}}, \tag{3.3}$$

where n_j could be now any positive or negative number.

In our case, we are working with the graphs where $E = 3$ and $k = 2$. So, from (3.2) we get $N_{sp} = 7$. As we can see from the chapter 2, our Feynman diagrams consist of six independent propagators. That means, if we want to express all our amplitudes in the form (3.3), we are forced to add one independent propagator. This procedure can be visualized by so-called Auxiliary graph. The Auxiliary graph of our problem is depicted in the figure 3.1. This graph has nothing to do with dynamics of our process (in means of Feynman diagrams). Its function is just to represent propagators. The general formula (3.3) can now be rewritten to the form

$$B(n_1, ..., n_7) = \int \mathrm{d}^d l \mathrm{d}^d k \frac{1}{\prod_{j=1}^{7} (P_j)^{n_j}}. \tag{3.4}$$

In the following text we will denote functions in the equation (3.4) as B functions.

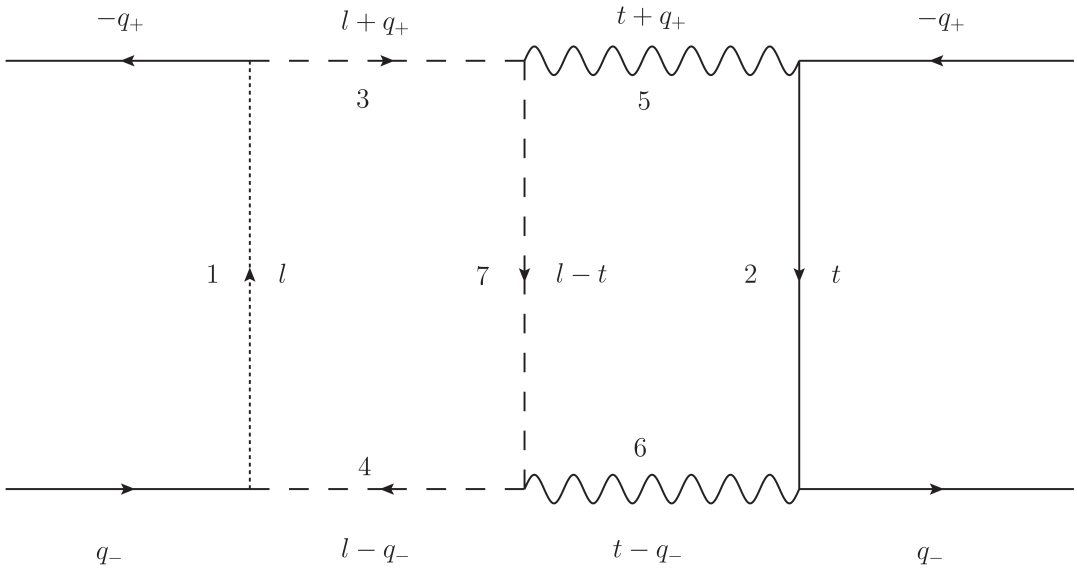

Figure 3.1: Auxiliary graph representing six propagators which are present in our two-loop calculations and the propagator which was added.

Finally, we will write out all the propagators which appear in B functions

$$\begin{aligned} P_1 &= l^2 - M_\pi^2, \\ P_2 &= t^2 - m^2, \\ P_3 &= (l + q_+)^2 - M_\pi^2, \\ P_4 &= (l - q_-)^2 - M_\pi^2, \\ P_5 &= (t + q_+)^2, \\ P_6 &= (t - q_-)^2, \\ P_7 &= (l - t)^2 - M_\pi^2, \end{aligned} \tag{3.5}$$

and all the independent scalar products expressed in terms of the propagators

(3.5)

$$
\begin{aligned}
l^2 &= P_1 + M_\pi^2, \\
t^2 &= P_2 - m^2, \\
l.q_+ &= \frac{P_3 - P_1 - m^2}{2}, \\
l.q_- &= \frac{P_1 - P_4 + m^2}{2}, \\
t.q_+ &= \frac{P_5 - P_2 - 2m^2}{2}, \\
t.q_- &= \frac{P_2 - P_6 + 2m^2}{2}, \\
l.t &= \frac{P_1 + P_2 - P_7 + m^2}{2}.
\end{aligned}
\tag{3.6}
$$

Now, we have all necessary ingredients for derivation of the NLO amplitudes introduced in (2.3). For better understanding, let us derive the amplitude corresponding to the second diagram in the figure 2.3. Firstly, for the determination of the P amplitude (2.15) we need to calculate 1-loop diagram

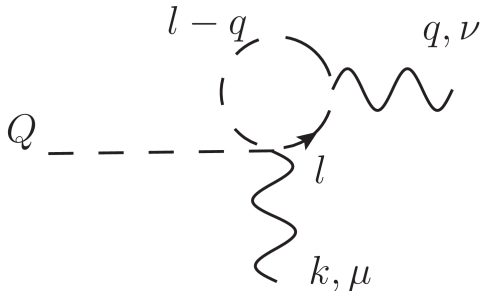

We can express this diagram, with use of the Feynman rules listed in the appendix A, in the dimensional regularization scheme as [1]

$$
\mathrm{i}\Gamma_{\mu\nu} = -\frac{\mathrm{i}e^2 N_C \epsilon_{\alpha\beta\gamma\mu}\mu^{4-n}}{12\pi^2 F_0^3} \int \frac{\mathrm{d}^n l}{(2\pi)^n} \frac{(l-q)^\alpha l^\beta Q^\gamma (2l-q)_\nu}{(l^2 - Q^2)((l+q)^2 - Q^2)}, \tag{3.7}
$$

which can be simplified, if we realize that two identical momenta coupled with the antisymmetric tensor $\epsilon_{\alpha\beta\gamma\mu}$ give zero contribution, just like the integral where in the numerator is the odd power of the loop momenta. Simplified integral reads then

$$
\mathrm{i}\Gamma_{\mu\nu} = \frac{\mathrm{i}e^2 N_C \epsilon_{\alpha\beta\gamma\mu}\mu^{4-n}}{6\pi^2 F_0^3} \int \frac{\mathrm{d}^n l}{(2\pi)^n} \frac{q^\alpha l^\beta Q^\gamma l_\nu}{(l^2 - Q^2)((l+q)^2 - Q^2}. \tag{3.8}
$$

Further, we can rewrite this integral to the form in which the loop momentum appears only in the denominator of propagators by the Passarino-Veltman reduction

$$
\mathrm{i}\Gamma_{\mu\nu} = \mathrm{i}q^\alpha Q^\gamma \frac{e^2 N_C \epsilon_{\alpha\gamma\mu\nu}\mu^{4-n}}{12\pi^2 F_0^3} \Big(\frac{A}{(1-n)} + \frac{B(4Q^2 - q^2)}{2(1-n)} \Big), \tag{3.9}
$$

[1] note that the $Q^2 = M_\pi^2$

where

$$A = \int \frac{\mathrm{d}^n l}{(2\pi)^n} \frac{1}{(l^2 - Q^2)} = \frac{\mathrm{i}M^2}{(4\pi)^2}\Big(\frac{1}{\epsilon} - \gamma_E - \ln\Big(\frac{M^2}{4\pi}\Big) + O(\epsilon)\Big), \tag{3.10}$$

$$\begin{aligned} B &= \int \frac{\mathrm{d}^n l}{(2\pi)^n} \frac{1}{(l^2 - Q^2)((q-l)^2 - Q^2)} \\ &= \frac{\mathrm{i}}{(4\pi)^2}\Big(\frac{1}{\epsilon} - \gamma_E - \int_0^1 \mathrm{d}x \, \ln\Big(\frac{M^2 - q^2 x(1-x)}{4\pi}\Big) + O(\epsilon)\Big). \end{aligned} \tag{3.11}$$

If we compare (3.9) with (2.12), then we get corresponding contribution to the pion transition form factor

$$F^{up-bubble}_{\pi^0\gamma\gamma} = -\frac{N_C}{12\pi^2 F_0^3}\Big(\frac{A}{(1-n)} + \frac{(4Q^2 - q^2)B}{2(1-n)}\Big). \tag{3.12}$$

Inserting this to the general formula (2.15), we can write the whole amplitude P in terms of B functions as

$$\begin{aligned} P(m^2, Q^2)^{up-bubble}_{\pi^0\gamma\gamma} =& \mathrm{i}\frac{e^4 m N_C}{12\pi^2 F_0^3 Q^2}\frac{\mu^{2(4-n)}}{(n-1)}\Big(\frac{1}{2}\{4Q^2\Big[Q^4 B(0,1,1,0,1,1,1) \\ &+ B(0,1,1,0,1,-1,1) + B(0,1,1,0,-1,1,1) \\ &- 2B(0,1,1,0,0,0,1) - 2Q^2 B(0,1,1,0,1,0,1) \\ &- 2Q^2 B(0,1,1,0,0,1,1)\Big] - \Big[Q^4 B(0,1,1,0,0,1,1) \\ &+ B(0,1,1,0,-2,1,1) + B(0,1,1,0,0,-1,1) \\ &- 2B(0,1,1,0,-1,0,1) - 2Q^2 B(0,1,1,0,-1,1,1) \\ &- 2Q^2 B(0,1,1,0,0,0,1)\Big]\} + Q^4 B(1,1,0,0,1,1,0) \\ &+ B(1,1,0,0,-1,1,0) + B(1,1,0,0,1,-1,0) \\ &- 2Q^2 B(1,1,0,0,0,1,0) - 2Q^2 B(1,1,0,0,1,0,0) \\ &- 2B(1,1,0,0,0,0,0)\Big). \end{aligned} \tag{3.13}$$

P amplitude corresponding to the third diagram in the figure 2.3 is symmetrical to the $P(m^2, Q^2)^{up-bubble}_{\pi^0\gamma\gamma}$, what leads to the result

$$P(m^2, Q^2)^{down-bubble}_{\pi^0\gamma\gamma} = P(m^2, Q^2)^{up-bubble}_{\pi^0\gamma\gamma}. \tag{3.14}$$

In order to calculate amplitude P corresponding to the tadpole diagram (first diagram in the figure 2.3), it is necessary to calculate 1-loop diagram

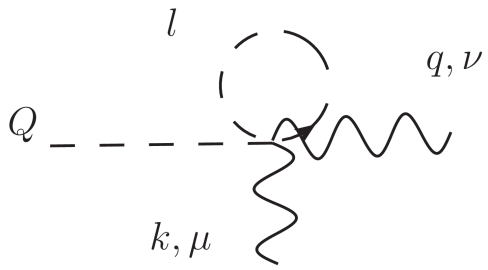

With the use of the Feynman rule for $\pi^0\pi^+\pi^-\gamma\gamma$ listed in the appendix A, we can express this loop in the sense of dimensional regularization as

$$\begin{aligned} \mathrm{i}\Sigma_{\mu\nu} &= \frac{\mathrm{i}4e^2N_C\epsilon_{\alpha\beta\mu\nu}\mu^{4-n}}{36\pi^2F_0^3}\int\frac{\mathrm{d}^n l}{(2\pi)^n}\frac{(q+k)^\alpha(q-k)^\beta}{(l^2-Q^2)} \\ &= -\frac{\mathrm{i}2e^2N_C\epsilon_{\alpha\beta\mu\nu}\mu^{4-n}}{9\pi^2F_0^3}q^\alpha k^\beta A, \end{aligned} \tag{3.15}$$

and for the corresponding contribution to the pion transition form factor (2.12) we get

$$F^{tadpole}_{\pi^0\gamma\gamma} = -\frac{2N_C}{9\pi^2F_0^3}A. \tag{3.16}$$

Finally, we obtain $P(m^2,Q^2)^{tadpole}_{\pi^0\gamma\gamma}$ in terms of B functions

$$\begin{aligned} P(m^2,Q^2)^{tadpole}_{\pi^0\gamma\gamma} =& \mathrm{i}\frac{2e^4m}{Q^2}\frac{N_C\mu^{2(4-n)}}{9\pi^2F_0^3}\Big[Q^4B(1,1,0,0,1,1,0) \\ &+ B(1,1,0,0,-1,1,0) + B(1,1,0,0,1,-1,0) \\ &- 2Q^2B(1,1,0,0,0,1,0) - 2Q^2B(1,1,0,0,1,0,0) \\ &- 2B(1,1,0,0,0,0,0)\Big]. \end{aligned} \tag{3.17}$$

3.2 Symmetry relations, restrictions and IBP identities

This section is divided to two subsections in which we will describe the methods which simplify computation of the particular amplitudes.

3.2.1 Symmetry relations and restrictions

As follows from the name, symmetry relations allow us to relate different B functions coupled with symmetry in one equation. Generally, we can write them in the form

$$B(n_1,....,n_I) = (-1)^{a_1n_1+.....+a_In_I}B(\sigma(n_1),....,\sigma(n_I)), \tag{3.18}$$

where σ represent a permutation and a_1 take the value of 1 or 0. If we want to find a symmetry relations in the particular case, the best way how to do it is to look on the auxiliary graph. In our case we see that we can make permutations ($3 \leftrightarrow 4$, $5 \leftrightarrow 6$) without change of the result. In mathematical form

$$B(n_1, n_2, n_3, n_4, n_5, n_6, n_7) = B(n_1, n_2, n_4, n_3, n_6, n_5, n_7). \tag{3.19}$$

In order to simplify and speed up our calculations, we will use some restrictions which tell us when the particular B function is equal to zero. For example, we can use the fact that massless tadpole gives zero contribution to the Feynman amplitude. In our case this can be written as

$$B(a_1, 0, a_2, a_3, a_4, 0, 0) = 0, \tag{3.20}$$

where a_i is any integer.

Surely, there exist more symmetry relations and the restrictions, but for our calculations the symmetry relations and the restrictions written above are sufficient.

3.2.2 IBP identities

Let's define a scalar Feynman integral

$$I(n_1, ..., n_N) = \int \mathrm{d}^n k_1 ..... \mathrm{d}^n k_L f(k_1, ..., k_L, p_1, ..., p_E), \tag{3.21}$$

$$f(k_1, ..., k_L, p_1, ..., p_E) = \frac{1}{P_1^{n_1} .... P_N^{n_N}}, \tag{3.22}$$

where P_i is the denominator of the scalar propagator. Now, if we multiply the integrand f with the momentum $q_{\mu,j}$ (any of the $L + E$ momenta) and take a four-divergence $\frac{\partial}{\partial k_i^\mu}$, we obtain from the d-dimensional Gauss theorem

$$\int d^n k_1 ..... d^n k_L \boldsymbol{O}_{ij} f = 0, \tag{3.23}$$

$$\boldsymbol{O}_{ij} = \frac{\partial}{\partial k_i^\mu} q_{\mu,j}, \tag{3.24}$$

where we assume a vanishing of the surface term in the infinity. Now, if we introduce so called shift operators defined as

$$\mathbf{i}^{\pm} I(n_1, ..., n_i, ..., n_N) = I(n_1, ..., n_i \pm 1, ..., n_N), \tag{3.25}$$

then we can rewrite operator $\boldsymbol{O}_{ij}$ as the linear combination of shift operators. These equations are called IBP identities [29, 30].

It is clear that this construction can be applied on our particular case, where we have eight different operators $\boldsymbol{O}_{ij}$ acting on the integrand of the B functions. Schematically, this can be written as

$$\int \frac{\mathrm{d}^n l}{(2\pi)^n} \frac{\mathrm{d}^n k}{(2\pi)^n} \begin{pmatrix} \frac{1}{\partial l^\mu} \\ \frac{1}{\partial k^\mu} \end{pmatrix} \begin{pmatrix} l^\mu & k^\mu & q_+^\mu & q_-^\mu \end{pmatrix} \frac{1}{\prod_{j=1}^7 (P_j)^{n_j}} = 0. \tag{3.26}$$

The individual relations of (3.26) in terms of the shift operators can be found in the appendix A.

Number of propagators	MI's
2	B(0,0,1,0,0,0,1)*, B(0,1,0,0,0,0,1)*, B(0,1,1,0,0,0,0)*, B(1,1,0,0,0,0,0)*
3	[B(-1,0,0,1,1,0,1), B(0,-1,0,1,1,0,1), B(0,0,0,1,1,0,1)], [B(-1,1,1,0,0,0,1), B(0,1,1,0,0,0,1)], B(0,0,0,0,1,1,1)*, B(0,0,1,0,1,1,0)*
4	[B(-1,1,0,1,1,0,1), B(0,1,0,1,1,0,1), B(0,1,-1,1,1,0,1)], B(0,1,0,0,1,1,1)*, B(0,1,1,0,1,1,0)*, B(1,1,0,0,1,1,0)*

Table 3.1: Table of MI classified by the number of propagators and topologies.

3.3 Reduction to master integrals by Laporta algorithm

It is known that any B function can be reduced by IBP identities to linear combination of the finite set of so-called master integrals (MI's). These MI's belongs to the same topology or subtopology as the original B function. With the topology, we mean set of integrals which contain the same denominators of propagators to the arbitrary positive integer power (we do not put any constrain on denominators of propagators with negative integer). The Laporta algorithm [31, 32] is based on the fact that number of MI's are finite. In general, it fixes some sector (topology) and starts generating IBP relations with the different index substitution. Since the number of integrals is finite, after some time the number of equations will be bigger than number of integrals and the system can be solved. Laporta algorithm is implemented to the software Mathematica by the package FIRE [33].

In the table 3.1, you can see the set of MI's in our particular problem and in the figures 3.4, 3.5 and 3.6 are depicted the Feynman diagrams of these MI's organized by numbers of propagators. MI's which can be solved trivially are marked with asterisk. The MI's in brackets belong to the same topology and will be solved by the differential equation method (see section 3.4).

3.4 Differential equation method

In the previous section we showed how to obtain MI's. Now, we show how to solve them by differential equation method (DEM) [34, 35]. First part of this section is devoted to the general scheme of this method. In the latter subsection, we will deal with the problems concerning decoupling of the equation and boundary conditions.

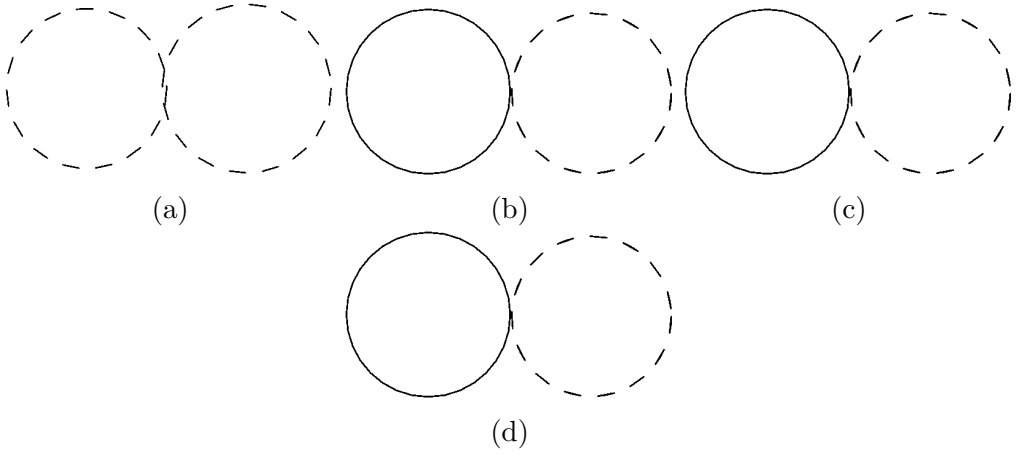

Figure 3.4: Subset of MI with 2 propagators. There are two different topologies on this picture, namely (a) and (b, c, d). The diagrams are ordered in accordance with the table 3.1.

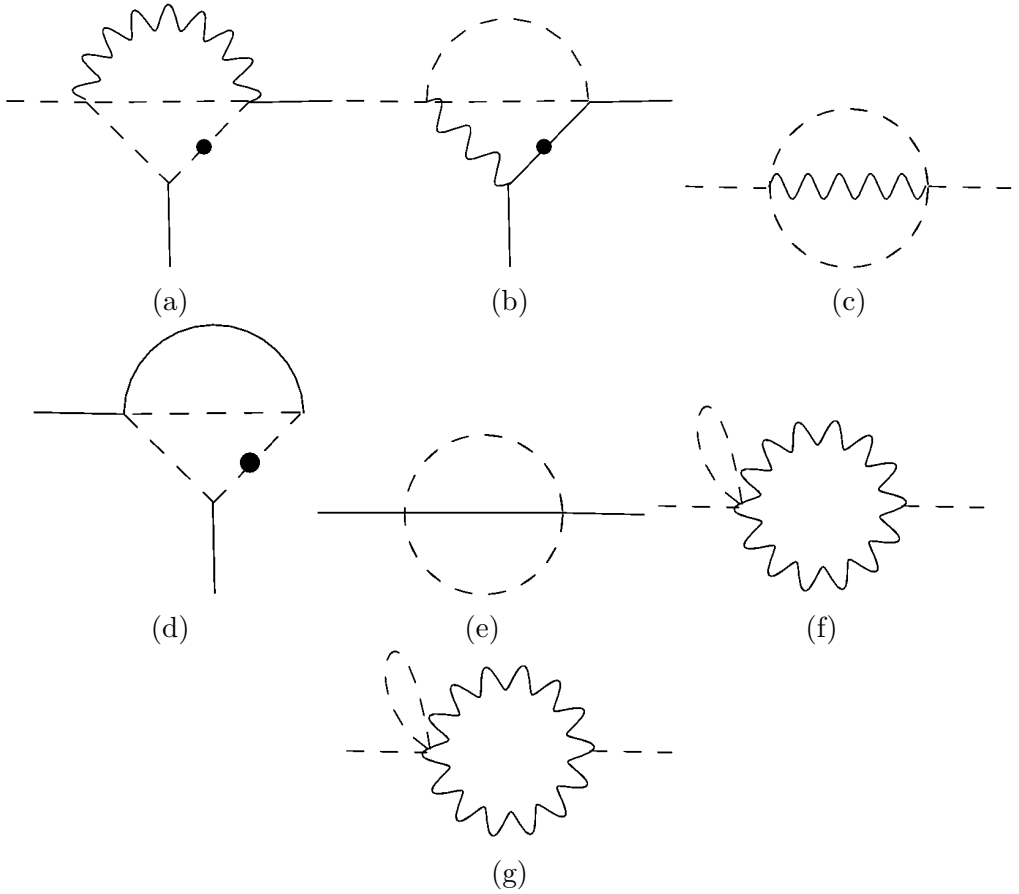

Figure 3.5: Subset of MI with 3 propagators. There are three different topologies on this picture, namely (a, b, c), (d, e), (f, g). The diagrams are ordered in accordance with the table 3.1. Black dot marks the negative power of the propagator in terms of B function.

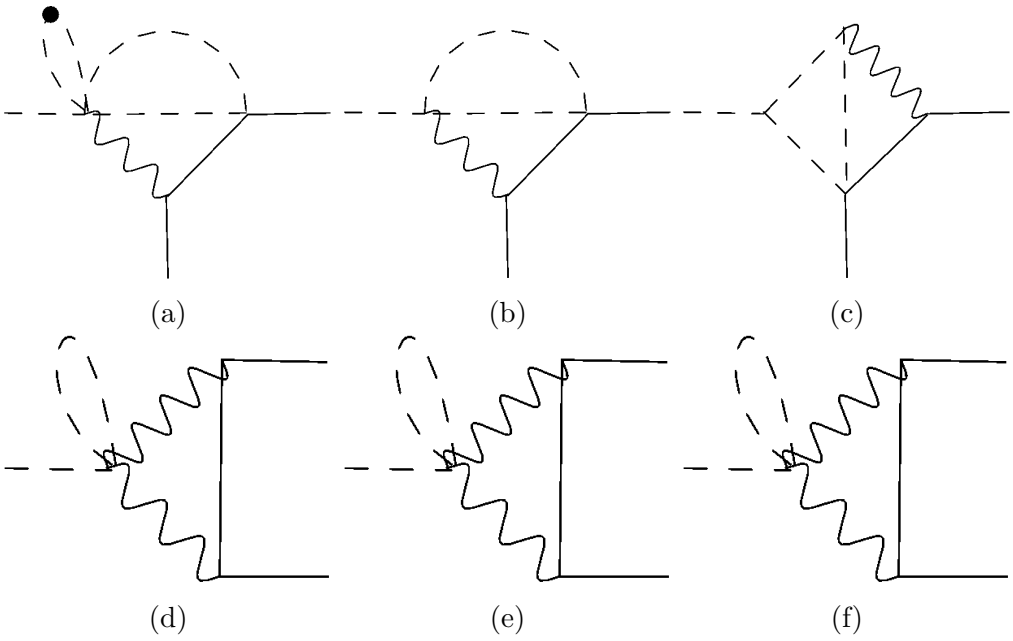

Figure 3.6: Subset of MI with 4 propagators. There are two different topologies on this picture, namely (a, b, c) and (d, e, f). The diagrams are ordered in accordance with the table 3.1. Black dot marks the negative power of the propagator in terms of B function.

3.4.1 General equations of DEM

Let us consider a situation where we are dealing with Feynman graphs with E external legs. Then the number of independent kinematical variables is

$$N = \frac{E(E-1)}{2}. \tag{3.27}$$

As was shown in the previous sections, the amplitude can be decomposed to the linear combination of MI's of the form

$$I(s_1, ..., s_N) = \int \mathrm{d}^n l_1 .... \mathrm{d}^n l_k \frac{1}{\prod_{j=1}^{I} (P_j)^{n_j}}, \tag{3.28}$$

where s_i is i-th kinematical variable. Now, let us differentiate MI by one of these kinematical variable. After the chain rule with external momenta q_j's we get

$$\begin{aligned} \frac{\partial I(s_1, ..., s_N)}{\partial s_i} &= \frac{\partial q_{j,\mu}}{\partial s_i} \frac{\partial I(s_1, ..., s_N)}{\partial q_{j,\mu}} \\ &= (\sum_{j,k=1}^{E} C_{jk}(s_1, ..., s_N) q_{k,\mu}) \frac{\partial I(s_1, ..., s_N)}{\partial q_{j,\mu}}. \end{aligned} \tag{3.29}$$

Coefficients $C_{jk}(s_1, ..., s_N)$ can be found by conditions which we impose on the solution. Consequently, the solution can be rewritten in terms of the shift operators (3.25). We illustrate this approach on our problem. As was mentioned in the chapter 2 our kinematical variable has the form

$$y = \frac{M_\pi^2}{4m^2}. \tag{3.30}$$

Let us denote the coefficients occurring in (3.29) as A, B and C (associated with momenta q_+, q_- and $(q_+ + q_-)$ respectively). The part with the coefficient C can be calculated trivially, if we realize that the square of momenta $(q_+ + q_-)^2$ occurs only as a mass of pion propagators. Schematically we can write this in the form

$$\Big(\frac{\partial}{\partial y}\Big)_1 = 4m^2(n_1\mathbf{1}^+ + n_3\mathbf{3}^+ + n_4\mathbf{4}^+ + n_7\mathbf{7}^+). \tag{3.31}$$

The coefficients A and B can be calculated as follows. First, we assume that our wanted operator is in the form

$$\Big(\frac{\partial}{\partial y}\Big)_2 = (Aq_{+,\mu} + Bq_{-,\mu})\frac{\partial}{\partial q^\mu_{+,-}}. \tag{3.32}$$

Next, let us impose the normalization condition and the on-shell condition

$$\Big(\frac{\partial}{\partial y}\Big)_2\Big(\frac{M^2}{4q^2_{+,-}}\Big) = 1, \tag{3.33a}$$

$$\Big[\Big(\frac{\partial}{\partial y}\Big)_2, q^2_{+,-}\Big] = 0, \tag{3.33b}$$

then we will get operator $\left(\frac{\partial}{\partial y}\right)_2$ as

$$\begin{aligned}\Big(\frac{\partial}{\partial y}\Big)_2 =& \frac{1}{2y(y-1)}[(2y-1)q_{+,\mu} - q_{-,\mu}]\frac{\partial}{\partial q^\mu_+}\\ =& \frac{1}{2y(y-1)}[(2y-1)q_{-,\mu} - q_{+,\mu}]\frac{\partial}{\partial q^\mu_-}\\ =& \frac{1}{y(y-1)}[-(2y-1)\Big(\frac{n_4+n_6}{2}\Big) + n_4y\mathbf{4}^+\mathbf{1}^- + n_6y\mathbf{6}^+\mathbf{2}^-\\ & - n_4\frac{\mathbf{4}^+\mathbf{3}^-}{2} - n_6\frac{\mathbf{6}^+\mathbf{5}^-}{2} + n_4m^2y\mathbf{4}^+ + 2n_6m^2y\mathbf{6}^+],\end{aligned} \tag{3.34}$$

and the resulting operator $\frac{\partial}{\partial y}$ as a sum

$$\begin{aligned}\frac{\partial}{\partial y} =& \Big(\frac{\partial}{\partial y}\Big)_1 + \Big(\frac{\partial}{\partial y}\Big)_2\\ =& \frac{1}{y(y-1)}[-(2y-1)\Big(\frac{n_4+n_6}{2}\Big) + n_4y\mathbf{4}^+\mathbf{1}^- + n_6y\mathbf{6}^+\mathbf{2}^-\\ & - n_4\frac{\mathbf{4}^+\mathbf{3}^-}{2} - n_6\frac{\mathbf{6}^+\mathbf{5}^-}{2} + n_4m^2y\mathbf{4}^+ + 2n_6m^2y\mathbf{6}^+]\\ & + 4m^2(n_1\mathbf{1}^+ + n_3\mathbf{3}^+ + n_4\mathbf{4}^+ + n_7\mathbf{7}^+).\end{aligned} \tag{3.35}$$

From (3.35) we can observe that operator $\frac{\partial}{\partial y}$ creates a combination of integrals which belong to the same topology or subtopology as the original integral. This means that every integral appearing on the RHS of the differential equation can be decomposed by the IBP identities to the linear combination of MI's belonging to the particular topology. So, if we use the operator (3.35) on every MI of a certain topology, we get the system of differential equations which can be solved in principle. An example of this method is showed in the chapter 6.

3.4.2 Decoupling of differential equations

We would like to solve the system of the differential equations after their obtaining. Unfortunately, in most cases the system of MI's is not decoupled in the lowest order of ϵ. In this situation, we are forced to find basis in which the equations decouple. The algorithm searching for the suitable basis works in following steps:

1. Choosing different integrals belonging to the same topology as MI which we want to solve.
2. Finding a solution of (3.35) for the chosen integrals in terms of MI's
3. Finding a relation between our chosen integrals and MI's by IBP relations
4. Substitution for MI's in terms of the chosen integrals in the point 2.
5. Repetition of this process until the system decouples

The algorithm of this type can be programmed for example in Mathematica. When the system decouples the integrals can be solved to the required order of ϵ. Now, the only remaining problem is to fix the integration constants from the boundary conditions.

3.4.3 Boundary conditions

Integration constants can be fixed from the singularity of integrals in some specific kinematic points. For this purpose, it is convenient to redefine our kinematical variable (for example when we want to have a singularity of the diagram in the point 0 instead of ∞). Actually, searching for the appropriate kinematical variable is a weak point of this method. There exists also another possibility how to fix the integration constant. Sometimes, the integrals was computed in some specific point of the kinematical variable in the literature. From this known solution we can fix the integration constant for the general case [36].

Chapter 4

General structure of renormalization

In this section we discuss the general scheme of a renormalization for one-loop and two-loop contributions. Within this thesis we use common dimensional regularization and non-renormalizable effective field theory renormalization scheme [37]. We write effective Lagrangian in the form

$$L = \sum_n \mu^{-2\epsilon n} L_n, \tag{4.1}$$

where $\mu^{-2\epsilon n}$ is the dimensional scale resulting from dimensional regularization scheme and L_n contains counterterms which are needed for renormalization of corresponding n-loop Feynman graphs. In the next sections, we follow the analysis from [14].

4.1 Renormalization of the one-loop contributions

Generally, for the renormalized one-loop Feynman graph we can write schematically

$$\begin{aligned}\delta^{1\text{–loop}} =& \mu^{-2\epsilon} m^D \Big[\Big(\frac{\mu}{m}\Big)^{2\epsilon} \Big(\frac{\delta_{-1}^{1\text{–loop}}}{\epsilon} + \delta_0^{1\text{–loop}} + \epsilon \delta_1^{1\text{–loop}} + O(\epsilon^2) \Big) \\ &+ \Big(\chi(\mu) - \frac{\delta_{-1}^{1\text{–loop}}}{\epsilon} \Big) \Big],\end{aligned} \tag{4.2}$$

where D is dimension of δ. In this formula the first bracket represents contribution of the bare loop while the second bracket represent the counterterm contribution.

We use here the renormalization scheme suitable for effective theories and require renormalization scale independence order by order in the loop expansion.

At one loop order this means that the term

$$\begin{aligned}\overline{\chi} &= \Big(\frac{\mu}{m}\Big)^{-2\epsilon}\Big(\chi(\mu) - \frac{\delta_{-1}^{1\text{–loop}}}{\epsilon}\Big) + \frac{\delta_{-1}^{1\text{–loop}}}{\epsilon} \\ &= \chi(\mu) + \delta_{-1}^{1\text{–loop}}\ln\Big(\frac{\mu^2}{m^2}\Big) + O(\epsilon),\end{aligned} \tag{4.3}$$

is μ independent. In terms of this scale invariant variables (4.2) can be rewritten to the form

$$\delta^{1\text{–loop}} = m^D\Big(\delta_0^{1\text{–loop}} + \overline{\chi} + O(\epsilon)\Big). \tag{4.4}$$

4.2 Renormalization of the two-loop contributions

At the two-loop level the corresponding contribution can be divided to the three categories

$$\delta^{2\text{–loop}} = \delta_G^{2\text{–loop}} + \delta_{CT}^{1\text{–loop}} + \delta_{CT}^{\text{tree}}, \tag{4.5}$$

where $\delta_G^{2\text{–loop}}$ is a genuine two-loop contribution which we can write in the form

$$\delta_G^{2\text{–loop}} = \mu^{-4\epsilon}m^D\Big(\frac{\mu}{m}\Big)^{4\epsilon}\Big(\frac{\delta_{-2}^{2\text{–loop}}}{\epsilon^2} + \frac{\delta_{-1}^{2\text{–loop}}}{\epsilon} + \delta_0^{2\text{–loop}} + \epsilon\delta_1^{1\text{–loop}} + O(\epsilon^2)\Big), \tag{4.6}$$

$\delta_{CT}^{1\text{–loop}}$ represent contribution of one-loop graphs with counterterms and can be written as

$$\begin{aligned}\delta_{\text{CT}}^{1\text{–loop}} =& \mu^{-4\epsilon}m^D\Big(\frac{\mu}{m}\Big)^{2\epsilon}\sum_i\Big(\frac{\eta_{-1}^{(i),1\text{–loop}}}{\epsilon} + \eta_0^{(i),1\text{–loop}} + \epsilon\eta_1^{(i),1\text{–loop}} + O(\epsilon^2)\Big) \\ &\times\Big(\chi(\mu)^{(i),1\text{–loop}} - \frac{\delta_{-1}^{(i),1\text{–loop}}}{\epsilon}\Big),\end{aligned} \tag{4.7}$$

where the bracket on the first line correspond to the pure loop contribution and the terms on second line corresponds to the counterterm vertex. $\delta_{CT}^{\text{tree}}$ represent tree counterterm graph which is necessary for renormalization of the remaining superficial divergences. Naively

$$\begin{aligned}\delta_{CT}^{\text{tree}} =& \mu^{-4\epsilon}m^D\Big[\chi(\mu)^{\text{tree}} - \frac{\delta_{-2}^{2\text{–loop}} - \sum_i \eta_{-1}^{(i),1\text{–loop}}\delta_{-1}^{(i),1\text{–loop}}}{\epsilon^2} \\ &- \frac{\delta_{-1}^{2\text{–loop}} - \sum_i\Big(\eta_0^{(i),1\text{–loop}}\delta_{-1}^{(i),1\text{–loop}} - \chi(\mu)^{(i),1\text{–loop}}\eta_{-1}^{(i),1\text{–loop}}\Big)}{\epsilon} \\ &- \ln\Big(\frac{\mu^2}{m^2}\Big)\frac{2\delta_{-2}^{2\text{–loop}} - \sum_i \eta_{-1}^{(i),1\text{–loop}}\delta_{-1}^{(i),1\text{–loop}}}{\epsilon}\Big],\end{aligned} \tag{4.8}$$

here the term $\chi(\mu)^{\text{tree}}$ consist of linear combinations of the two-loop couplings $\chi(\mu)^{(i),2\text{–loop}}$ and powers of external momenta. However, the sum $\delta_G^{2\text{–loop}} + \delta_{CT}^{1\text{–loop}}$

should be free from non-local divergences (divergences containing terms proportional to $\ln\left(\frac{\mu^2}{m^2}\right)$) , i.e. only divergences which contain polynomials of external momenta and masses remain. This leads to the constraints

$$2\delta_{-2}^{2\text{–loop}} - \sum_i \eta_{-1}^{(i),1\text{–loop}} \delta_{-1}^{(i),1\text{–loop}} = 0, \tag{4.9}$$

$$\delta_{-1}^{2\text{–loop}} - \sum_i \eta_{0}^{(i),1\text{–loop}} \delta_{-1}^{(i),1\text{–loop}} = \left(\delta_{-1}^{2\text{–loop}}\right)_l, \tag{4.10}$$

where $\left(\delta_{-1}^{2\text{–loop}}\right)_l$ is local.

Now, if we introduce invariant couplings $\overline{\chi}^{(i),1\text{–loop}}$ and $\overline{\chi}^{\text{tree}}$ in the same manner as (4.3), namely

$$\overline{\chi}^{(i),1\text{–loop}} = \left(\frac{\mu}{m}\right)^{-2\epsilon}\left(\chi(\mu)^{(i),1\text{–loop}} - \frac{\delta_{-1}^{(i),1\text{–loop}}}{\epsilon}\right) + \frac{\delta_{-1}^{(i),1\text{–loop}}}{\epsilon}, \tag{4.11}$$

$$\begin{aligned}\overline{\chi}^{\text{tree}} =& \left(\frac{\mu}{m}\right)^{-4\epsilon}\Bigg[\chi(\mu)^{\text{tree}} + \frac{\delta_{-2}^{(i),2\text{–loop}}}{\epsilon^2} \\ &- \frac{\left(\delta_{-1}^{2\text{–loop}}\right)_l + \sum_i \chi(\mu)^{(i),1\text{–loop}} \eta_{-1}^{(i),1\text{–loop}}}{\epsilon}\Bigg] \\ &- \frac{\delta_{-2}^{(i),2\text{–loop}}}{\epsilon^2} + \frac{\left(\delta_{-1}^{2\text{–loop}}\right)_l + \sum_i \overline{\chi}^{(i),1\text{–loop}} \eta_{-1}^{(i),1\text{–loop}}}{\epsilon},\end{aligned} \tag{4.12}$$

then we are able to rewrite $\delta_G^{2\text{–loop}} + \delta_{CT}^{1\text{–loop}}$ as

$$\begin{aligned}\delta_G^{2\text{–loop}} + \delta_{CT}^{1\text{–loop}} =& \mu^{-4\epsilon} m^D \left(\frac{\mu}{m}\right)^{4\epsilon}\Bigg[\frac{\delta_{-2}^{2\text{–loop}}}{\epsilon^2} \\ &+ \frac{\left(\delta_{-1}^{2\text{–loop}}\right)_l + \sum_i \left(\overline{\chi}^{(i),1\text{–loop}} \eta_{-1}^{(i),1\text{–loop}}\right)}{\epsilon} + \delta_0^{2\text{–loop}} \\ &+ \sum_i \left(\overline{\chi}^{(i),1\text{–loop}} \eta_0^{(i),1\text{–loop}} - \delta_{-1}^{1\text{–loop}} \eta_1^{(i),1\text{–loop}}\right) + O(\epsilon)\Bigg],\end{aligned} \tag{4.13}$$

and the tree-level counterterm graph to the form

$$\begin{aligned}\delta_{CT}^{\text{tree}} =& \mu^{-4\epsilon} m^D \left(\frac{\mu}{m}\right)^{4\epsilon}\Bigg[\overline{\chi}^{\text{tree}} + \frac{\delta_{-2}^{2\text{–loop}}}{\epsilon^2} \\ &+ \frac{\left(\delta_{-1}^{2\text{–loop}}\right)_l + \sum_i \left(\overline{\chi}^{(i),1\text{–loop}} \eta_{-1}^{(i),1\text{–loop}}\right)}{\epsilon}\Bigg].\end{aligned} \tag{4.14}$$

As a result we get for $\delta^{2\text{–loop}}$ the form which is invariant with respect to change of the renormalization scale μ

$$\begin{aligned}\delta^{2\text{–loop}} =& m^D\Bigg[\delta_0^{2\text{–loop}} + \overline{\chi}^{\text{tree}} + \delta_0^{2\text{–loop}} \\ &+ \sum_i \left(\overline{\chi}^{(i),1\text{–loop}} \eta_0^{(i),1\text{–loop}} - \delta_{-1}^{1\text{–loop}} \eta_1^{(i),1\text{–loop}}\right) + O(\epsilon)\Bigg].\end{aligned} \tag{4.15}$$

Chapter 5

Counterterm technique of renormalization

This chapter is devoted to the counterterm diagrams necessary for the renormalization of the genuine two-loop loop diagrams $\delta_G^{2\text{–loop}}$, i. e. we introduce the diagrams contributing to $\delta_{CT}^{1\text{–loop}} + \delta_G^{\text{tree}}$.

5.1 One-loop counterterm diagrams

In this section we firstly introduce the one-loop diagrams, where the divergent one-loop subgraphs are replaced by point-like counterterm vertices (this correspond to the first bracket contribution in the (4.7)). After that, we evaluate the divergent part of one-loop subgraphs in order to renormalize our Lagrangian and subsequently we determine $\delta_{-1}^{1\text{–loop}}$ from the second bracket of (4.7).

5.1.1 One-loop counterterm diagrams with counterterm vertices

All necessary one-loop counterterm diagrams are depicted in the figure 5.1. The effective one-particle irreducible vertex (defined in (2.2)) of the triangle diagram can be written as

$$\begin{aligned} \mathrm{i}\mathcal{V}^{tr}(q_+, q_-) = &- \frac{K_{\pi_0\gamma\gamma}\alpha^2}{F_0}\frac{\epsilon_{\mu\nu\alpha\beta}}{\pi}\int \frac{\mathrm{d}^n l}{(2\pi)^n}(l+q_+)^\alpha (l-q_-)^\beta \\ &\times \frac{\gamma^\mu(\not{l}+m)\gamma^\nu}{(l^2-m^2)(l-q_-)^2(l+q_+)^2}. \end{aligned} \tag{5.1}$$

With use of (2.12) and (2.15) we can find the P form factor for this counterterm diagram (in fact this loop diagram with exception of the counterterm was

calculated in the section 2.3.2) in terms of the B functions

$$\begin{aligned} P^{tr}(m^2, M^2) = &- \mathrm{i}\frac{K_{\pi_0\gamma\gamma}\alpha^2}{F_0(4\pi^2)}\frac{m}{M^2}\{M^4 B(0,1,0,0,1,1,0) \\ &+ B(0,1,0,0,-1,1,0) + B(0,1,0,0,1,-1,0) \\ &- 2\Big[B(0,1,0,0,0,1,0) + B(0,1,0,0,1,0,0)\Big] \\ &- 2B(0,1,0,0,0,0,0)\}. \end{aligned} \tag{5.2}$$

The effective one-particle irreducible vertex of the second diagram depicted in the figure 5.1 has the following form

$$\mathrm{i}\mathcal{V}^{tad}(q_+, q_-) = -\frac{iK_{\pi^0\pi^+\pi^-e^+e^-}\alpha^2 N_C}{12F_0^3\pi^2}\int\frac{\mathrm{d}^n l}{(2\pi)^n}\frac{\not{Q}\gamma_5}{(l^2-m^2)}. \tag{5.3}$$

As one can observe, for this type of the diagram we cannot use the formula (2.15) for the determination of P amplitude as before, but we need to derive the corresponding amplitude from the relation (2.7). If we insert the equation (5.3) to (2.7) we get (after the anticommutation of γ_5 matrices)

$$\begin{aligned} P^{tad}(m^2, M^2) = &- \lim_{q_\pm^2\to m^2}\frac{K_{\pi^0\pi^+\pi^-e^+e^-}\alpha^2 N_C}{24M^2F_0^3\pi^2}\mathrm{Tr}\Big[(\not{q}_- + m)\not{Q}(\not{q}_+ + m)\Big] \\ &\times B(1,0,0,0,0,0,0) \\ = &- \frac{mK_{\pi^0\pi^+\pi^-e^+e^-}\alpha^2 N_C}{6F_0^3\pi^2}B(1,0,0,0,0,0,0). \end{aligned} \tag{5.4}$$

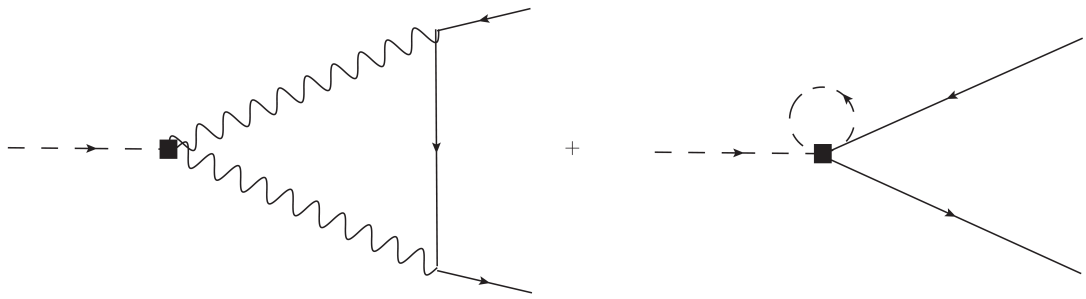

Figure 5.1: One-loop counterterm diagrams necessary for renormalization.

5.1.2 Renormalization of the Lagrangian

All divergent one-loop subgraphs which we need to renormalize in order to get rid all necessary divergences in our calculations are depicted in the figure 5.2.

Bubble insertion diagram

The first diagram we are dealing with is the bubble insertion diagram 5.2a. This loop was expressed in the dimensional regularization scheme in (3.7) which can

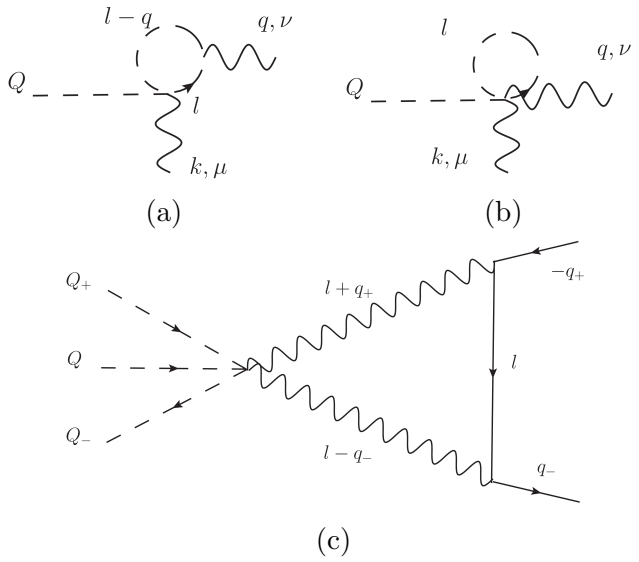

Figure 5.2: Set of the divergent loop diagrams necessary for renormalization.

be simplified to the form (3.9). This expression can be rewritten by Feynman parametrization and subsequently calculated with master formula of the general form

$$\int \frac{\mathrm{d}^n l}{(2\pi)^n} \frac{(l^2)^r}{(l^2-C^2)^s} = \mathrm{i}\frac{(-1)^{r+s}}{(4\pi)^{n/2}} \frac{\Gamma(r+\frac{n}{2})\Gamma(s-r-\frac{n}{2})}{\Gamma(\frac{n}{2})\Gamma(s)} \Big(C^2\Big)^{r+\frac{n}{2}-s}. \tag{5.5}$$

This formula was used in (3.10) and (3.11) and for the UV divergent part of (3.9) we get (note we denote here the loop contribution as Σ instead of Γ in order to do not confuse it with gamma function)

$$\mathrm{i}\Sigma_{\mu\nu}^{\mathrm{BID,div}} = -\frac{q^\alpha k^\beta}{\epsilon} \frac{e^2 N_C \epsilon_{\alpha\beta\mu\nu}}{36\pi^2 F_0^3} \frac{3M^2 - \frac{m^2}{2}}{(4\pi)^2}. \tag{5.6}$$

Let us now renormalize the Lagrangian of our particular process. The part of the Lagrangian which should subtract the divergence above is of the form

$$\mathcal{L}^{(4)}_{CT,\pi\gamma\gamma} = \frac{\pi^0}{8} K_{\pi\gamma\gamma} \Big(\frac{\alpha}{\pi}\Big) \epsilon_{\mu\nu\alpha\beta} F^{\mu\nu} F^{\alpha\beta}, \tag{5.7}$$

where the constant $K_{\pi\gamma\gamma}$ in the spirit of the fourth chapter can be written as (see (4.7))

$$K_{\pi\gamma\gamma} = \mu^{-2\epsilon}(1 - \frac{\delta_{-1}^{(\mathrm{BID}),1\,-\,\mathrm{loop}}}{\epsilon} + \chi^{(\mathrm{BID}),1\,-\,\mathrm{loop}} - \frac{\delta_{-1}^{(\mathrm{Tad}),1\,-\,\mathrm{loop}}}{\epsilon} + \chi^{(\mathrm{Tad}),1\,-\,\mathrm{loop}}), \tag{5.8}$$

where $\frac{-\delta_{-1}^{(\mathrm{BID}),1-\mathrm{loop}}}{\epsilon} + \chi^{(\mathrm{BID}),1-\mathrm{loop}}$ corresponds to the part renormalizing the bubble insertion diagram and $-\frac{\delta_{-1}^{(\mathrm{Tad}),1-\mathrm{loop}}}{\epsilon} + \chi^{(\mathrm{Tad}),11-\mathrm{loop}}$ renormalize the tadpole diagram discussed in the following content. The term $\delta_{-1}^{(\mathrm{BID}),1-\mathrm{loop}}$ can be derived from comparison of the (5.8) with the Feynman rule for the $\pi\gamma\gamma$ vertex listed in the appendix A with result

$$\delta_{-1}^{(BID),1-\mathrm{loop}} = -\frac{\mathrm{i}N_C}{144\pi^3 F_0^2}\Big(3M^2 - \frac{m^2}{2}\Big). \tag{5.9}$$

Tadpole diagram

Next diagram of our interest is the tadpole diagram depicted in the figure 5.2b. The analytical structure of this loop was written in (3.15). The divergent part of the diagram can be calculated by the use of (5.5) with the result

$$\mathrm{i}\Sigma_{\mu\nu}^{\mathrm{Tad,div}} = -\frac{1}{\epsilon}\frac{2e^2 N_C \epsilon_{\alpha\beta\mu\nu} k^\alpha q^\beta}{9\pi^2 F_0^3}\frac{M_\pi^2}{(4\pi)^2}. \tag{5.10}$$

As in the previous case this divergence is subtracted by the renormalization of the Lagrangian part corresponding to (5.7). Factor $\delta_{-1}^{\mathrm{Tad}),1-\mathrm{loop}}$ has then the form

$$\delta_{-1}^{(\mathrm{Tad}),1-\mathrm{loop}} = \frac{\mathrm{i}N_C M_\pi^2}{18\pi^3 F_0^2}. \tag{5.11}$$

Triangle diagram

The last diagram which is necessary to calculate in order to renormalize the relevant parts of the Lagrangian is the triangle diagram depicted in the figure 5.2c. The loop can be written in the dimensional regularization scheme as

$$\begin{aligned}\mathrm{i}\Sigma^{\mathrm{Triangle}} = &-\frac{\mathrm{i}\mu^{4-n}e^4 N_C \epsilon^{\alpha\beta\mu\nu}}{36\pi^2 F_0^3}(4Q - 2Q_- - 2Q_+)_\beta \\ &\times \int \frac{\mathrm{d}^n l}{(2\pi)^n}\frac{(2l + q_+ - q_-)_\alpha(\gamma_\mu(\not{l} + m)\gamma_\nu)}{((l+q_+)^2 - M^2)((l-q_-)^2 - M^2)(l^2 - M^2)}.\end{aligned} \tag{5.12}$$

Now, if we notice that the only divergent part originate from the term which is proportional in the numerator of the integrand to l^2 than we can after the Feynman parametrization for the divergent part of the loop $\mathrm{i}\Sigma^{\mathrm{Triangle}}$ write

$$\begin{aligned}\mathrm{i}\Sigma^{\mathrm{Triangle,div}} = &-\frac{\mathrm{i}e^4 N_C \epsilon^{\alpha\beta\mu\nu}}{36\pi^2 F_0^3}(4Q - 2Q_- - 2Q_+)_\beta \\ &\times \int\int \frac{4\mathrm{d}x\mathrm{d}y}{n}\int \frac{\mathrm{d}^n l}{(2\pi)^n}\frac{l^2(\gamma_\mu\gamma_\alpha\gamma_\nu)}{(l^2 - C^2)^3}.\end{aligned} \tag{5.13}$$

Let us focus on the term $\epsilon^{\alpha\beta\mu\nu}\gamma_\mu\gamma_\alpha\gamma_\nu$. This term can be written in the basis of γ matrices (in general this basis is spanned by 16 matrices 1, γ_μ, $\gamma_\mu\gamma_5$ and $\sigma_{\mu\nu}$) only as

$$\epsilon^{\alpha\beta\mu\nu}\gamma_\mu\gamma_\alpha\gamma_\nu = C\gamma_5\gamma_\beta, \tag{5.14}$$

where C is a appropriate constant. This constant can be determined if we calculate trace of (5.14) multiplied with $\gamma^\beta\gamma_5$. Then we get

$$4\mathrm{i}\epsilon^{\alpha\beta\mu\nu}\epsilon_{\alpha\beta\mu\nu} = 16C, \tag{5.15}$$

and with the use of the identity $\epsilon^{\alpha\beta\mu\nu}\epsilon_{\alpha\beta\mu\nu} = -4!$ we have for the constant C

$$C = -6\mathrm{i}. \tag{5.16}$$

If we use the master formula (5.5) then we can express the whole result for $\mathrm{i}\Sigma^{\mathrm{Triangle,div}}$ as

$$\mathrm{i}\Sigma^{\mathrm{Triangle,div}} = -\frac{\mathrm{i}}{\epsilon}\frac{e^4 N_C}{96\pi^4 F_0^3}\gamma_5(2\not{Q} - \not{Q}_- - \not{Q}_+). \tag{5.17}$$

The relevant part which subtract this divergence is included in the renormalized part of the Lagrangian

$$\begin{aligned}\mathcal{L}^{(6)}_{CT,\pi^0\pi^-\pi^+e^+e^-} =& \frac{K_{\pi^0\pi^-\pi^+e^+e^-}}{24F_0^3}\Big(\frac{\alpha}{\pi}\Big)^2\overline{\psi}\gamma^\mu\gamma_5\psi(\pi^-\pi^0\partial_\mu\pi^+ \\ & - 2\pi^-\partial_\mu\pi^0\pi^+ + \partial_\mu\pi^-\pi^0\pi^+),\end{aligned} \tag{5.18}$$

where $K_{\pi^0\pi^-\pi^+e^+e^-}$ has the form

$$K_{\pi^0\pi^-\pi^+e^+e^-} = (1 - \frac{\delta^{(\mathrm{Triangle}),1\,-\,\mathrm{loop}}_{-1}}{\epsilon}). \tag{5.19}$$

Term $\delta^{(\mathrm{Triangle}),1\,-\,\mathrm{loop}}_{-1}$ is obtained after the comparison of (5.17) with the vertex $\pi^0\pi^-\pi^+e^+e^-$ which is listed in the appendix A. The result reads then (note we used $\delta^{(\mathrm{Triangle}),1\,-\,\mathrm{loop}}_{-1}$ instead of -4χ)

$$\delta^{(\mathrm{Triangle}),1\,-\,\mathrm{loop}}_{-1} = \frac{\mathrm{i}N_C}{4\pi^2}. \tag{5.20}$$

5.2 Tree level counterterm diagram

For the subtraction of the remaining divergences, we introduce the tree level counterterm diagram depicted in the figure 5.3. Let us remind that remaining divergences after the sum of two-loop diagrams with one-loop counterterm diagrams should be local. Unfortunately, due to lack of time we were not able to determine the explicit form of the complete tree level counterterm Lagrangian since it has complicated structure. However, the corresponding vertex should have the similar form as (1.62). Schematically

$$\mathcal{L}^{(6)}_{CT,\pi^0e^+e^-} = -\Big(\frac{\alpha}{\pi}\Big)^2\frac{K_{\mathrm{tree}}(M^2,\partial)}{16F_0}\overline{\psi}\gamma_\mu\gamma_5\psi\partial^\mu\pi^0, \tag{5.21}$$

where $K_{\mathrm{tree}}(M^2,\partial)$ is a second order polynomial of the external momenta and masses.

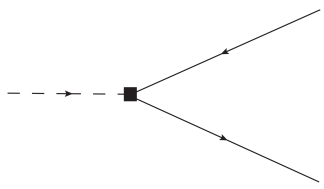

Figure 5.3: Tree level counterterm diagram necessary for renormalization.

Chapter 6

Results for the master integrals

In this section we firstly introduce our convention for normalization of integrals and we show the importance of the correctly chosen kinematical variable on example. The other part of the section is devoted to the analytical results of the diagrams depicted in the figure 2.3.

6.1 Normalization of integrals and substitution of kinematical variables

In order to maximally simplify calculations of differential equations, we introduce the dimensionless integral b defined as

$$B(n_1,...,n_7) = \Big(\mathrm{i}\Gamma(1+\epsilon)(4\pi)^{\epsilon-2}\Big)^2\left(\frac{\mu}{m}\right)^{4\epsilon} m^{2(4-\sum_i n_i)} b(n_1,...,n_7). \tag{6.1}$$

Differential equations are then solved to the desired order in ϵ of b functions. Schematically

$$b(n_1,...,n_7) = \sum_{i\geq -2} b(n_1,...,n_7)^{(i)}\epsilon^i. \tag{6.2}$$

Another important part of the calculation is the correct selection of the kinematical variable. In order to express all our results in harmonic polylogarithms (see appendix C), we were forced to use two different kinematical variables

$$x = \frac{1}{\sqrt{4y}} = \frac{m}{M_\pi}, \tag{6.3}$$

$$z = -\frac{\sqrt{1-\frac{1}{y}}-1}{\sqrt{1-\frac{1}{y}}+1}. \tag{6.4}$$

6.2 Example of calculation by differential equation technique

In this subsection we will show in detail the calculation in both lowest orders of the Laurent expansion for the one of the MI's subtopologies. All of these calculations will be expressed in the kinematical variable x. Let us consider the integrals with the following topology

$b(0,1,1,0,0,0,1) \equiv b_1$

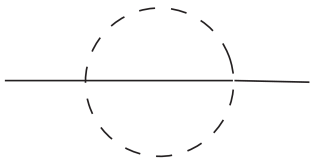

$b(-1,1,1,0,0,0,1) \equiv b_2$

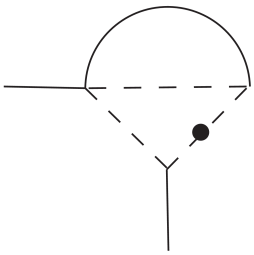

$b(0,0,1,0,0,0,1) \equiv t_1$

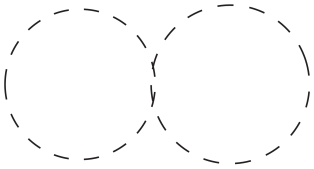

$b(0,1,0,0,0,0,1) \equiv t_2$

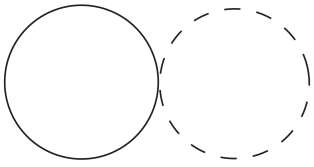

RHS of differential equations contains also tadpole diagrams (MI's of two propagator topology) which Laurent expansions is known since they can be calculated by the Feynman parametrization and will be expressed in concrete calculations as known functions of the kinematical variable. For completeness, let us list the

results for the tadpoles in two lowest orders expressed in the variable x

$$t_1^{(-2)} = \frac{1}{x^2}, \tag{6.5a}$$
$$t_1^{(-1)} = \frac{2(\mathrm{HPL}(\{0\},x)+1)}{x^2}, \tag{6.5b}$$

$$t_2^{(-2)} = \frac{1}{x^4}, \tag{6.6a}$$
$$t_2^{(-1)} = \frac{4\mathrm{HPL}(\{0\},x)+2}{x^4}. \tag{6.6b}$$

The system of the differential equations in the lowest order for the basis of the MI's is of the form

$$\frac{\partial b_1^{(-2)}}{\partial y} = \frac{4y(b_1^{(-2)}+4y+2)-3b_2^{(-2)}}{2y(4y-1)}, \tag{6.7a}$$
$$\frac{\partial b_2^{(-2)}}{\partial y} = \frac{2b_1^{(-2)}-6b_2^{(-2)}+6}{1-4y} + \frac{3b_2^{(-2)}}{2y} - 10. \tag{6.7b}$$

As one can see, the differential equations did not decouple for this choice of the basis. So, it is necessary to find different basis in which the differential equations decouple. One of the possibility is the basis

$$b(0,1,2,0,0,0,1) \equiv r_1, \tag{6.8a}$$
$$b(-1,2,1,0,0,0,2) \equiv r_2. \tag{6.8b}$$

The relations between this two basis (in terms of the kinematic variable y) are following

$$\begin{aligned} b_1 =& r_1\Big(\frac{27y\epsilon^3}{2} + \frac{9\epsilon^3}{2(4y-1)} + \frac{11\epsilon^3}{(1-4y)^2} - \frac{2\epsilon^3}{(4y-1)^3} + 9y\epsilon^2 + \frac{3\epsilon^2}{4y-1} \\ &- \frac{2\epsilon^2}{(1-4y)^2} + 6y\epsilon - \frac{2\epsilon}{4y-1} + 4y - \frac{95\epsilon^3}{8} + \frac{11\epsilon^2}{4} - \frac{7\epsilon}{2} - 1\Big) \\ &+ r_2\Big(-\frac{18\epsilon^3}{4y-1} + \frac{4\epsilon^3}{(1-4y)^2} + \frac{4\epsilon^2}{4y-1} + 13\epsilon^3 - 2\epsilon^2 + 4\epsilon\Big) + t_1\Big(\frac{51\epsilon^3}{64y^2} \\ &- \frac{7\epsilon^2}{32y^2} + \frac{\epsilon}{16y^2} - \frac{13\epsilon^3}{64y} + \frac{17\epsilon^3}{4(4y-1)} - \frac{13\epsilon^3}{2(1-4y)^2} + \frac{\epsilon^3}{(4y-1)^3} \\ &+ \frac{33\epsilon^2}{32y} - \frac{5\epsilon^2}{2(4y-1)} + \frac{\epsilon^2}{(1-4y)^2} - \frac{\epsilon}{16y} + \frac{\epsilon}{4y-1} + \frac{1}{8y}\Big) \\ &+ t_2\Big(-\frac{461\epsilon^3}{32y} + \frac{37\epsilon^3}{4y-1} - \frac{6\epsilon^3}{(1-4y)^2} + \frac{65\epsilon^2}{16y} - \frac{6\epsilon^2}{4y-1} - \frac{9\epsilon}{8y} + \frac{1}{4y}\Big), \end{aligned} \tag{6.9}$$

$$
\begin{aligned}
b_2 =& r_1\Big(-\frac{86}{3}y^2\epsilon^3 - \frac{56y^2\epsilon}{3} - \frac{11y\epsilon^3}{6} + \frac{35\epsilon^3}{6(4y-1)} + \frac{3\epsilon^3}{(1-4y)^2} \\
&- \frac{2\epsilon^3}{3(4y-1)^3} - \frac{(2y(4y(4y(68y-89)+125)-55)+5)\epsilon^2}{6(1-4y)^2} + \frac{10y\epsilon}{3} \\
&- \frac{2\epsilon}{3(4y-1)} + 4(1-4y)y + \frac{7\epsilon^3}{12} - \epsilon\Big) + r_2\Big(\frac{44y\epsilon^3}{3} - \frac{14\epsilon^3}{3(4y-1)} \\
&+ \frac{4\epsilon^3}{3(1-4y)^2} - \frac{8y(8y(6y-5)+9)\epsilon^2}{3(1-4y)^2} + \frac{4\epsilon^2}{3(1-4y)^2} + \frac{16y\epsilon}{3} - \frac{20\epsilon^3}{3}\Big) \\
&+ t_1\Big(-\frac{5\epsilon^3}{96y^2} + \frac{(4y-1)\left(24y^2-98y+25\right)\epsilon^2}{48(1-4y)^2y} + \frac{\epsilon^2}{48(1-4y)^2y^2} \\
&+ \frac{157\epsilon^3}{96y} - \frac{13\epsilon^3}{12(4y-1)} - \frac{11\epsilon^3}{6(1-4y)^2} + \frac{\epsilon^3}{3(4y-1)^3} + \frac{\epsilon}{8y} + \frac{\epsilon}{3(4y-1)} \\
&+ \frac{3\epsilon^3}{16} + \frac{\epsilon}{12} + \frac{1}{2}\Big) + t_2\Big(\frac{17\epsilon^3}{16y} + \frac{31\epsilon^3}{3(4y-1)} - \frac{2\epsilon^3}{(1-4y)^2} \\
&+ \frac{(4y-1)(2y(220y-93)+7)\epsilon^2}{24(1-4y)^2y} + \frac{\epsilon}{12y} - \frac{73\epsilon^3}{8} - \frac{11\epsilon}{6} + 1\Big).
\end{aligned}
\tag{6.10}
$$

The solution of the integrals r_i is searched as the Laurent expansion to the desired order of ϵ. Schematically

$$
r_i = \sum_{j\geq -2} r_i^{(j)}\epsilon^j \tag{6.11}
$$

Notice the dependence of b_1 and b_2 on the integral r_2 in the (6.9, 6.10). This integral does not appear in the 0th order in ϵ. So, it is enough to calculate r_2 in terms of the Laurent expansion (6.11) to the power of ϵ which is one less in the order as it is in case of r_1. Now, we switch to the kinematic variable x in order to get differential equations which solutions can be expressed in HPL's (appendix C). System of the differential equations in the lowest order reads now

$$
\frac{\partial r_1^{(-2)}}{\partial x} = \frac{1-2r_1^{(-2)}}{(x-x^3)}, \tag{6.12a}
$$

$$
\frac{\partial r_2^{(-2)}}{\partial x} = \frac{x^2(2r_1^{(-2)} - 4r_2^{(-2)} + 3) + 4(r_2^{(-2)} - 1)}{4x(x^2-1)}. \tag{6.12b}
$$

As we can see the differential equation for $r_1^{(-2)}$ is decoupled. The calculation of $r_1^{(-2)}$ can be done (as all other orders) by the technique of the variation of constants. We get

$$
r_1^{(-2)} = \frac{1}{2} + (-1 + \frac{1}{x^2})C_1^{(-2)}. \tag{6.13}
$$

Finally, the integration constant $C_1^{(-2)}$ is fixed from [36], where the MI of this subtopology were calculated for the limits of $x \to 1$ and $x \to \infty$. After the comparison of results (which are $b_1^{(-2)}(x=1) = \frac{3}{2}$ and $b_1^{(-2)}(x=\infty) = \frac{1}{2}$) we get for the integral constant $C_1^{(-2)}$ and $r_1^{(-2)}$

$$
C_1^{(-2)} = 0, \tag{6.14a}
$$

$$r_1^{(-2)} = 1/2. \tag{6.14b}$$

Now, the calculation of the r_2^{-2} can be also performed

$$r_2^{(-2)} = \frac{(C_2^{(-2)} + x)}{x}. \tag{6.15}$$

In order to fix constant $C_2^{(-2)}$, we need also know $r_1^{(-1)}$. The differential equation has the following form (note appearance of $\mathrm{HPL}(\{0\}, x)$ from the tadpoles diagrams (6.5) and (6.6))

$$\frac{\partial r_1^{(-1)}}{\partial x} = \frac{4\mathrm{HPL}(\{0\}, x) + 4C_2^{(-2)}x - 2r_1^{-1} - 2x^2 + 3}{x - x^3}. \tag{6.16}$$

The differential equation for $r_1^{(-1)}$ can be solved trivially

$$\begin{aligned} r_1^{(-1)} =& \frac{1}{4x^2}\Big(4C_2^{(-2)}\left(x^2-1\right)\mathrm{HPL}(\{\mathrm{p}\}, x) + 8x^2\mathrm{HPL}(\{0\}, x) \\ & - 4C_1^{(-1)}\left(x^2-1\right) - C_2^{(-2)}(4 - 4(x-2)x) + x^2 + 1\Big). \end{aligned} \tag{6.17}$$

The integration constants $C_1^{(-1)}$, $C_2^{(-2)}$ are fixed as before from the knowledge of the analytical form of the MI's in limiting cases (here the results are $b_1^{(-1)}(x = 1) = \frac{17}{4}$ and $b_1^{(-1)}(x = \infty) = \frac{5}{4}$). We get

$$C_2^{(-2)} = 0, \tag{6.18a}$$

$$C_1^{(-1)} = -\frac{1}{4}. \tag{6.18b}$$

The result for $r_2^{(-2)}$ and $r_1^{(-1)}$ reads then

$$r_2^{(-2)} = 1, \tag{6.19a}$$

$$r_1^{(-1)} = 2\mathrm{HPL}(\{0\}, x) + \frac{1}{2}. \tag{6.19b}$$

This procedure is repeated in the calculation of the following orders. Complete results for all MI's are given in the appendix E.

6.3 Results of two-loop graphs

In this section we list the results for the pure two-loop diagrams (i. e. contribution $\delta_G^{2\text{–loop}}$ without counterterms) depicted in the figure 2.3. The results will be expressed in the kinematic variable y defined in (2.8). We express the results through form factor P defined in (2.3) (see also (2.4) and (2.5)). The structure of the form factors P_{NLO} for all two-loop diagrams calculated here in terms of B functions can be seen in (3.13), (3.14) and (3.17). Decomposition of the individual B functions appearing in (3.13, 3.14, 3.17) to MI's can be found in the

appendix D. The results for each MI are listed in appendix E. Finally, let us list these amplitudes in terms of MI's

$$
\begin{aligned}
P(m^2,y)^{up-bubble}_{\pi^0\gamma\gamma} =& \mathrm{i}\frac{e^4N_C}{12\pi^2F_0^3 4my}\frac{\mu^{2(4-n)}}{(n-1)}\{32m^4y^2B(0,1,1,0,1,1,0)\\
&+16m^4y^2B(1,1,0,0,1,1,0)\\
&-\frac{8}{3}m^4y(37y-2)B(0,1,0,1,1,0,1)\\
&-\frac{16}{3}m^2yB(-1,1,0,1,1,0,1)\\
&-\frac{8}{3}m^2(y-1)B(0,0,0,1,1,0,1)\\
&-8m^2yB(0,1,-1,1,1,0,1)\\
&+4m^2yB(0,1,1,0,0,0,1)(4m^2+8y-1)\\
&+2(5-8m^2)yB(-1,1,1,0,0,0,1)\\
&+B(0,0,1,0,0,0,1)(8(m^2-1)y+\frac{4}{3})\\
&+4(2m^2-3)yB(0,1,0,0,0,0,1)\\
&+8(m^2-1)yB(0,1,1,0,0,0,0)\\
&-\frac{8}{3}B(-1,0,0,1,1,0,1)-\frac{4}{3}B(0,-1,0,1,1,0,1)\\
&+\epsilon\Big[-32m^4y^2B(0,1,1,0,1,1,0)\\
&+\frac{4}{3}m^4y(100y-11)B(0,1,0,1,1,0,1)\\
&+\frac{44}{3}m^2yB(-1,1,0,1,1,0,1)\\
&+\frac{22}{3}m^2(y-1)B(0,0,0,1,1,0,1)\\
&+8m^2yB(0,1,-1,1,1,0,1)\\
&+\frac{8}{3}m^2(1-24y)yB(0,1,1,0,0,0,1)\\
&-12yB(-1,1,1,0,0,0,1)\\
&+(8y-\frac{11}{3})B(0,0,1,0,0,0,1)\\
&-\frac{26}{3}yB(0,1,0,0,0,0,1)-\frac{2}{3}yB(0,1,1,0,0,0,0)\\
&+\frac{22}{3}B(-1,0,0,1,1,0,1)+\frac{11}{3}B(0,-1,0,1,1,0,1)\Big]\\
&+\epsilon^2\Big[\frac{4}{3}m^4y(4y+1)B(0,1,0,1,1,0,1)\\
&-\frac{4}{3}m^2yB(-1,1,0,1,1,0,1)\\
&-\frac{2}{3}m^2(y-1)B(0,0,0,1,1,0,1)\\
&-\frac{4}{3}m^2yB(0,1,1,0,0,0,1)\\
&-\frac{52}{3}yB(0,1,0,0,0,0,1)-\frac{28}{3}yB(0,1,1,0,0,0,0)
\end{aligned}
\tag{6.20}
$$

$$
\begin{aligned}
&- \frac{2}{3}B(-1,0,0,1,1,0,1) - \frac{1}{3}B(0,-1,0,1,1,0,1) \\
&+ \frac{1}{3}B(0,0,1,0,0,0,1)\Big] + O(\epsilon^3)\}.
\end{aligned}
$$

$$
P(m^2,Q^2)^{down-bubble}_{\pi^0\gamma\gamma} = P(m^2,Q^2)^{up-bubble}_{\pi^0\gamma\gamma}. \tag{6.21}
$$

$$
\begin{aligned}
P(m^2,y)^{tadpole}_{\pi^0\gamma\gamma} =& \mathrm{i}\frac{2e^4}{4my}\frac{N_C\mu^{2(4-n)}}{9\pi^2F_0^3}\{4y(4m^4yB(1,1,0,0,1,1,0) \\
&- 3B(0,1,0,0,0,0,1)) - 8\epsilon\Big[yB(0,1,0,0,0,0,1)\Big] \\
&- 16\epsilon^2\Big[yB(0,1,0,0,0,0,1)\Big] + O\left(\epsilon^3\right)\}.
\end{aligned} \tag{6.22}
$$

Conclusion

In this diploma thesis the chiral corrections to the decay $\pi^0 \to e^+e^-$ are studied in a detailed way. Firstly, χPT was presented with all the relevant parts of the χPT Lagrangian describing the dynamics of our particular process. Subsequently, we introduced the diagrams calculated in the presented work. Mainly, we focused on the two-loop chiral corrections of the order $O(\alpha^2 p^4)$. In order to calculate these diagrams, we firstly calculated the pion transition form factor $F_{\pi^0\to\gamma\gamma}$ (2.12) for each of these diagrams. With this knowledge, we were able to determine P amplitudes (defined in (2.3)) with the use of (2.15) in terms of scalar integrals (also called B functions (3.4)). To calculate all the P amplitudes we expressed necessary scalar integrals to linear combinations of so-called MI's. This reduction was done by Laporte algorithm based on IBP relations. MI's themselves was then calculated by the differential equation method.

Following content was dedicated to the renormalization of the two-loop Feynman diagrams we were dealing with. Firstly, we set the general structure of renormalization. After that, we introduced all the necessary one-loop counterterm diagrams. The counterterm vertices were determined in the classical way, i. e. we firstly calculated divergent parts of all the relevant one-loop subgraphs and then we subtracted these divergences by the renormalized Lagrangian. All these results together with the results for the P amplitudes of two-loop graphs are presented.

Unfortunately, due to lack of time we were not able to do all the necessary calculations to get the final and finite results for the relevant two-loop diagrams. With these results we would be able to determine finite contributions of one-loop counterterm diagrams $\chi^{(1\text{ - loop})}(\mu)$ describing the high-energy loop contribution (since the χPT is the effective field theory). However, in this work all the results necessary for the determination of $\chi^{(1\text{ - loop})}(\mu)$ was presented and we hope that in the following months, we will be able express these parameters also numerically.

Appendix

A Feynman rules

In this appendix we list the Feynman rules for the corresponding vertices used in this master thesis

- $e^+e^-\gamma$ vertex:

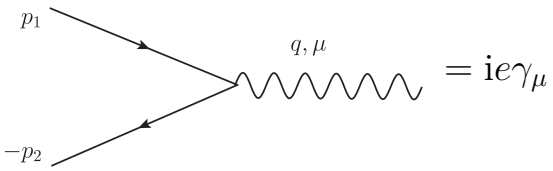

Figure 2: Feynman rule for $e^+e^-\gamma$ vertex.

- πe^+e^- vertex:

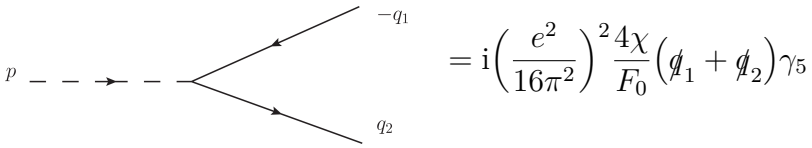

Figure 3: Feynman rule for πe^+e^- vertex.

- $\pi 2\gamma$ vertex:

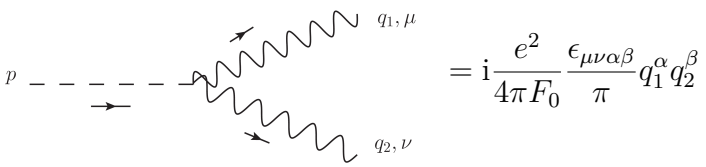

Figure 4: Feynman rule for $\pi 2\gamma$ vertex.

- $2\pi\gamma$ vertex:

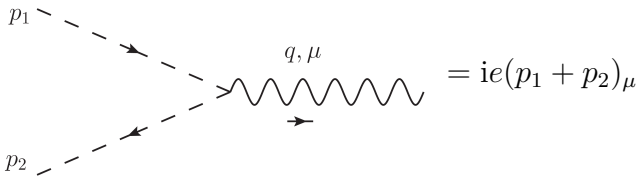

Figure 5: Feynman rule for $2\pi\gamma$ vertex.

- $3\pi\gamma$ vertex:

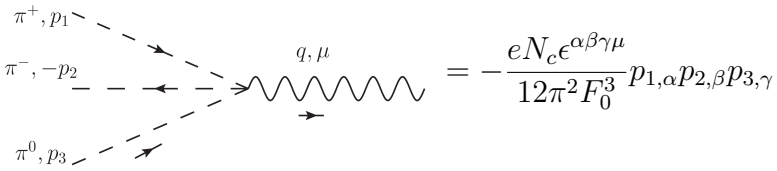

Figure 6: Feynman rule for $3\pi\gamma$ vertex.

- $3\pi 2\gamma$ vertex:

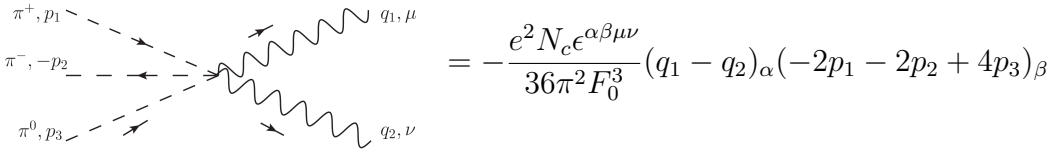

Figure 7: Feynman rule for $3\pi 2\gamma$ vertex.

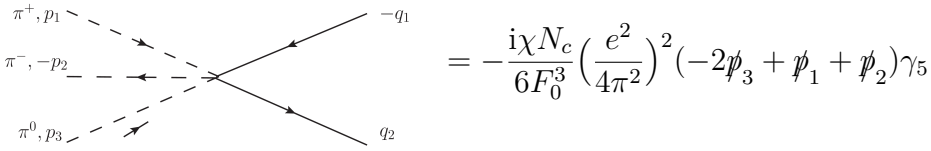

Figure 8: Feynman rule for $3\pi e^+e^-$ vertex.

B IBP identities

In this appendix the set of IBP identities (3.26) are listed individually. They are written in terms of the shifting operators (3.25) and are presented in the form

(3.24) where $i = l, t$ and $j = l, t, q_\pm$

$$
\begin{aligned}
\boldsymbol{O}_{lq_+} =& n_1\mathbf{1}^+(\mathbf{1}^- - \mathbf{3}^- + m^2) + n_3\mathbf{3}^+(-\mathbf{3}^- + \mathbf{1}^- - m^2) \\
&+ n_4\mathbf{4}^+(-\mathbf{3}^- + \mathbf{1}^- - m^2 + 4m^2y) \\
&+ n_7\mathbf{7}^+(-\mathbf{3}^- + \mathbf{1}^- + \mathbf{5}^- - \mathbf{2}^- - m^2),
\end{aligned}
$$

$$
\begin{aligned}
\boldsymbol{O}_{lq_-} =& n_1\mathbf{1}^+(-\mathbf{1}^- + \mathbf{4}^- - m^2) + n_3\mathbf{3}^+(-\mathbf{4}^- - \mathbf{1}^- + m^2 - 4m^2y) \\
&+ n_4\mathbf{4}^+(\mathbf{4}^- - \mathbf{1}^- + m^2) + n_7\mathbf{7}^+(\mathbf{4}^- - \mathbf{1}^- + \mathbf{2}^- - \mathbf{6}^- + m^2),
\end{aligned}
$$

$$
\begin{aligned}
\boldsymbol{O}_{lt} =& n_1\mathbf{1}^+(-\mathbf{1}^- - \mathbf{2}^- + \mathbf{7}^- - m^2) + n_3\mathbf{3}^+(-\mathbf{1}^- + \mathbf{7}^- - \mathbf{5}^- + m^2) \\
&+ n_4\mathbf{4}^+(-\mathbf{1}^- + \mathbf{7}^- - \mathbf{6}^- + m^2) \\
&+ n_7\mathbf{7}^+(-\mathbf{1}^- + \mathbf{2}^- + \mathbf{7}^- - \mathbf{6}^- - 3m^2),
\end{aligned}
$$

$$
\begin{aligned}
\boldsymbol{O}_{ll} =& 2n_1\mathbf{1}^+(-\mathbf{1}^- - 4m^2y) + n_3\mathbf{3}^+(-\mathbf{1}^- - \mathbf{3}^- - 8m^2y + m^2) \\
&+ n_4\mathbf{4}^+(-\mathbf{1}^- - \mathbf{4}^- - 8m^2y + m^2) \\
&+ n_7\mathbf{7}^+(-\mathbf{1}^- + \mathbf{2}^- - \mathbf{7}^- - \mathbf{6}^- - 8m^2y + m^2),
\end{aligned}
$$

$$
\begin{aligned}
\boldsymbol{O}_{tq_+} =& n_2\mathbf{2}^+(-\mathbf{5}^- + \mathbf{2}^- + 2m^2) + n_5\mathbf{5}^+(-\mathbf{5}^- + \mathbf{2}^-) \\
&+ n_6\mathbf{6}^+(-\mathbf{3}^- + \mathbf{2}^- + 4m^2y) + n_7\mathbf{7}^+(\mathbf{1}^- - \mathbf{4}^- - \mathbf{3}^- + \mathbf{2}^- + m^2),
\end{aligned}
$$

$$
\begin{aligned}
\boldsymbol{O}_{tq_-} =& n_2\mathbf{2}^+(-\mathbf{2}^- + \mathbf{6}^- - 2m^2) + n_5\mathbf{5}^+(-\mathbf{6}^- + \mathbf{2}^- + 4m^2y) \\
&+ n_6\mathbf{6}^+(-\mathbf{2}^- + \mathbf{6}^-) + n_7\mathbf{7}^+(\mathbf{1}^- - \mathbf{4}^- - \mathbf{2}^- + \mathbf{6}^- - m^2),
\end{aligned}
$$

$$
\begin{aligned}
\boldsymbol{O}_{tl} =& n_2\mathbf{2}^+(-\mathbf{1}^- - \mathbf{2}^- + \mathbf{7}^- - m^2) + n_5\mathbf{5}^+(-\mathbf{2}^- + \mathbf{7}^- - \mathbf{3}^-) \\
&+ n_6\mathbf{6}^+(-\mathbf{2}^- + \mathbf{7}^- - \mathbf{4}^-) + n_7\mathbf{7}^+(\mathbf{1}^- - \mathbf{2}^- + \mathbf{7}^- + 8m^2y - m^2),
\end{aligned}
$$

$$
\begin{aligned}
\boldsymbol{O}_{tt} =& 2n_2\mathbf{2}^+(-\mathbf{2}^- + m^2) + n_5\mathbf{5}^+(-\mathbf{5}^- - \mathbf{2}^- + 4m^2) \\
&+ n_6\mathbf{6}^+(-\mathbf{2}^- - \mathbf{6}^- + 4m^2) + n_7\mathbf{7}^+(\mathbf{1}^- - \mathbf{2}^- - \mathbf{7}^- + 3m^2).
\end{aligned}
$$

C Generalized Harmonic Polylogarithms

In this appendix we introduce functions by which we expressed two-loop contributions calculated in this thesis in an analytical form.

C.1 Harmonic Polylogarithms

The harmonic polylogarithms (HPL's) [38] are a generalization of the usual polylogarithms and of the Nielsen polylogarithms. These functions are popular in multi-loop calculations because of the ease with which we can perform an analytic continuation to the arbitrary region and their brevity. They are a function

of one variable x and labeled by a vector $a = (a_1, ..., a_n)$. The indices a_i can acquire three different values $0, 1, -1$. The dimension of the vector n is called the weight of the function. The functions through we define HPL's have the form

$$f_0(x) = \frac{1}{x}, \tag{23a}$$

$$f_1(x) = \frac{1}{1-x}, \tag{23b}$$

$$f_{-1}(x) = \frac{1}{1+x}. \tag{23c}$$

Then the HPL's of the weight one are written as

$$\mathrm{HPL}(0; x) = \log(x), \tag{24a}$$

$$\mathrm{HPL}(1; x) = \int_0^x f_1(t)\mathrm{d}t = -\log(1-x), \tag{24b}$$

$$\mathrm{HPL}(-1; x) = \int_0^x f_{-1}(t)\mathrm{d}t = \log(1+x) \tag{24c}$$

and higher weights HPL's can be written schematically by the general formula

$$\mathrm{HPL}(\{0_1, ..., 0_n\}; x) = \frac{1}{n!}\log^n(x), \tag{25a}$$

$$\mathrm{HPL}(\{a, a_1, ..., a_k\}; x) = \int_0^x f_a(t)\mathrm{HPL}(\{a_1, ..., a_k\}; t)\mathrm{d}t. \tag{25b}$$

Let us also introduce the linear combinations of the HPL's because of the maximal brevity of the solution

$$\mathrm{HPL}(+; x) = \mathrm{HPL}(1; x) + \mathrm{HPL}(-1; x), \tag{26a}$$

$$\mathrm{HPL}(-; x) = \mathrm{HPL}(1; x) - \mathrm{HPL}(-1; x), \tag{26b}$$

$$\mathrm{HPL}(\{\pm, a_1, ..., a_k\}; x) = \mathrm{HPL}(\{1, a_1, ..., a_k\}; x) \pm \mathrm{HPL}(\{-1, a_1, ..., a_k\}; x). \tag{26c}$$

As one can imagine, in the calculation of multi-loop Feynman diagrams by the differential equation technique, we often encounter the integral consist of the HPL's and polynomials. The integrals which are possible to express after the integration as a product of the HPL's and polynomials can be derived from (25) and have the form

$$\begin{aligned} &\int \frac{Ct^i}{(1-t^2)^k}\mathrm{HPL}(...; t)\mathrm{d}t, \\ &\int \frac{Ct^i}{(1-t)^k}\mathrm{HPL}(...; t)\mathrm{d}t, \\ &\int \frac{Ct^i}{(1+t)^k}\mathrm{HPL}(...; t)\mathrm{d}t, \\ &\int Ct^i\mathrm{HPL}(...; t)\mathrm{d}t. \end{aligned} \tag{27}$$

where C is an arbitrary constant and $k > 0$ is an integer.

As another important rule consider the product of two HPL's. Imagine, we have two arbitrary HPL's $\mathrm{HPL}(\{u_1,.....,u_{q1}\};x)$ and $\mathrm{HPL}(\{v_2,.....,v_{q2}\};x)$. Then their product can be decomposed as

$$\begin{aligned}\mathrm{HPL}(\{u_1,.....,u_{q1}\};x)\mathrm{HPL}(\{v_2,.....,u_{q2}\};x) &= \mathrm{HPL}(\mathbf{u};x)\mathrm{HPL}(\mathbf{v};x)\\ &= \sum_{\mathbf{w}\in\mathbf{u}\uplus\mathbf{v}}\mathrm{HPL}(\mathbf{w},x),\end{aligned} \tag{28}$$

where $\mathbf{u}\uplus\mathbf{v}$ means all possible combinations of $\mathbf{u}$ and $\mathbf{v}$ where the internal order of both components of vectors is preserved. For example, for vectors $\mathbf{u}=(a,b)$ and $\mathbf{v}=(c,d)$ we have

$$\begin{aligned}\mathrm{HPL}(\{a,b\};x)H(\{c,d\};x) &= \mathrm{HPL}(\{a,b,c,d\};x)+\mathrm{HPL}(\{a,c,d,b\};x)\\ &+\mathrm{HPL}(\{c,a,b,d\};x)+\mathrm{HPL}(\{c,a,d,b\};x)\\ &+\mathrm{HPL}(\{c,d,a,b\};x)+\mathrm{HPL}(\{a,c,b,d\};x).\end{aligned} \tag{29}$$

HPL's with its properties are implemented to various programming languages such as Mathematica [39], FORTRAN [40] and C++ [41].

C.2 Generalized Harmonic Polylogarithms

Unfortunately, there exist cases when the indices $0,1$ and -1 of a_i are not sufficient to describe a particular Feynman diagram. In this situation we are forced to find all the remaining singularities occurring in our calculations and define generalized harmonic polylogarithms (GHPL's) [42]. Let us illustrate this process on our particular case. In the appendix E.3 we calculate three MI of four propagator topology in kinematical variable

$$z=-\frac{\sqrt{1-\frac{1}{y}}-1}{\sqrt{1-\frac{1}{y}}+1}. \tag{30}$$

As we can see in 0th order appear harmonic polylogarithms with new indices a and $-a$ corresponding to the functions through we define HPL's

$$f_a(z)=\frac{1}{(-\frac{1}{2}+\frac{\mathrm{i}\sqrt{3}}{2})-z}, \tag{31a}$$

$$f_{-a}(z)=\frac{1}{(\frac{1}{2}+\frac{\mathrm{i}\sqrt{3}}{2})+z}. \tag{31b}$$

Singularities of this functions are roots of the equation $1+z+z^2=0$ and lie on a complex unit circle deviated from real axis by 120 ° and 240 ° respectively. GHPL's of the weight one have then the form

$$\mathrm{HPL}(a;z)=\int_0^z f_a(t)\mathrm{d}t=-\log((-\frac{1}{2}+\frac{\mathrm{i}\sqrt{3}}{2})-z)+\log(-\frac{1}{2}+\frac{\mathrm{i}\sqrt{3}}{2}), \tag{32a}$$

$$\mathrm{HPL}(-a;z)=\int_0^z f_{-a}(t)\mathrm{d}t=\log((\frac{1}{2}+\frac{\mathrm{i}\sqrt{3}}{2})+z)-\log(\frac{1}{2}+\frac{\mathrm{i}\sqrt{3}}{2}). \tag{32b}$$

GHPL's obey same properties as was discussed for HPL's. In addition to integrals (27) we are able to calculate integrals of the form

$$\int \frac{Ct^i}{(1+t+t^2)^k}\mathrm{HPL}(...;t)\mathrm{d}t, \tag{33a}$$

$$\int \frac{Ct^i}{((-\frac{1}{2}+\frac{\mathrm{i}\sqrt{3}}{2})-t)^k}\mathrm{HPL}(...;t)\mathrm{d}t, \tag{33b}$$

$$\int \frac{Ct^i}{((\frac{1}{2}+\frac{\mathrm{i}\sqrt{3}}{2})+t)^k}\mathrm{HPL}(...;t)\mathrm{d}t. \tag{33c}$$

Finally, let us give the example where the usefulness of the GHPL's is illustrated. Consider that we want to substitute variable z for variable x in the term $\mathrm{HPL}(\{\mathrm{minus},0\},x)$ (this example is used in our calculations). Firstly, we rewrite this term to the integral form in the variable z

$$\begin{aligned}\mathrm{HPL}(\{\mathrm{minus},0\},x) =&\mathrm{HPL}(\{1,0\},\sqrt{\frac{z}{(1+z)^2}})-\mathrm{HPL}(\{-1,0\},\sqrt{\frac{z}{(1+z)^2}})\\ =&\int_0^z \mathrm{d}z\,\log\Big(\frac{\sqrt{z}}{(1+z)}\Big)\frac{2z}{\sqrt{\frac{z}{(z+1)^2}}\,(z^2+z+1)}\\ &\times\Big(-\frac{z-1}{2\sqrt{\frac{z}{(z+1)^2}}(z+1)^3}\Big),\end{aligned} \tag{34}$$

where the last factor comes from the differential $\mathrm{d}x$. This equation can be further simplified to the form

$$\mathrm{HPL}(\{\mathrm{minus},0\},x)=\int_0^z \mathrm{d}z\Big(\frac{\log(z)}{2}-\log(1+z)\Big)\frac{1-z}{(z+1)\,(z^2+z+1)}. \tag{35}$$

Here we see in the denominator polynomial (z^2+z+1) which roots define GHPL's of our particular case. If we expand further equation (35) in the sense of complex numbers, we get

$$\begin{aligned}\mathrm{HPL}(\{\mathrm{minus},0\},x) =&\int_0^z \mathrm{d}z\,\Big(\frac{\log(z)}{2}-\log(1+z)\Big)\\ &\times(-\frac{1}{z+(\frac{1}{2}+\frac{\mathrm{i}\sqrt{3}}{2})}+\frac{1}{-z+(-\frac{1}{2}+\frac{\mathrm{i}\sqrt{3}}{2})}+\frac{2}{z+1}).\end{aligned} \tag{36}$$

As one can observe this equation can be written in terms of HPL's and GHPL's introduced above. The final formula reads then

$$\begin{aligned}\mathrm{HPL}(\{\mathrm{minus},0\},x) =&\frac{1}{2}\Big(2\mathrm{HPL}(\{-a,-1\},z)-\mathrm{HPL}(\{-a,0\},z)\\ &-2\mathrm{HPL}(\{a,-1\},z)+\mathrm{HPL}(\{a,0\},z)\\ &-\mathrm{HPL}(\{\mathrm{minus},0\},z)+\mathrm{HPL}(\{\mathrm{plus},0\},z)\\ &-4\mathrm{HPL}(\{-1,-1\},z)\Big).\end{aligned} \tag{37}$$

D Decomposition to master integrals

In this appendix we list the decomposition of non-master B functions contributing to P^{NLO} in terms of master integrals

$$\begin{aligned}
B(0,1,1,0,-1,1,1) =&\frac{1}{2m^2y}\Big(4m^4yB(0,1,0,1,1,0,1)\\
&+2m^2(-2yB(-1,1,0,1,1,0,1)\\
&-(y-1)B(0,0,0,1,1,0,1))+2y(B(0,1,0,0,0,0,1)\\
&+B(0,1,1,0,0,0,0))-2B(-1,0,0,1,1,0,1)\\
&-B(0,-1,0,1,1,0,1)+B(0,0,1,0,0,0,1)\Big)\\
&+\frac{\epsilon}{m^2}\Big(B(0,1,0,0,0,0,1)+B(0,1,1,0,0,0,0)\Big)\\
&+\frac{2\epsilon^2}{m^2}\Big(B(0,1,0,0,0,0,1)+B(0,1,1,0,0,0,0)\Big)+O\left(\epsilon^3\right),
\end{aligned}$$

$$\begin{aligned}
B(0,1,1,0,1,-1,1) =&\frac{1}{8m^2\epsilon}\Big(3(-4m^2yB(0,1,1,0,0,0,1)-B(-1,1,1,0,0,0,1)\\
&+B(0,0,1,0,0,0,1)+B(0,1,0,0,0,0,1)\\
&+B(0,1,1,0,0,0,0))\Big)-\frac{1}{8m^2}\Big(-9m^2B(0,1,1,0,0,0,1)\\
&-3B(-1,1,1,0,0,0,1)-3B(0,0,1,0,0,0,1)\\
&+B(0,1,0,0,0,0,1)+B(0,1,1,0,0,0,0)\Big)\\
&+\frac{\epsilon}{4m^2}\Big(3B(0,0,1,0,0,0,1)+B(0,1,0,0,0,0,1)\\
&+B(0,1,1,0,0,0,0)\Big)+\frac{\epsilon^2}{2m^2}\Big(3B(0,0,1,0,0,0,1)\\
&+B(0,1,0,0,0,0,1)+B(0,1,1,0,0,0,0)\Big)+O\left(\epsilon^3\right),
\end{aligned}$$

$$\begin{aligned}
B(0,1,1,0,1,1,1) =&\frac{3}{128m^6y^2\epsilon}\Big(-4m^2yB(0,1,1,0,0,0,1)-B(-1,1,1,0,0,0,1)\\
&+B(0,0,1,0,0,0,1)+B(0,1,0,0,0,0,1)\\
&+B(0,1,1,0,0,0,0)\Big)\\
&-\frac{1}{128\left(m^6y^3\right)}\Big(8m^2yB(-1,1,0,1,1,0,1)\\
&+y(m^2(8m^2(4y-1)B(0,1,0,1,1,0,1)\\
&-32m^2yB(0,1,1,0,1,1,0)+(3-64y)B(0,1,1,0,0,0,1)\\
&+4B(0,0,0,1,1,0,1)+8B(0,1,-1,1,1,0,1))\\
&-15B(-1,1,1,0,0,0,1)+13B(0,0,1,0,0,0,1)\\
&+B(0,1,0,0,0,0,1)+9B(0,1,1,0,0,0,0))\\
&-4m^2B(0,0,0,1,1,0,1)+4B(-1,0,0,1,1,0,1)
\end{aligned}$$

$$
\begin{aligned}
&+ 2B(0,-1,0,1,1,0,1) - 2B(0,0,1,0,0,0,1)\Big) \\
&+ \frac{\epsilon}{64m^6y^3}\Big(8m^2yB(-1,1,0,1,1,0,1) \\
&+ y(2m^2(4m^2(8y-1)B(0,1,0,1,1,0,1) \\
&- 8m^2yB(0,1,1,0,1,1,0) + (1-16y)B(0,1,1,0,0,0,1) \\
&+ 2B(0,0,0,1,1,0,1) + 2B(0,1,-1,1,1,0,1)) \\
&- 6B(-1,1,1,0,0,0,1) + 3B(0,0,1,0,0,0,1) \\
&+ B(0,1,0,0,0,0,1) + B(0,1,1,0,0,0,0))+ \\
&2(-2m^2B(0,0,0,1,1,0,1) + B(0,-1,0,1,1,0,1) \\
&- B(0,0,1,0,0,0,1)) + 4B(-1,0,0,1,1,0,1)\Big) \\
&- \frac{\epsilon^2}{32(m^6y^2)}\Big((B(0,0,1,0,0,0,1) - B(0,1,0,0,0,0,1) \\
&+ B(0,1,1,0,0,0,0)\Big) + O\left(\epsilon^3\right),
\end{aligned}
$$

$$
\begin{aligned}
B(0,1,1,0,-2,1,1) =& \frac{1}{3}(-32m^4(y-2)yB(0,1,0,1,1,0,1) \\
&- 64m^2yB(-1,1,0,1,1,0,1) \\
&- 32m^2(y-1)B(0,0,0,1,1,0,1) \\
&+ 6m^2(1-4y)B(0,1,1,0,0,0,1) \\
&+ 30yB(0,1,0,0,0,0,1) + 30yB(0,1,1,0,0,0,0) \\
&- 32B(-1,0,0,1,1,0,1) - 6B(-1,1,1,0,0,0,1) \\
&- 16B(0,-1,0,1,1,0,1) + 19B(0,0,1,0,0,0,1) \\
&+ 3(B(0,1,0,0,0,0,1) + B(0,1,1,0,0,0,0))) \\
&+ \frac{2}{3}\epsilon(4m^2yB(-1,1,0,1,1,0,1) \\
&+ 2m^2(y-1)B(0,0,0,1,1,0,1) \\
&+ 2y(-2m^4(4y+1)B(0,1,0,1,1,0,1) \\
&+ 2m^2B(0,1,1,0,0,0,1) \\
&+ 7B(0,1,0,0,0,0,1) + 7B(0,1,1,0,0,0,0)) \\
&+ 2B(-1,0,0,1,1,0,1) + B(0,-1,0,1,1,0,1) \\
&- B(0,0,1,0,0,0,1)) + \frac{2}{3}\epsilon^2(4m^2yB(-1,1,0,1,1,0,1) \\
&+ 2m^2(y-1)B(0,0,0,1,1,0,1) \\
&+ 4y(m^4(-(4y+1))B(0,1,0,1,1,0,1) \\
&+ m^2B(0,1,1,0,0,0,1) + 7B(0,1,0,0,0,0,1) \\
&+ 7B(0,1,1,0,0,0,0)) + 2B(-1,0,0,1,1,0,1) \\
&+ B(0,-1,0,1,1,0,1) - B(0,0,1,0,0,0,1)) + O(\epsilon^3),
\end{aligned}
$$

$$
B(0,1,1,0,1,0,1) = \frac{3}{32m^4y\epsilon}\Big(- 4m^2yB(0,1,1,0,0,0,1)
$$

$$
\begin{aligned}
&- B(-1,1,1,0,0,0,1) + B(0,0,1,0,0,0,1) \\
&+ B(0,1,0,0,0,0,1) + B(0,1,1,0,0,0,0)\Big) \\
&- \frac{1}{32\,(m^4 y)}\Big(m^2(-(16y+1))B(0,1,1,0,0,0,1) \\
&- 3B(-1,1,1,0,0,0,1) + B(0,0,1,0,0,0,1) \\
&+ B(0,1,0,0,0,0,1) + B(0,1,1,0,0,0,0)\Big) \\
&+ \frac{\epsilon}{16m^4 y}\Big(B(0,0,1,0,0,0,1) + B(0,1,0,0,0,0,1) \\
&+ B(0,1,1,0,0,0,0)\Big) + \frac{\epsilon^2}{8m^4 y}\Big(B(0,0,1,0,0,0,1) \\
&+ B(0,1,0,0,0,0,1) + B(0,1,1,0,0,0,0)\Big) \\
&+ O\left(\epsilon^3\right),
\end{aligned}
$$

$$
\begin{aligned}
B(0,1,1,0,0,-1,1) =& 2m^2 B(0,1,1,0,0,0,1) + (4y-2)B(-1,1,1,0,0,0,1) \\
&- (2y-1)(B(0,1,0,0,0,0,1) + B(0,1,1,0,0,0,0)) \\
&+ B(0,0,1,0,0,0,1),
\end{aligned}
$$

$$
\begin{aligned}
B(0,1,1,0,-1,0,1) =& 2m^2 B(0,1,1,0,0,0,1) - 2B(-1,1,1,0,0,0,1) \\
&+ B(0,0,1,0,0,0,1) + B(0,1,0,0,0,0,1) \\
&+ B(0,1,1,0,0,0,0),
\end{aligned}
$$

E Results for MI

In this appendix we list the analytical results for the individual MI's listed in the table 3.1. Note that some results are listed in the different basis as the original one. We do not list the transformation formulas of these basis explicitly since some of them are extremely long. However, all of these formulas are known.

E.1 Two propagator topology

This topology contains two MI's depicted in the figure 9. Both MI's can be calculated by Feynman parametrization technique with results

$$
b_1 = \frac{(4y)^{1-\epsilon}\Gamma(\epsilon-1)^2}{\Gamma(\epsilon+1)^2}, \tag{38}
$$

$$
b_2 = \frac{(16y^2)^{1-\epsilon}\Gamma(\epsilon-1)^2}{\Gamma(\epsilon+1)^2}. \tag{39}
$$

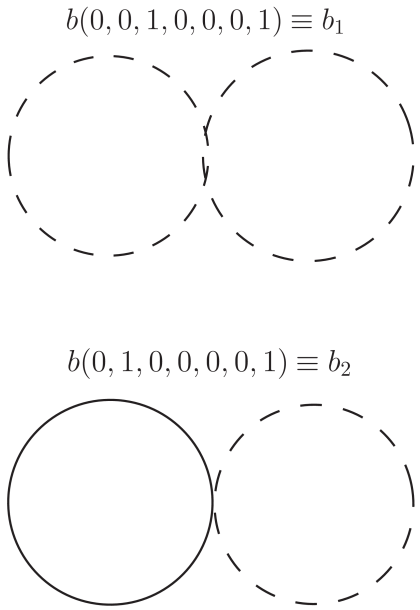

Figure 9: Two propagator topology

These results have the following expansions (in the variable z)

$$
\begin{aligned}
b_1^{(-2)} =& \frac{(z+1)^4}{z^2} \\
b_1^{(-1)} =& -\frac{4(z+1)^4\mathrm{HPL}(\{-1\},z)}{z^2} + \frac{2(z+1)^4\mathrm{HPL}(\{0\},z)}{z^2} + \frac{2(z+1)^4}{z^2} \\
b_1^{(0)} =& \frac{8(z+1)^4\mathrm{HPL}(\{-1\},z)^2}{z^2} + \frac{2(z+1)^4\mathrm{HPL}(\{0\},z)^2}{z^2} \\
&+ \frac{4(z+1)^4\mathrm{HPL}(\{0\},z)}{z^2} + \mathrm{HPL}(\{-1\},z)(-\frac{8(z+1)^4\mathrm{HPL}(\{0\},z)}{z^2} \\
&- \frac{8(z+1)^4}{z^2}) + \frac{3(z+1)^4}{z^2} \\
b_1^{(1)} =& -\frac{32(z+1)^4\mathrm{HPL}(\{-1\},z)^3}{3z^2} + \frac{4(z+1)^4\mathrm{HPL}(\{0\},z)^3}{3z^2} \\
&+ \frac{4(z+1)^4\mathrm{HPL}(\{0\},z)^2}{z^2} + \frac{6(z+1)^4\mathrm{HPL}(\{0\},z)}{z^2} \\
&+ \mathrm{HPL}(\{-1\},z)^2(\frac{16(z+1)^4\mathrm{HPL}(\{0\},z)}{z^2} + \frac{16(z+1)^4}{z^2}) \\
&+ \mathrm{HPL}(\{-1\},z)(-\frac{8(z+1)^4\mathrm{HPL}(\{0\},z)^2}{z^2} - \frac{16(z+1)^4\mathrm{HPL}(\{0\},z)}{z^2} \\
&- \frac{12(z+1)^4}{z^2}) + \frac{4(z+1)^4}{z^2}.
\end{aligned}
$$

$$
\begin{aligned}
b_2^{(-2)} =& z + \frac{1}{z} + 2 \\
b_2^{(-1)} =& -\frac{2(z+1)^2\mathrm{HPL}(\{-1\},z)}{z} + (z + \frac{1}{z} + 2)\mathrm{HPL}(\{0\},z) + \frac{2(z+1)^2}{z}
\end{aligned}
$$

$$
\begin{aligned}
b_2^{(0)} =& \frac{2(z+1)^2\mathrm{HPL}(\{-1\},z)^2}{z} + \frac{(z+1)^2\mathrm{HPL}(\{0\},z)^2}{2z} \\
&+ \frac{2(z+1)^2\mathrm{HPL}(\{0\},z)}{z} + \mathrm{HPL}(\{-1\},z)(-\frac{2(z+1)^2\mathrm{HPL}(\{0\},z)}{z} \\
&- \frac{4(z+1)^2}{z}) + \frac{3(z+1)^2}{z} \\
b_2^{(1)} =& \frac{4(\mathrm{HPL}(\{0\},x)(4\mathrm{HPL}(\{0\},x)(2\mathrm{HPL}(\{0\},x)+3)+9)+3)}{3x^4}.
\end{aligned}
$$

E.2 Three propagator topology, type a

$b(0,0,0,1,1,0,1) \equiv b_1$

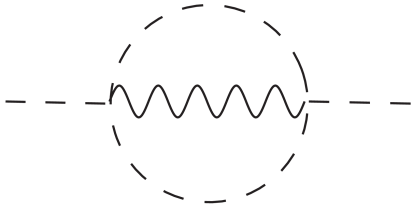

$b(-1,0,0,1,1,0,1) \equiv b_2$

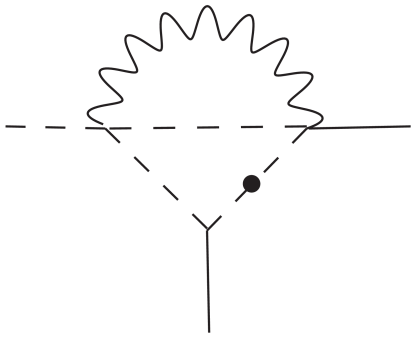

$b(0,-1,0,1,1,0,1) \equiv b_3$

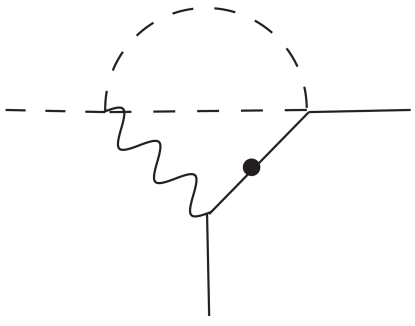

Figure 10: Three propagator topology, type a

There are three MI's in this topology depicted in the figure 10. The pioneering calculation for these types of diagrams was done in [36]. The basis in which the calculation was done is following

$$r_1 \equiv b(0,0,0,1,1,0,1)$$

$$r_2 \equiv b(0,0,0,3,1,0,1)$$

$$r_3 \equiv b(0,0,0,2,1,0,2).$$

The result expressed in Laurent expansion reads then (in the variable z)

$$\begin{aligned}
r_1^{(-2)} =& z + \frac{1}{z} + 2 \\
r_1^{(-1)} =& -\frac{4(z+1)^2\mathrm{HPL}(\{-1\},z)}{z} + \frac{2(z+1)^2\mathrm{HPL}(\{0\},z)}{z} + \frac{11(z+1)^2}{4z} \\
r_1^{(0)} =& \frac{8(z+1)^2\mathrm{HPL}(\{-1\},z)^2}{z} + \frac{2(z+1)^2\mathrm{HPL}(\{0\},z)^2}{z} \\
&+ \frac{11(z+1)^2\mathrm{HPL}(\{0\},z)}{2z} + \mathrm{HPL}(\{-1\},z)(-\frac{8(z+1)^2\mathrm{HPL}(\{0\},z)}{z} \\
&- \frac{11(z+1)^2}{z}) + \frac{(35+4\sqrt{3}\pi)(z+1)^2}{8z} \\
r_1^{(1)} =& -\frac{32(z+1)^2\mathrm{HPL}(\{-1\},z)^3}{3z} + (\frac{16(z+1)^2\mathrm{HPL}(\{0\},z)}{z} \\
&+ \frac{22(z+1)^2}{z})\mathrm{HPL}(\{-1\},z)^2 + (-\frac{8(z+1)^2\mathrm{HPL}(\{0\},z)^2}{z} \\
&- \frac{22(z+1)^2\mathrm{HPL}(\{0\},z)}{z} - \frac{(35+4\sqrt{3}\pi)(z+1)^2}{2z})\mathrm{HPL}(\{-1\},z) \\
&+ \frac{4(z+1)^2\mathrm{HPL}(\{0\},z)^3}{3z} + \frac{11(z+1)^2\mathrm{HPL}(\{0\},z)^2}{2z} \\
&+ \frac{(35+4\sqrt{3}\pi)(z+1)^2\mathrm{HPL}(\{0\},z)}{4z} \\
&+ \frac{(z+1)^2(324S_2+5-4\sqrt{3}\pi(\log(729)-13))}{16z}.
\end{aligned}$$

$$\begin{aligned}
r_2^{(-1)} =& -\frac{z}{2(z+1)^2} \\
r_2^{(0)} =& \frac{2z\mathrm{HPL}(\{-1\},z)}{(z+1)^2} - \frac{z\mathrm{HPL}(\{0\},z)}{(z+1)^2} + \frac{(\sqrt{3}\pi-6)z}{6(z+1)^2} \\
r_2^{(1)} =& -\frac{4z\mathrm{HPL}(\{-1\},z)^2}{(z+1)^2} + (\frac{4z\mathrm{HPL}(\{0\},z)}{(z+1)^2} \\
&- \frac{2(\sqrt{3}\pi-6)z}{3(z+1)^2})\mathrm{HPL}(\{-1\},z) - \frac{z\mathrm{HPL}(\{0\},z)^2}{(z+1)^2} \\
&+ \frac{(\sqrt{3}\pi-6)z\mathrm{HPL}(\{0\},z)}{3(z+1)^2} + \frac{z(9(27S_2-8)+\pi^2-6\sqrt{3}\pi(\log(27)-2))}{36(z+1)^2}.
\end{aligned}$$

$$r_3^{(0)} = -\frac{\pi^2 z}{9(z+1)^2}$$

$$r_3^{(1)} = \frac{4\pi^2 z \mathrm{HPL}(\{-1\}, z)}{9(z+1)^2} - \frac{2\pi^2 z \mathrm{HPL}(\{0\}, z)}{9(z+1)^2} + \frac{2z\zeta(3)}{3(z+1)^2}.$$

E.3 Three propagator topology, type b

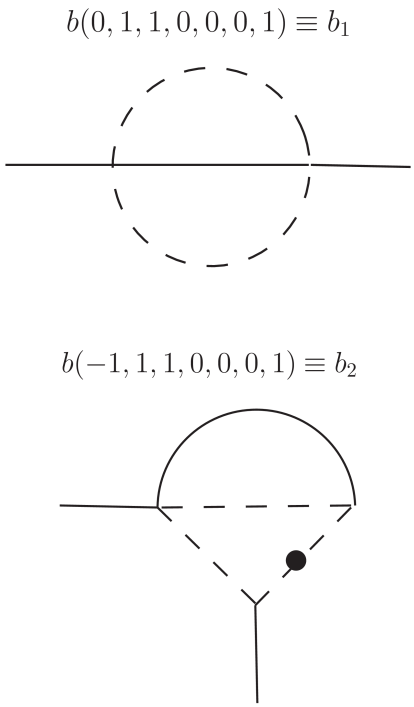

Figure 11: Three propagator topology, type b

There are two MI's in this topology depicted in the figure 11. An integration constant was fixed from [14], where these integrals were calculated in the limit $x \to \infty$ and $x \to 1$. The basis in which the calculation was done is following

$$r_1 \equiv b(0,1,2,0,0,0,1)$$

$$r_2 \equiv b(-1,2,2,0,0,0,1)$$

The result expressed in Laurent expansion reads then (in the variable x)

$$\begin{aligned}
r_1^{(-2)} =& \frac{1}{2} \\
r_1^{(-1)} =& 2\mathrm{HPL}(\{0\}, x) + \frac{1}{2} \\
r_1^{(0)} =& (2 - \frac{2}{x^2})\mathrm{HPL}(\{\mathrm{minus}, 0\}, x) + 4\mathrm{HPL}(\{0\}, x) + 8\mathrm{HPL}(\{0,0\}, x) - \frac{1}{2} \\
r_1^{(1)} =& (6 - \frac{2}{x^2})\mathrm{HPL}(\{\mathrm{minus}, 0\}, x) - \frac{12\mathrm{HPL}(\{0, \mathrm{minus}, 0\}, x)}{x^2} \\
& - \frac{12\mathrm{HPL}(\{\mathrm{minus}, 0, 0\}, x)}{x^2} - \frac{6\mathrm{HPL}(\{\mathrm{minus}, \mathrm{minus}, 0\}, x)}{x^2}
\end{aligned}$$

$$
\begin{aligned}
&+ 12\mathrm{HPL}(\{0,\mathrm{minus},0\},x) + 12\mathrm{HPL}(\{\mathrm{minus},0,0\},x)\\
&+ 6\mathrm{HPL}(\{\mathrm{minus},\mathrm{minus},0\},x) + \frac{2\mathrm{HPL}(\{\mathrm{plus},\mathrm{plus},0\},x)}{x^2}\\
&- \frac{4\mathrm{HPL}(\{\mathrm{plus},0\},x)}{x} - 2\mathrm{HPL}(\{\mathrm{plus},\mathrm{plus},0\},x) + 8\mathrm{HPL}(\{0\},x)\\
&+ 20\mathrm{HPL}(\{0,0\},x) + 32\mathrm{HPL}(\{0,0,0\},x) - \frac{11}{2}.
\end{aligned}
$$

$$
\begin{aligned}
r_2^{(-2)} =& 1\\
r_2^{(-1)} =& 2\mathrm{HPL}(\{0\},x)\\
r_2^{(0)} =& \mathrm{HPL}(\{\mathrm{minus},0\},x) - \frac{2\mathrm{HPL}(\{\mathrm{plus},0\},x)}{x} + 4\mathrm{HPL}(\{0\},x)\\
&+ 4\mathrm{HPL}(\{0,0\},x) - 4.
\end{aligned}
$$

E.4 Three propagator topology, type c

$$b(0,0,1,0,1,1,0) \equiv b_1$$

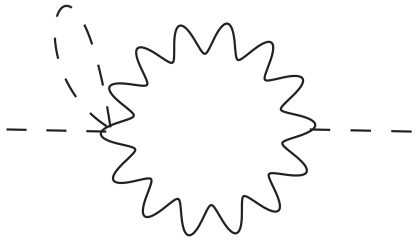

Figure 12: Three propagator topology, type c

This topology contain one MI depicted in the figure 12. This MI can be calculated by Feynman parametrization technique with results

$$b_1 = -\frac{1}{(-1+\epsilon)}\frac{x^{4\epsilon}}{\epsilon^2 x^2} \tag{43}$$

The result expressed in Laurent expansion reads then (in the variable x)

$$
\begin{aligned}
b_1^{(-2)} =& \frac{1}{x^2}\\
b_1^{(-1)} =& \frac{4\mathrm{HPL}(\{0\},x)}{x^2} + \frac{1}{x^2}\\
b_1^{(0)} =& \frac{8\mathrm{HPL}(\{0\},x)^2}{x^2} + \frac{4\mathrm{HPL}(\{0\},x)}{x^2} + \frac{1}{x^2}\\
b_1^{(1)} =& \frac{32\mathrm{HPL}(\{0\},x)^3}{3x^2} + \frac{8\mathrm{HPL}(\{0\},x)^2}{x^2} + \frac{4\mathrm{HPL}(\{0\},x)}{x^2} + \frac{1}{x^2}.
\end{aligned}
$$

E.5 Four propagator topology, type a

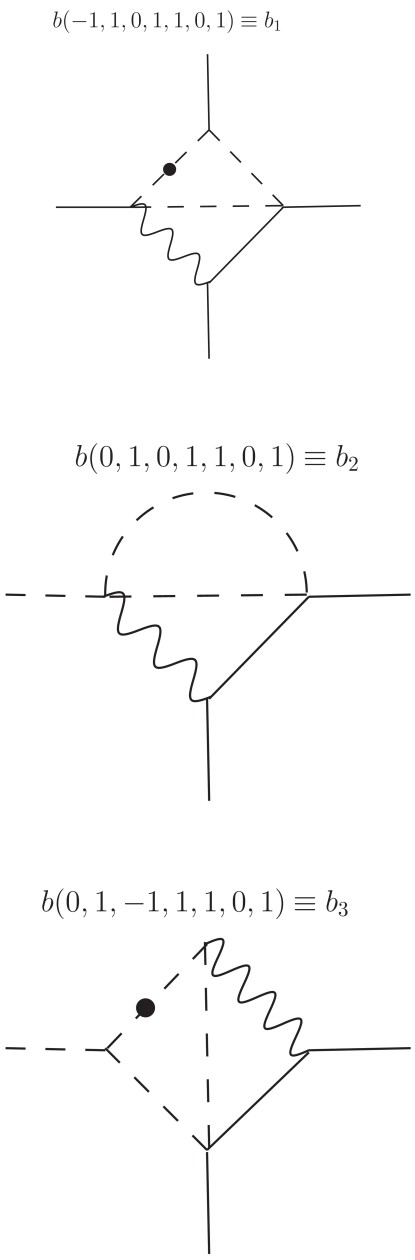

Figure 13: Four propagator topology, type a

As we can see in the figure 13, there are three MI's in this topology. The suitable point for fixing integration constants is $z = 1$. Instead of original basis we use the more appropriate basis

$$r_1 \equiv b(0,1,0,2,1,0,1)$$

$$r_2 \equiv b(0,1,0,1,1,0,2)$$

$$r_3 \equiv b(0,2,0,1,1,0,1).$$

These integrals have the following Laurent expansion (in z variable)

$$
\begin{aligned}
r_1^{(0)} =&\frac{2z\mathrm{HPL}(\{0,-a,-1\},z)}{z^2-1}+\frac{z\mathrm{HPL}(\{0,-a,0\},z)}{1-z^2}-\frac{2z\mathrm{HPL}(\{0,a,-1\},z)}{z^2-1}\\
&+\frac{z\mathrm{HPL}(\{0,a,0\},z)}{z^2-1}+\frac{z\mathrm{HPL}(\{0,\mathrm{minus},0\},z)}{1-z^2}\\
&+\frac{z\mathrm{HPL}(\{0,\mathrm{plus},0\},z)}{z^2-1}+\frac{\pi^2 z\mathrm{HPL}(\{0\},z)}{18-18z^2}-\frac{4z\mathrm{HPL}(\{-2,-1\},z)}{z^2-1}\\
&+\frac{1}{54(1-z^2)}\Big(z(-9(24(\mathrm{Li}_3(\frac{1}{6}(3-i\sqrt{3}))+\mathrm{Li}_3(\frac{1}{6}(3+i\sqrt{3})))\\
&+3(\mathrm{Li}_2(\frac{1}{6}(1-i\sqrt{3}))+2\mathrm{Li}_2(\frac{1}{6}(3-i\sqrt{3}))\\
&+4\mathrm{Li}_2(\frac{1}{6}(3+i\sqrt{3}))-2\mathrm{Li}_2(\frac{1}{6}i(3i+\sqrt{3})))\log(3)+2\log^3(3))\\
&-2\pi(-18i(3\mathrm{Li}_2(-\frac{i}{\sqrt{3}})-3\mathrm{Li}_2(\frac{i}{\sqrt{3}})+\mathrm{Li}_2(\frac{3}{4}-\frac{i\sqrt{3}}{4})\\
&-2\mathrm{Li}_2(\frac{1}{6}(3-i\sqrt{3}))+2\mathrm{Li}_2(\frac{1}{6}(3+i\sqrt{3}))-\mathrm{Li}_2(\frac{1}{4}(3+i\sqrt{3})))+\\
&\sqrt{3}\psi^{(1)}(\frac{1}{6})+\sqrt{3}\psi^{(1)}(\frac{1}{3})-\sqrt{3}\psi^{(1)}(\frac{2}{3})\\
&-\sqrt{3}\psi^{(1)}(\frac{5}{6}))+240\zeta(3)+6\pi^2\log\Big(\frac{16}{3}\Big)\Big)\Big).
\end{aligned}
$$

$$
\begin{aligned}
r_2^{(0)} =&\frac{2z\mathrm{HPL}(\{0,-a,-1\},z)}{z^2-1}+\frac{z\mathrm{HPL}(\{0,-a,0\},z)}{1-z^2}-\frac{2z\mathrm{HPL}(\{0,a,-1\},z)}{z^2-1}\\
&+\frac{z\mathrm{HPL}(\{0,a,0\},z)}{z^2-1}+\frac{z\mathrm{HPL}(\{0,\mathrm{minus},0\},z)}{1-z^2}\\
&+\frac{z\mathrm{HPL}(\{0,\mathrm{plus},0\},z)}{z^2-1}+\frac{\pi^2 z\mathrm{HPL}(\{0\},z)}{18-18z^2}-\frac{4z\mathrm{HPL}(\{-2,-1\},z)}{z^2-1}\\
&+\frac{1}{54(1-z^2)}\Big(z(-9(24(\mathrm{Li}_3(\frac{1}{6}(3-i\sqrt{3}))+\mathrm{Li}_3(\frac{1}{6}(3+i\sqrt{3})))\\
&+3(\mathrm{Li}_2(\frac{1}{6}(1-i\sqrt{3}))+2\mathrm{Li}_2(\frac{1}{6}(3-i\sqrt{3}))\\
&+4\mathrm{Li}_2(\frac{1}{6}(3+i\sqrt{3}))-2\mathrm{Li}_2(\frac{1}{6}i(3i+\sqrt{3})))\log(3)+2\log^3(3))\\
&-2\pi(-18i(3\mathrm{Li}_2(-\frac{i}{\sqrt{3}})-3\mathrm{Li}_2(\frac{i}{\sqrt{3}})+\mathrm{Li}_2(\frac{3}{4}-\frac{i\sqrt{3}}{4})\\
&-2\mathrm{Li}_2(\frac{1}{6}(3-i\sqrt{3}))+2\mathrm{Li}_2(\frac{1}{6}(3+i\sqrt{3}))-\mathrm{Li}_2(\frac{1}{4}(3+i\sqrt{3})))+\\
&\sqrt{3}\psi^{(1)}(\frac{1}{6})+\sqrt{3}\psi^{(1)}(\frac{1}{3})-\sqrt{3}\psi^{(1)}(\frac{2}{3})\\
&-\sqrt{3}\psi^{(1)}(\frac{5}{6}))+240\zeta(3)+6\pi^2\log\Big(\frac{16}{3}\Big)\Big)\Big).
\end{aligned}
$$

$$
\begin{aligned}
r_3^{(-2)} =&\frac{1}{2}\\
r_3^{(-1)} =&\frac{(z+1)\mathrm{HPL}(\{\mathrm{minus}\},z)}{2(z-1)}+\frac{(z+1)\mathrm{HPL}(\{\mathrm{plus}\},z)}{2-2z}
\end{aligned}
$$

$$
\begin{aligned}
&+\frac{2\mathrm{HPL}(\{-1\},z)}{z-1}+\frac{1}{2}\mathrm{HPL}(\{0\},z)-\frac{\pi}{2\sqrt{3}}+1\\
r_3^{(0)}=&\frac{((-1-i\sqrt{3})z-i\sqrt{3}+1)\mathrm{HPL}(\{-a,-1\},z)}{z-1}\\
&+\frac{(i\sqrt{3}z+z+i\sqrt{3}-1)\mathrm{HPL}(\{-a,0\},z)}{2(z-1)}\\
&+\frac{(-i\sqrt{3}z+z-i\sqrt{3}-1)\mathrm{HPL}(\{a,-1\},z)}{z-1}\\
&+\frac{(i(\sqrt{3}+i)z+i\sqrt{3}+1)\mathrm{HPL}(\{a,0\},z)}{2(z-1)}\\
&+\frac{(z+1)\mathrm{HPL}(\{\mathrm{minus},\mathrm{plus}\},z)}{2-2z}+\frac{(3z+3)\mathrm{HPL}(\{\mathrm{plus},\mathrm{minus}\},z)}{2-2z}\\
&-\frac{(\sqrt{3}\pi-6)(z+1)\mathrm{HPL}(\{\mathrm{minus}\},z)}{3(z-1)}\\
&+\frac{(z+1)\mathrm{HPL}(\{0,\mathrm{minus}\},z)}{2(z-1)}+\frac{1}{2}\mathrm{HPL}(\{\mathrm{minus},0\},z)\\
&+\frac{(z+1)\mathrm{HPL}(\{\mathrm{minus},\mathrm{minus}\},z)}{2(z-1)}+\frac{(\sqrt{3}\pi-6)(z+1)\mathrm{HPL}(\{\mathrm{plus}\},z)}{3(z-1)}\\
&+\frac{(z+1)\mathrm{HPL}(\{0,\mathrm{plus}\},z)}{2-2z}-\frac{1}{2}\mathrm{HPL}(\{\mathrm{plus},0\},z)\\
&+\frac{3(z+1)\mathrm{HPL}(\{\mathrm{plus},\mathrm{plus}\},z)}{2(z-1)}+\frac{2\mathrm{HPL}(\{-2\},z)}{z-1}\\
&+\frac{2(3z-2\sqrt{3}\pi+9)\mathrm{HPL}(\{-1\},z)}{3(z-1)}+(\frac{\pi-3\pi z}{2\sqrt{3}(z-1)}+1)\mathrm{HPL}(\{0\},z)\\
&-\frac{8\mathrm{HPL}(\{-1,-1\},z)}{z-1}-\mathrm{HPL}(\{-1,0\},z)+\frac{1}{2}\mathrm{HPL}(\{0,0\},z)\\
&-\frac{2(z+1)\mathrm{HPL}(\{1,-1\},z)}{z-1}+\frac{1}{36(z-1)}\Big(-3(z(-12i\sqrt{3}\mathrm{Li}_2(2\sqrt[3]{-1})\\
&+12i\sqrt{3}\mathrm{Li}_2(-2(-1)^{2/3})-24-\psi^{(1)}(\frac{1}{6})-3\psi^{(1)}(\frac{1}{3})+3\psi^{(1)}(\frac{2}{3})+\psi^{(1)}(\frac{5}{6}))\\
&+12i\sqrt{3}\mathrm{Li}_2(-2(-1)^{2/3})-12i\sqrt{3}\mathrm{Li}_2(2\sqrt[3]{-1})+81\mathrm{S}_2(z-1)\\
&+24+\psi^{(1)}(\frac{5}{6})+3\psi^{(1)}(\frac{2}{3})-3\psi^{(1)}(\frac{1}{3})-\psi^{(1)}(\frac{1}{6}))+2\pi^2(z-1)\\
&+6\sqrt{3}\pi(z(\log(1728)-2)+2+\log\Big(\frac{64}{27}\Big))\Big).
\end{aligned}
$$

E.6 Four propagator topology, type b

This topology contain one MI depicted in the figure 14. The suitable point for fixing integration constants is $z = 1$. This integral has the following Laurent

$$b(0,1,1,0,1,1,0) \equiv b_1$$

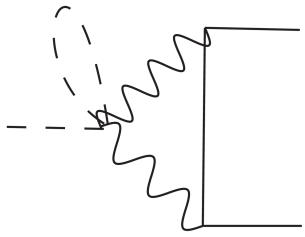

Figure 14: Four propagator topology, type b

expansion (in z variable)

$$\begin{aligned}
b_1^{(-1)} =& \frac{2(z+1)\mathrm{HPL}(\{-2\},z)}{z-1} + \frac{2(z+1)\mathrm{HPL}(\{0\},z)}{z-1} \\
&+ \frac{(z+1)\mathrm{HPL}(\{0,0\},z)}{1-z} - \frac{\pi^2(z+1)}{6(z-1)} \\
b_1^{(0)} =& - \frac{\pi^2(z+1)\mathrm{HPL}(\{\mathrm{minus}\},z)}{6(z-1)} + \frac{2(z+1)\mathrm{HPL}(\{\mathrm{minus},0\},z)}{z-1} \\
&+ \frac{(z+1)\mathrm{HPL}(\{\mathrm{minus},0,0\},z)}{1-z} + \frac{\pi^2(z+1)\mathrm{HPL}(\{\mathrm{plus}\},z)}{2(z-1)} \\
&- \frac{6(z+1)\mathrm{HPL}(\{\mathrm{plus},0\},z)}{z-1} + \frac{3(z+1)\mathrm{HPL}(\{\mathrm{plus},0,0\},z)}{z-1} \\
&+ \frac{8(z+1)\mathrm{HPL}(\{-3\},z)}{z-1} - \frac{6(z+1)\mathrm{HPL}(\{-2\},z)}{z-1} \\
&- \frac{(\pi^2-12)\,(z+1)\mathrm{HPL}(\{0\},z)}{6(z-1)} - \frac{12(z+1)\mathrm{HPL}(\{-2,-1\},z)}{z-1} \\
&+ \frac{6(z+1)\mathrm{HPL}(\{-2,0\},z)}{z-1} - \frac{8(z+1)\mathrm{HPL}(\{-1,-2\},z)}{z-1} \\
&+ \frac{5(z+1)\mathrm{HPL}(\{0,0\},z)}{z-1} - \frac{4(z+1)\mathrm{HPL}(\{1,-2\},z)}{z-1} \\
&- \frac{4(z+1)\mathrm{HPL}(\{0,0,0\},z)}{z-1} - \frac{5(z+1)(6\zeta(3)+\pi^2)}{6(z-1)}.
\end{aligned}$$

Bibliography

[1] M Passera. The standard model prediction of the muon anomalous magnetic moment. *Journal of Physics G: Nuclear and Particle Physics*, 31(5):R75, 2005.

[2] S. D. Drell. Direct decay $\pi^0 \to e^+e^-$. *Il Nuovo Cimento (1955-1965)*, 11(5):693–697, Mar 1959.

[3] S. M. Berman and D. A. Geffen. The electromagnetic structure and alternative decay modes of the π^0. *Il Nuovo Cimento (1955-1965)*, 18(6):1192–1202, Dec 1960.

[4] L. Bergström, E. Massó, Ll. Ametller, and A. Bramon. Q2 duality and rare pion decays. *Physics Letters B*, 126(1):117 – 121, 1983.

[5] Martin J Savage, Michael Luke, and Mark B Wise. The rare decays $\pi^0 \to e^+e^-, \eta \to e^+e^-$ and $\eta \to \mu^+\mu^-$ in chiral perturbation theory. *Physics Letters B*, 291(4):481–483, 1992.

[6] Ll Ametller, A Bramon, and E Masso. The $\pi^0 \to e^+e^-$ and $\eta \to \mu^+\mu^-$ Decays Revisited. *arXiv preprint hep-ph/9302304*, 1993.

[7] M Knecht, S Peris, M Perrottet, and E De Rafael. Decay of pseudoscalars into lepton pairs and large N_C QCD. *Physical Review Letters*, 83(25):5230, 1999.

[8] Marc Knecht and Andreas Nyffeler. Resonance estimates of $O(p^{(6)})$ low-energy constants and QCD short-distance constraints. *The European Physical Journal C-Particles and Fields*, 21(4):659–678, 2001.

[9] E Abouzaid, M Arenton, AR Barker, L Bellantoni, A Bellavance, E Blucher, GJ Bock, E Cheu, R Coleman, MD Corcoran, et al. Measurement of the rare decay $\pi^0 \to e^+e^-$. *Physical Review D*, 75(1):012004, 2007.

[10] L. Bergström. Radiative corrections to pseudoscalar meson decays. *Zeitschrift für Physik C Particles and Fields*, 20(2):135–140, Jun 1983.

[11] Alexander E Dorokhov and Mikhail A Ivanov. Rare decay $\pi^0 \to e^+e^-$: Theory confronts KTeV data. *Physical Review D*, 75(11):114007, 2007.

[12] J Gronberg, TS Hill, R Kutschke, DJ Lange, S Menary, RJ Morrison, HN Nelson, TK Nelson, C Qiao, JD Richman, et al. Measurements of the

meson-photon transition form factors of light pseudoscalar mesons at large momentum transfer. *Physical Review D*, 57(1):33, 1998.

[13] AE Dorokhov, EA Kuraev, Yu M Bystritskiy, and M Sečanskỳ. QED radiative corrections to the decay $\pi^0 \to e^+e^-$. *The European Physical Journal C*, 55(2):193–198, 2008.

[14] Petr Vasko and Jiri Novotny. Two-loop QED radiative corrections to the decay $\pi^0 \to e^+e^-$: The virtual corrections and soft-photon bremsstrahlung. *JHEP*, 10:122, 2011.

[15] Tomáš Husek, Karol Kampf, and Jiří Novotný. Rare decay $\pi^0 \to e^+e^-$: on corrections beyond the leading order. *The European Physical Journal C*, 74(8):3010, 2014.

[16] Steven Weinberg. Phenomenological Lagrangians. *Physica A: Statistical Mechanics and its Applications*, 96(1):327 – 340, 1979.

[17] J Gasser and H Leutwyler. Chiral perturbation theory to one loop. *Annals of Physics*, 158(1):142 – 210, 1984.

[18] J. Gasser and H. Leutwyler. Chiral perturbation theory: Expansions in the mass of the strange quark. *Nuclear Physics B*, 250(1):465 – 516, 1985.

[19] Res Urech. Virtual photons in chiral perturbation theory. *Nuclear Physics B*, 433(1):234–254, 1995.

[20] M Knecht, H Neufeld, H Rupertsberger, and P Talavera. Chiral perturbation theory with virtual photons and leptons. *The European Physical Journal C-Particles and Fields*, 12(3):469–478, 2000.

[21] Jeffrey Goldstone, Abdus Salam, and Steven Weinberg. Broken Symmetries. *Phys. Rev.*, 127:965–970, Aug 1962.

[22] K. Agashe et al. Review of Particle Physics. *Phys. Rev. D*, 98:030001, Aug 2018.

[23] Stefan Scherer and Matthias R. Schindler. A Chiral perturbation theory primer. 2005.

[24] J. Gasser and H. Leutwyler. Chiral Perturbation Theory to One Loop. *Annals Phys.*, 158:142, 1984.

[25] J. Gasser and H. Leutwyler. Chiral Perturbation Theory: Expansions in the Mass of the Strange Quark. *Nucl. Phys.*, B250:465–516, 1985.

[26] J. Wess and B. Zumino. Consequences of anomalous Ward identities. *Phys. Lett.*, 37B:95–97, 1971.

[27] Edward Witten. Global Aspects of Current Algebra. *Nucl. Phys.*, B223:422–432, 1983.

[28] L. Bergström. Rare decay of a pseudoscalar meson into a lepton pair—A way to detect new interactions? *Zeitschrift für Physik C Particles and Fields*, 14(2):129–134, Jun 1982.

[29] A. G. Grozin. Integration by parts: An Introduction. *Int. J. Mod. Phys.*, A26:2807–2854, 2011.

[30] K.G. Chetyrkin and F.V. Tkachov. Integration by parts: The algorithm to calculate β-functions in 4 loops. *Nuclear Physics B*, 192(1):159 – 204, 1981.

[31] Stefano Laporta. High-precision calculation of multiloop Feynman integrals by difference equations. *International Journal of Modern Physics A*, 15(32):5087–5159, 2000.

[32] S Laporta and E Remiddi. The analytical value of the electron $(g-2)$ at order α^3 in QED. *Physics Letters B*, 379(1-4):283–291, 1996.

[33] AV Smirnov and FS Chuharev. FIRE6: Feynman Integral REduction with Modular Arithmetic. *arXiv preprint arXiv:1901.07808*, 2019.

[34] A.V. Kotikov. Differential equations method. New technique for massive Feynman diagram calculation. *Physics Letters B*, 254(1):158 – 164, 1991.

[35] Mario Argeri and Pierpaolo Mastrolia. Feynman diagrams and differential equations. *International Journal of Modern Physics A*, 22(24):4375–4436, 2007.

[36] J. Fleischer, M. Yu. Kalmykov, and A. V. Kotikov. Two loop selfenergy master integrals on-shell. *Phys. Lett.*, B462:169–177, 1999. [Erratum: Phys. Lett.B467,310(1999)].

[37] Johan Bijnens and Lisa Carloni. The Massive $O(N)$ Non-linear Sigma Model at High Orders. *Nucl. Phys.*, B843:55–83, 2011.

[38] Ettore Remiddi and Jos AM Vermaseren. Harmonic polylogarithms. *International Journal of Modern Physics A*, 15(05):725–754, 2000.

[39] Daniel Maître. Extension of HPL to complex arguments. *arXiv preprint hep-ph/0703052*, 2007.

[40] Thomas Gehrmann and Ettore Remiddi. Numerical evaluation of two-dimensional harmonic polylogarithms. *Computer physics communications*, 144(2):200–223, 2002.

[41] Jens Vollinga and Stefan Weinzierl. Numerical evaluation of multiple polylogarithms. *Computer physics communications*, 167(3):177–194, 2005.

[42] R Bonciani, G Degrassi, and A Vicini. On the generalized harmonic polylogarithms of one complex variable. *Computer Physics Communications*, 182(6):1253–1264, 2011.

List of Figures

List of Tables